

2



This is to certify that the

dissertation entitled

ASSESSING AND MODELING THE SPATIAL VARIABILITY OF SOIL WATER REDISTRIBUTION AND WHEAT YIELD ALONG A SLOPING LANDSCAPE presented by

AYMAN ABDALLAH AHMED SULEIMAN

has been accepted towards fulfillment of the requirements for

DOCTOR OF PHILOSOPHY degree in _CROP_AND_SOIL_SCIENCES

De J. Litchie

Major professor

Date 26 Oct. 1999

LIBRARY Michigan State University

PLACE IN RETURN BOX to remove this checkout from your record.

TO AVOID FINES return on or before date due.

MAY BE RECALLED with earlier due date if requested.

DATE DUE	DATE DUE	DATE DUĖ

11/00 c:/CIRC/DateDue.p65-p.14

ASSESSING AND MODELING THE SPATIAL VARIABILITY OF SOIL WATER REDISTRIBUTION AND WHEAT YIELD ALONG A SLOPING LANDSCAPE

By

AYMAN ABDALLAH AHMED SULEIMAN

A DISSERTATION

Submitted to
Michigan State University
in partial fulfillment of the requirements
for the degree of

DOCTOR OF PHILOSOPHY

Department of Crop and Soil Sciences

1999

yield mana

appro

mode

and (

yield

versi

resid

repre

soil e

three

input

avail

coeff evapo

drain

ABSTRACT

ASSESSING AND MODELING THE SPATIAL VARIABILITY OF SOIL WATER REDISTRIBUTION AND WHEAT YIELD ALONG A SLOPING LANDSCAPE

By

AYMAN ABDALLAH AHMED SULEIMAN

Assessing and modeling the spatial variability of soil water redistribution and crop yield along a sloping landscape is a prerequisite for a better understanding of site-specificmanagement. The objectives of this research were to (1) evaluate and improve, when appropriate, the vertical soil water dynamics in the water balance portion of the CERES model, (2) develop a simple functional model to simulate lateral downslope soil water flow, and (3) combine remote sensing and crop modeling to predict the spatial variability of wheat yield grown on a sloping landscape. The daily change of soil water content (SWC) in a recent version of the crop model CERES is estimated from the difference between the initial and residual SWC of the water balance components multiplied by a transfer coefficient representing the fraction of the remaining soil water that can be removed in the processes of soil evaporation, vertical drainage and root water uptake. The transfer coefficients for the three processes is assumed to be fixed for all soils. The residual SWC values depend on the input soil properties for the SWC at air dry, drained upper limit, and lower limit of plant availability, respectively. Testing the dependancy of the drainage and evaporation transfer coefficients on soil characteristics was done by monitoring the SWC. The drainage and evaporation transfer coefficients were found to be soil specific and highly correlated with the drained upper limit SWC. Refinements in the drainage and second stage evaporation models

re fie yi in lea in fiel mo to ta

sl

m

in o

improved their accuracy for different soils.

A functional model was developed to simulate downslope lateral soil water flow based on Darcy's Law and equations for estimating unsaturated and saturated hydraulic conductivity. The model requires inputs of the drained upper limit and saturated SWC, water table level, slope, and the amount of incoming flow. Soil water profiles and water table levels were monitored at 15 locations along a sloping landscape to test the model. The model performed reasonably well in estimating lateral soil water drainage. A wheat crop grown on the 6 ha field where lateral flow was studied provided an opportunity to assess spatial variation in yield as influenced by soil spatial variability of differences in water supply related to position in the landscape. Remote sensing from an aircraft helped to quantify spatial variability in leaf area index (LAI) in the field. When this spatial variation in LAI at anthesis was input in the CERES-Wheat model as an alternative to predicting LAI uniformly for the whole field, the modeled spatial variation in yield agreed quite well with the variation in yields monitored for the entire field. The experiments done for this research demonstrated the need to take both vertical and horizontal water flow into account for sloping land in humid regions in order to adequately describe causes of spatial variability in crop yields.

DEDICATION

To

Muna, my wife, for her understanding, patience, and support

Zena, my daughter, for the enjoyable time she has given us

Dr

Th

gu

Dr.

Dr

Dr.

Baı

fiel

Bri

my

Ma: infr

Hor Dr.

Roti

stay

My

My I

ACKNOWLEDGMENTS

I would like to express my appreciation and gratitude to:

Dr. Joe Ritchie, my major advisor, for his financial support, friendship, and enlightening guidance throughout my study at Michigan State University.

The graduate committee:

Dr. Harold Belcher, Dr. James Flore, Dr. David Lusch, and Dr. Alvin Smucker.

Dr. Joe Ritchie.

Bary Darling, University Farms manager, and his crew for their great help throughout my field research.

Brian Graff, Crop Science Field Lab manager, and his staff for their great help throughout my research.

Marc Hooper and Sharon, from Grower Service Corporation, for their help in getting the infrared images.

Homer Nowlin group: Bruno Basso, Brian Baer, Dr. Samira Daroub, Dr. Aris Gerakis,
Dr. Alagarswamy Gopalsamy, Eirini Katsalirou, Carlos Paglis, Scott Piggott, Sharlene
Rotman, and Dr. Serena Stornaiuolo for their sincere friendship and assistant throughout my

stay at Michigan State University.

My parents and all my family members for their continuous care and concern.

My parents in-law, and all their family members for their invaluable gift!

T

I

(

СН

CHA

TABLE OF CONTENTS

LIST OF TABLES viii
LIST OF FIGURES ix
INTRODUCTION1
References
CHAPTER ONE
ASSESSING AND MODELING SOIL WATER DISTRIBUTION UNDER
SECOND STAGE EVAPORATION9
Introduction9
Theory
Second stage evaporation
Second Stage Evaporation Model in CERES Water Balance
Materials and methods
Laboratory Experiments
Field Experiment
Laboratory Results
Effect of Water Table
References
CHAPTER TWO
ASSESSING AND MODELING VERTICAL SOIL WATER DRAINAGE 37
Introduction
Theory
Drainage Model in CERES Water Balance
Materials and Methods
Laboratory Experiments45
Field Experiment
Results and Discussion45
Laboratory Results
Field Results60
Conclusions
References
CHAPTER THREE
CHAPTER THREE
ASSESSING AND MODELING DOWNSLOPE LATERAL SOIL WATER FLOW ALONG A SLOPING LANDSCAPE
Introduction
Theory
Material and Methods
2-2007-0-2001 0010-0-1-1-0-1-1-1-1-1-1-1-1-1-1-1-1

	Data Collection	78
	Site Description	80
	TDR Description	82
	Data Analysis	84
	Results and Discussion	84
	Water table	89
	Leaf Area Index	91
	Lateral downslope soil water flow	95
	Conclusions	101
	References	102
CHAI	PTER FOUR	
	ASSESSING AND MODELING THE SPATIAL VARIABILITY OF	WHEAT
	YIELD WITHIN A SLOPING LANDSCAPE	104
	Introduction	104
	Materials and Methods	105
	Site Description	109
	Field Management	
	Normalized Difference Vegetation Index and LAI	111
	Integrating CERES-WHEAT Model and Remote Sensing	112
	Results and Discussion	113
	Spatial Variability Along Access Tube Transect	113
	Model Performance Along Access Tube Transect	116
	Infrared Images Interpretation	118
	Modeling Spatial Variability of Grain Yield	120
	Conclusions	127
	References	128
SUM	MARY AND CONCLUSIONS	131
APPE	ENDICES	
	Appendix A. Soil properties at access tube locations	134
	Appendix B. Daily solar radiation (SR), maximum (T _{max}) and minimum	
	temperature (T _{min}), and Rainfall (R) for the sloping landscape	137
	Appendix C. List of abbreviations	147

Table

Table

LIST OF TABLES

Table 1.1. Soil physical properties of profile 1 and profile 2 for soil field in Lansing 16
Table 4.1. Measured and simulated grain yield near all access tube locations 117

F Fi Fi

> Fig Fig

> Fig

Figu

Figu

Figu

Figu

Figu

Figu

LIST OF FIGURES

Figure	1.1. Daily solar radiation (SR), maximum (Tmax) and minimum (Tmin) temperatures, and rainfall (R) from DOY 200 to 280 in 1997
Figure	1.2. Measured and simulated soil water content profiles of 60-cm columns of loam and sandy loam soils drying during second stage evaporation
Figure	1.3. Measured and simulated soil water content profiles of 60-cm columns of loam and sandy loam soils drying during second stage evaporation 20
Figure	1.4. Relationship between α and θ_{dul} of 8 soils: Loamy and Sandy loam soils from Michigan and 6 soils from D.A. Rose (1968)
Figure	1.7. Soil water content profiles of 60-cm columns of loamy and sandy loam soils versus Boltzmann transform under second stage evaporation
Figure	1.8. Soil water content profiles at six depths of sandy loam soil profile in 1997. 26
Figure	1.9. Measured, simulated (using Eq. [8] with n=-2 and a=0.63), simulated (M) (using Eq. [8] with n=2.09 and a=0.47) soil water content of a bare soil in Lansing field in 1997 at six different depths
Figure	1.10. Soil water content profiles of 150-cm columns of loamy soil drying during second stage evaporation
Figure	1.11. Soil water content profiles of 150-cm columns of sandy loam soil drying during second stage evaporation
Figure	1.12. Soil water content profiles of 150-cm columns of loamy and sandy loam soils versus Boltzmann transform during second stage evaporation
Figure	1.13. Cumulative evaporation of 150-cm column of loamy and sandy loam soils during second stage evaporation
Figure	2.1. Relationships between C_1 , C_2 , and C with $(\ln \alpha)^{1/n}$ for any realistic possible combination of θ_s and θ_{dul}
Figure	2.2. Measured and estimated C using Eq. [20] of the international soils versus (lnα) ^{1/n}
Figure	2.3. Relationship between C and θ_{dul} for any possible realistic combination of θ_s and θ_{dul}

F F Fi Fig Fig Fig Figi Figu Figu Figu Figu Figu Figu

Figure	2.4. Measured and estimated C using Eq. [21] of the international soil versus θ_{dul} 50
Figure	2.5. Relationship between C and Q_i for a soil of $\theta_s = 0.4$ cm ³ cm ⁻³ and $\theta_{dul} = 0.4$ cm ³ cm ⁻³
Figure	2.6.a. Soil water content profiles for a 150-cm column of loamy soil during drainage cycle at 3, 6, 9, 12, 15 and 25 cm depths
Figure	2.6.b. Soil water content profiles for a 150-cm column of loamy soil during drainage cycle at 35, 45, 55, 65, and 75 cm depths
Figure	2.7.a. Soil water content profiles for a 150-cm column of sandy loam soil during drainage cycle at 3, 6, 9, 12, 15 and 25 cm depths
Figure	2.7.b. Soil water content profiles for a 150-cm column of sandy loam soil during drainage cycle at 35, 45, 55, 65, and 75 cm depths
Figure	2.8. Daily drainage rate of a 150-cm column of loamy soil and a 150-cm column of sandy loam soil
Figure	2.9. Cumulative drainage of a 150-cm column of loamy soil and a 150-cm column of sandy loam soil
Figure	2.10.a. Soil water content profiles for profile 1 of sandy loam soil during drainage cycle at 3, 6, 9, 12, 15, and 25 cm depths
Figure	2.10.b. Soil water content profiles of profile 1 of sandy loam soil during drainage cycle at 35, 45, 55, 65, and 75 cm depths
_	2.11.a. Soil water content profiles for profile 2 of sandy loam soil during drainage cycle at 3, 6, 9, 12, 15, and 25 cm depths
Figure	2.12. Daily drainage rate of profile 1 and profile 2 of sandy loam soil 66
Figure	2.13. Cumulative drainage of profile 1 and profile 2 of sandy loam soil versus time
Figure	3.1. Cartesian rectangular space coordinate x and z and rotated coordinates x. and z
Figure	3.2. (a) Elevation (ft), slope (%), and access tube locations within the field. (b) relative soil surface height (cm), water table (WT) height (cm), and restricted layer (at 150 cm depth)
Figure	3.3 Daily solar radiation (MJ m ⁻²), temperature (C°), and rainfall (mm) from DOY

Figu Figui

	1 through DOY 200 in 1998
Figure	3.4. A discontinuous TDR probe (DTDR150) and a typical wave 83
Figure	3.5. Relationship between C and C $\sin \gamma$ with $\sin \gamma$ and θ_{dul} at representative combinations of θ_{dul} and $\sin \gamma$
Figure	3.6. Example of a typical relationship between C_x and x_{\bullet} for a soil 86
Figure	3.7. Example of a typical relationship between C _p and Q _i for a soil 90
Figure	3.8. Measured and simulated change of soil water table depth (cm) from DOY 124 to 146
Figure	3.9.a. Corrected simulated LAI at L1 through L8 from DOY 90 through 200.
Figure	3.9.b. Corrected simulated LAI at L9 through L15 from DOY 90 through 200 and mean and standard deviation of LAI for the 15 locations
Figure	3.10. Mean and standard deviation of simulated daily actual (E _{ta}) and potential (E _{tp}) evapotranspiration from DOY 124 to 146
Figure	3.11. Estimated C and C sin γ at all access tube locations
Figure	3.12. Measured and simulated cumulative lateral down slope (L) flow at all access tube locations from DOY 124-132, 132-140, and 140-146
Figure	3.13. Measured and simulated daily lateral downslope soil water flow (L) at the middle of L12 and L13
Figure	4.1. Elevation, contours, slope, and access tube locations within the experimental field
Figure	4.2. Daily solar radiation, maximum (Tmax) and minimum (Tmin) temperature, and rainfall from DOY 1 through 200 in 1998
Figure	4.3. Infrared images were captured (from left to right) on April 4, April 28, June 4, and July 14, 1998
Figure	4.4. Elevation, slope, and some soil properties (total nitrogen, organic matter, soil texture, and bulk density) of the surface layer
Figure	4.5. Crop characteristics at harvest time (plant density, heads number, number of grains per head, head weight, unit grain weight, grain number, and grain yield. 115

Figu

Figu

Figu

Figu

Figu

_	4.6. Normalized difference vegetation index (NDVI) (from left to right) on April 4, April 28, June 4, and July 14, 1998
_	4.7. Leaf area index (LAI) (from left to right) on April 4, April 28, June 4, and July 14, 1998
_	4.8. Relationship between simulated stem weight and simulated leaf area index at anthesis
_	4.9. Relationship between measured grain yield and measured seed number near access tube locations
Figure 4	4.10. Measured and simulated grain yield maps

tr

INTRODUCTION

ASSESSING AND MODELING THE SPATIAL VARIABILITY OF SOIL WATER REDISTRIBUTION AND WHEAT YIELD ALONG A SLOPING LANDSCAPE

By

AYMAN ABDALLAH AHMED SULEIMAN

A model has been defined as a small imitation of the real thing or as system of postulates, data and inferences presented as a mathematical description of an entity or state of affairs (Hanks and Ritchie, 1991). Crop models are valuable as: (i) aids in interpreting experimental results, (ii) agronomic research tools, or (iii) agronomic grower tools (Whisler et al., 1986). Boote et al. (1996) proposed three primary uses or reasons for crop modeling: research knowledge synthesis (combining Whisler's first two categories), crop system decision management, and policy analysis (such as climate change and sustainable agriculture). The genesis of such models can be traced to the arrival of mainframe computers in the early 1960's, and their rapid growth in the past decade has been simulated by the ubiquity of desktop computers (Monteith, 1996; Passioura, 1996). Further advances in computer technology should facilitate the continued development and refinement of crop simulation models.

Most models used for evaluating crop production systems can be categorized as mechanistic or functional. Mechanistic models are usually based on dynamic rate concepts (Ritchie and Crum, 1989). They incorporate basic mechanisms of processes such as Darcy's Law or Fourier's Law and the appropriate continuity equations for water and heat flux, respectively. Functional models are usually based on capacity factors and treat processes in a more simplified manner, reducing the amount of input required. Every

model of the plant-soil-atmosphere system, whether mechanistic or functional, uses some level of empiricism in order to reduce the need for input information. Thus it may be somewhat difficult to distinguish between mechanistic and functional models. The most important difference between mechanistic and functional models is their usefulness as either research or management tools. Mechanistic models are useful primarily as research tools used to improve understanding of an integrated system, and usually are not widely used due to their complexity. The functional models have modest input requirements making them useful for management purposes. Because of their simplicity, functional models are more widely used and independently validated than their mechanistic counterparts.

Mechanistic modeling of soil water flow is based on Darcy's Law and the Richards equation. Darcy's Law is the basic concept for one-dimensional water flow in a homogeneous soil (Philip, 1995). However, for two or three-dimensional water flow in homogeneous soil, Richards equation may be useful. According to Youngs (1995), Richard (1931) derived his equation from Darcy's Law using the same two basic parameters: hydraulic conductivity and hydraulic water potential. Richards' equation is a good theoretical description for the homogeneous soil water flow. However, it may not be appropriate under field conditions. Youngs (1995) mentioned seven factors that often make Richards' model an inappropriate basis for computing soil-water flow under field conditions. These factors are: the influence of the air phase on the soil water movement, the effect of soil heterogeneity, soil swelling, soil aggregation and soil instability, deviation from Darcy's Law, thermal effects, and the hysteresis in soil water relationships.

19

So

w:a

un

cO1

(A

stra

cro

and

whe

inte

relat subr

for q

for t

subr

run(

evid

Although a well-defined laboratory experiment can be a preliminary step (Rose, 1996), the real challenge is to describe the soil water flow dynamics in field conditions. Soil in the field is rarely homogeneous and is a dynamic system. Approximations to soil water flow problems in the field may be used. But even if Richards' equation is valid under field conditions, its use can be difficult because measurements of soil hydraulic conductivity or soil water diffusivity in the field are time consuming and expensive (Ahuja et al., 1993).

The CERES program, a functional model, is designed to continuously simulate crop, soil, water and nutrient conditions under different management strategies. These strategies may include various crop rotations, planting dates, plant populations, irrigation and fertilizer applications, and tillage regimes. The program can simulate plant growth and soil conditions daily (during growing seasons and fallow periods) for any time period when weather sequences are available. This also provides a framework whereby the interaction between different areas under different management practices can be compared easily.

CERES consists of many subroutines which take into consideration many factors related to the soil-plant-atmosphere continuum. One of the most important CERES subroutines deals with water balance. The water balance subroutine in CERES is adapted for different soils, climatic conditions, and crops. The water balance subroutine accounts for the water coming to the profile as well as to the water going out of the profile. This subroutine simulates the temporal soil water contents, evapotranspiration, drainage, and runoff, however it does not account for soil water lateral flow. Soil water lateral flow is evident in sloping landscapes and it may account for 20% of the water balance.

re

sat wa

esti

and

coul

and y

are a

moni

varia

reduc

field.

of tir

to so

cond

the a

Therefore accurate modeling of the soil water balance is important for efficient water management and for simulating crop performance (Savage et al., 1996; Ritchie, 1972; Ritchie, 1981).

The soil water balance in CERES has been built using simplified approaches that require few soil inputs. Drained upper limit and lower limit soil water contents and saturated hydraulic conductivity are needed to run the soil water balance in CERES. It was found that the soil water limits as well as saturated hydraulic conductivity can be estimated reasonably well from texture and bulk density (Ritchie et al., 1999; Suleiman and Ritchie, 1999).

The movement of water from one location to another within a sloping landscape could explain crop spatial variability. Differences in crop production within agricultural fields vary by a factor of two to four. Applications of Global Positioning System (GPS) and yield-sensors allow expression of such differences. Differences of yields within fields are also obvious in many developing countries, even without access to GPS and yield monitoring equipments (Bouma et al., 1995). Finding the reasons why yield spatial variability occur is a primary step in the development of management procedures that can reduce or make use of these differences (Bouma et al. 1995). Differences in yield within a field is a consequence of the variability of the microenvironment.

The spatial covariance between soil and crop and its transformation as a function of time remains largely unexplored in the agricultural science as well as their application to soil specific framing (Nielsen et al., 1995). Some research, however, has been conducted on soil water variability. Rosek (1994), found that soil physical properties and the amount of soil water within a sloping landscape are largely determined by landscape

position. This is in agreement with Miller et al. (1988) findings, where a strong spatial dependency was found between soil properties and wheat yield.

According to Miller et al. (1988) no correlation was found between percent slope and yield or soil properties, using the standard regression analysis, but semiveriograms and cross-semiveriograms showed a strong correlation among them. Geostatistics, which is regionalized variable analysis, has been used to improve the assessment of soil and crop attributes within site specific domains (Burrough, 1991; Mulla, 1993; Nielsen and Alemi, 1989; Robert et al., 1993; Trangmar et al., 1985). The Geostatistics techniques in soil specific farming have been giving a good explanation for the spatial variability and their future is expected to be bright (Nielsen et al., 1995).

The spatial variability affects, in turn, the temporal variability. For instance, soil erosion creates spatial variability of clay content as well as a variation of the clay content over time at a certain spot. On the basis of that, determining the effect of time on the variability structure is necessary as well as determining the spatial variability for sustainable farming.

The Geographical Information System (GIS) is widely used to describe the spatial variability and to help in decision making. The early development and commercial success of GIS were fueled more by the need for efficient spatial inventory rather than decision making (Eastman et al., 1993). The GIS is an important tool that makes use of remote sensing data. The combined use of remote sensing, GIS, geostatistical techniques, and crop simulation models has the potential for improving agricultural management. This study aimed to:

1. Evaluate the vertical soil water movement dynamics during vertical drainage

and second stage evaporation in the water balance component of CERES,

- 2. Develop and evaluate a simple functional model to simulate lateral downslope soil water flow along a sloping landscape, and
- 3. Integrate CERES-WHEAT and remote sensing in order to simulate the spatial variability of wheat yield within a sloping landscape.

References

- Ahuja, L.R., O. Wendroth, and D.R. Nielsen. 1993. Relationship between initial drainage of surface soil and average profile saturated conductivity. Soil Sci Soc. Am. J. 57:19-25.
- Boote, K.J., J.W. Jones, and N.B. Pickering. 1996. Potential uses and limitations of crop models. Agron. J. 88:705-716.
- Bouma, J., J. Brouwer, A. Verhagen, and H.W.G. Booltink. 1995. Site specific management on field level: high and low tech approaches. Kluwer Academic Publishers in cooperation with International Potato Center. Netherlands.
- Burrough, P.A. 1991. Sampling design for quantifying map unit composition. p. 89-127. In M.J. Mausbach, and L.P. Wilding (ed.) Spatial variabilities of soils and landform. SSSA Spec. Publ. No.28. Soil Sci Soc. Am., Madison, WI.
- Hanks, J., and J.T. Ritchie. 1991. Modeling plant and soil systems. Number 31 in the series of Monograghs. Agronomy. Madison, Wisconsin, USA.
- Eastman, J.R., Kyem, P.A.K., Toledano, J., and W. Jin. 1993. Introduction: GIS and decision making. Explorations in Geographic Information Systems Technology, Vol 4, Geneva: Unitary European Office, p. 1-20, 93-98.
- Miller, M.P., M.J. Singer, and D.R. Nielsen. 1988. Spatial variability of wheat yield and soil properties on complex hill.
- Monteith, J.L. 1996. The quest for balance in crop modeling. Agron. J. 88:695-697.
- Mulla, D.J. 1993. Mapping and managing spatial patterns in soil fertility and crop yield. In P.C. Robert et al. (ed.) Proceedings of soil specific crop management: A workshop on research and development issues. SSSA Spec. Publ. No. 28. Soil Sci Soc. Am., Madison, WI.
- Nielsen, D.R, and H. Alemi. 1989. Statistical opportunities for analyzing spatial and temporal heterogeneity of field soils. p. 261-272. *In* M. Clarholm, and L. Bergströn (ed.) Ecology of arable land-perspectives and challenges. Proc. of an International Symposium, 9-12 June 1987, Swedish University of Agricultural Science, Uppsala, Sweden. Kluwer Academic publishers, Dordrecht.
- Nielsen, D.R., Owendroth, and M.B. Parlange. 1995. Opportunities for examining onfarm soil variability. Mausbach, and L.P. Wilding (ed.) Spatial variabilities of soils and landform. SSSA Spec. Publ. No. 28. Soil Sci Soc. Am., Madison, WI.
- Passioura, J.B. 1996. Simulation models: science, snake oil, education or engineering?.

- Agron. J. 88:690-694.
- Philip, J.R. 1995. Desperately seeking Darcy in Dijon. Soil Sci. Soc. Am. J. 59:319-324.
- Ritchie, J.T. 1972. Model for predicting evaporation from a row crop with incomplete cover. USDA Soil and water Conservation Research Division, Blackland Conservation Research Center, Temple, Texas.
- Ritchie, J.T. 1981. Water dynamics in soil-plant-atmosphere. Plant Soil 58:81-96.
- Ritchie, J.T., and J. Crum. 1989. Converting soil survey characterization data into IBSNAT crop model input. p.155-167. *In* J. Bouma and A.K. Brget (ed.) Land Qualities in space and time. Wageningen, The Netherlands.
- Ritchie, J.T., A. Gerakis, and A.A. Suleiman. 1999. Estimation of soil water content limits for water balance models from soil survey data. ASAE. (In review).
- Robert, P.C., R.H. Rust and W.E. Larson. 1993. Proceedings of soil specific crop management: A workshop on research and development issues. SSSA Spec. Publ. No. 28. Soil Sci Soc. Am., Madison, WI.
- Rose, D.A. 1996. The dynamics of soil water following single surface wettings. European Journal of soil science. 47:21-31.
- Rosek, M.J. 1994. Spatial and temporal soil water content changes within a sloping landscape. Doctoral Dissertation. Crop and Soil Sciences Department. Michigan State University, East Lansing, Michigan, USA.
- Savage, M.J., J.T Ritchie, W.L. Bland, and W.A. Dugas. 1996. Lower limit of soil water availability. Agron. J. 88:644-651.
- Suleiman, A.A., and J.T. Ritchie. 1999. Estimating saturated hydraulic conductivity from drained upper limit water content and bulk density. ASAE. (In review).
- Trangmar, B.B., R.S. Yost, and G. Uehara. 1985. Applications of geostatistics to spatial studies of soil properties. Advances in Agron. 38:45-94.
- Whisler, F.D., B. Acock, D.N. Baker, R.E. Fye, H.F. Hodges, J.R. Lambert, H.E. Lemmon, J.M. McKinion, and V.R. Reddy. 1986. Crop simulation models in agronomic systems. Adv. Agron. 40:141-208.
- Youngs, E.G. 1995. Developments in the physics of infiltration. Soil Sci. Soc. Am. J. 59:307-313.

- -

CHAPTER ONE

ASSESSING AND MODELING SOIL WATER DISTRIBUTION UNDER SECOND STAGE EVAPORATION

Introduction

Soil water evaporation is a large component of the water balance (Ritchie 1972). The water evaporation from a soil surface (E_s) can be divided into two stages: (1) the constant rate stage in which E_s is limited only by the supply of energy to the surface and (2) the falling rate stage in which water movement to the evaporation sites near the surface is controlled by the hydraulic properties of the soil (Ritchie, 1972). The constant rate stage of evaporation vary not only with the prevailing atmospheric environment, but also with soil surface features such as soil surface color, aerodynamic roughness (Mcllroy, 1984). The falling rate stage of evaporation requires an internal movement of water to the regions where vaporization is actually occurring (near-soil surface) (Mcllroy, 1984).

Several mechanistic models have been reported in which Richard's equation of water flow is used as a basis to calculate E_s (C.W. Rose, 1968; Gardner and Gardner, 1969; van Bavel and Hillel, 1976; Hillel and Talpaz, 1977; Feddes et al., 1978; Norman and Campbell, 1983; Hanks, 1991; Evett and Lascano, 1993; Farahani and Ahuja, 1996). Ritchie and Johnson (1990) stated that functional models for estimation of E_s are less evident in the literature and few evaluation have been conducted on such functional models (Gabrielle et al., 1995).

Ritchie and Johnson (1990) showed that mechanistic and functional models may

have very similar outcomes in estimating soil evaporation even though mechanistic models require more inputs. Mechanistic models usually require data of hourly weather (global radiation, air temperature, rainfall/irrigation, dew point temperature, wind speed), soil (water retention curve, K vs. θ , soil albedo vs. θ , Ksat, and porosity), and initial values of (θ vs. depth and temperature vs. depth). Functional models require data of daily weather (global radiation, maximum and minimum temperature, and rainfall/irrigation), soil (soil albedo and DUL), and initial values of (θ vs. depth). Increasing interest in regional evaporation models emphasizes the need to quantify the spatial distribution of evaporation (Lascano and Hatfield 1992). This would enhance the need for models that require less inputs.

D.A. Rose (1968) showed that diffusivity theory explained the soil water distribution under second stage evaporation for homogenous soils whose initial soil water content was equal to the drained upper limit soil water content. In a study on a bare soil, Black et al. (1969) examined the diffusivity theory in the field and demonstrated that E_s was function of soil diffusivity. Both of D.A. Rose (1968) and Black et al. (1969) approved that the cumulative soil evaporation, under second stage evaporation, was function of the square root of time. On the basis of the diffusivity theory and the published work of both D.A. Rose (1968) and Black et al.(1969), Ritchie (1972) developed a simple functional model to estimate E_s, under second stage evaporation. This model has been used worldwide to estimate E_s, because of its validity and simplicity.

The objective of this research was to test upward soil water flow dynamics and second stage soil water evaporation model in the water balance of CERES crop simulation model family. In many agricultural fields, especially those with restricted soil

lay

eva

was

Th

who

is s

Sec

sub

rela

rate

θ=

 $heta_{ss}$ $ext{E}_{sa}$

layer in the root zone, water table may have a profound impact on second stage evaporation, and hence the impact of water table on the rate of second stage evaporation was assessed.

Theory

The generalized vertical flow equation can be written as follows (Philip, 1957):

$$\frac{\partial \theta}{\partial t} = \frac{\partial}{\partial z} \left(D(\theta) \frac{\partial \theta}{\partial z} \right) - \frac{\partial K(\theta)}{\partial z}$$

(1)

where $D(\theta)$ and $K(\theta)$ are soil water diffusivity and hydraulic conductivity, respectively, θ is soil water content, and t and z are time and distance, respectively.

Second stage evaporation

When a semi-infinite soil column z > 0, initially at a uniform water content θ_{dul} , subsequently has its surface maintained at the water content θ_{ad} in equilibrium with the relative humidity of the atmosphere, the initial and boundary conditions governing flow rate are:

$$\theta = \theta_{dul} \qquad z \ge 0 \quad t = 0$$

$$\theta_{ss} = \theta_{ad} \qquad z = 0 \quad t > 0$$

$$E_{sa} < E_p \qquad t > 0$$

e

wł

Z

teri

an

cap

 θ_{ad}

au

z =

(E_{c.}

Q =

wher

where θ is volumetric soil water content, θ_{dul} volumetric drained upper limit soil water content, θ_{ss} is volumetric soil water content at the soil surface, θ_{ad} air dry volumetric soil water content, z is depth, t is time, E_{sa} is actual soil evaporation, and E_p is potential soil evaporation.

The solution of Eq. [1] subject to these conditions is, for all except large t,

$$z(\theta,t) = \sum_{n=1}^{\infty} \lambda_n t^{\frac{n}{2}}$$
 (2)

where $\lambda = zt^{-1/2}$ is the Boltzmann transform. The λ_n are all single-valued functions of θ , and the series converges so rapidly that, except when $t\to\infty$, only the three or four leading terms are needed to describe flow problems of practical interest, e.g. infiltration, or capillary rise above a water table. When gravity can be ignored (e.g. horizontal flow) or neglected without serious errors (e.g. drying a vertical column of well-structured soil with $\theta_{ad} < \theta_i \le \theta_{dul}$) only the first term of the series is needed and then, dropping the sub,

$$z = \lambda(\theta)t^{1/2} \tag{3}$$

Thus, the quantity of water lost by evaporation (Q cm) or cumulative evaporation (E_c cm) is given by

$$Q = E_c = \int_{\theta_i}^{\theta_{ad}} z d\theta = \alpha t^{\frac{1}{2}}$$
 (4)

where

$$\alpha = \int_{\theta_{ad}}^{\theta_{dul}} \lambda(\theta) d\theta \tag{5}$$

and the evaporation rate

$$E = dQ/dt = \frac{1}{2}t^{-1/2}\alpha \tag{6}$$

The assumptions in the analysis are justified, and the boundary conditions are satisfied when, for a given material, evaporation yields water content profiles invariant with zt^{-1/2}, i.e. when $\lambda(\theta)$ is uniquely dependent on θ . Diffusivities controlling evaporation are functions of water content alone (Philip, 1957; D.A. Rose, 1968).

Second Stage Evaporation Model in CERES Water Balance

The change of volumetric soil water content in a day at any depth > 2 cm under second stage evaporation can be estimated as follows:

$$\Delta \theta = C \left(\theta - \theta_{ad} \right) \tag{7}$$

where θ is the volumetric soil water content at any time, C is constant function of depth (d) as follows:

$$C = a d^{n}$$
 (8)

where a and n are constants and equal to 0.63 and -2, respectively.

The change of volumetric soil water content at 1 cm depth is calculated as follows:

$$C = a d^{n} (0.82 - 4.7 (0.45 - \theta_{dul})^{n})$$
(9)

Air dry volumetric soil water content (θ_{ad}) is estimated as follows:

$$\theta_{ad} = 0.44 \; \theta_{dul}^{2} \tag{10}$$

Cumulative evaporation (E_c) from soil under the following initial and boundary conditions

$$\theta_v = \theta_{dul}$$
 $z \ge 0$ $t = 0$

$$\theta_{vs} = \theta_{ad} \hspace{1cm} z = 0 \hspace{1cm} t > 0$$

$$E_{sa} < E_{p}$$
 $t > 0$

is estimated from Eq. [4] assuming α is a constant and equal to 3.75 mmd^{-1/2}.

Materials and methods

Laboratory and field experiments were conducted to study the upward soil water flow dynamics during drying cycle. Besides the laboratory and field experiments, data of six different soils from D.A. Rose (1968) were used for comparison.

Laboratory Experiments

Two different soils from Michigan were used to measure the second stage evaporation rate. One of the soils was obtained from Saginaw area and it was loamy soil (25.4 % clay and 43 % sand). The second one was obtained from Lansing area and it was sandy loam soil (9.4 % clay and 65.4 % sand). The two soils were air dried, sieved through 2 mm screen, and then assembled into PVC columns of 60 cm height and 30 cm diameter. Twenty cm time domain reflectometry probes (TDR) were installed horizontally at depths of 3, 6, 9, 12, and 15 cm from the surface. The top 25 cm of the soil columns were saturated by adding water on soil surface and then the soil surface was covered to avoid evaporation. The soil columns were allowed to drain for 10 days and

th so

c

st

9.

th

di hi

ev

F

15

Jυ

so

de

su pr

rai

then the soil surface was uncovered. A light source and a fan were directed toward the soil surface of each column to ensure high potential evaporative losses. Soil water content was monitored at the 5 depths every 15 minutes for about two months.

The two soils were also used to evaluate the effect of water table on the second stage evaporation rate. The air dried soils were assembled into PVC columns of 150 cm height and 30 cm diameter. Twenty cm TDR were installed horizontally at depths of 3, 6, 9, 12, 15, 25, 35, 45, 55, 65, and 75 cm from the surface. The soils were saturated from the bottom using constant head of 150 cm. The soils were allowed to drain the excess water for 10 days while the soil surface was covered. A light source and a fan were directed toward the soil surface of each column at the end of drainage cycle to ensure high potential evaporative losses. Soil water content was monitored at the eleven depths every 20 minutes for two months.

Field Experiment

Two sets of 20-cm TDR probes were installed horizontally at depths of 3, 6, 9, 12, 15, 25, 35, 45, 55, 65 and 75 cm from the surface in a flat bare field in Lansing area on July 10, 1997. The two sets were 3 m apart. The soil water content was monitored at all depths every 20 minutes for a month. The soil was saturated using ponding and then the soil surface was covered for 15 days on August 15, 1997. After the drainage, the soil surface was uncovered again for 10 days. The soils texture and bulk density are presented in Table 1.1. Daily solar radiation, maximum and minimum temperatures, and rainfall from day of year (DOY) 200 to 280 of 1997 are shown in Figure 1.1.

Ta

_

†

Table 1.1. Soil physical properties of profile 1 and profile 2 for soil field in Lansing.

Depth	Profile 1			Profile 2		
	Clay	Sand	B†	Clay	Sand	В
cm	•	%		%		g cm ⁻³
10	11.3	65.3	1.44	14.6	62.7	1.42
15	11.3	68.1	1.45	27.9	57.3	1.40
25	11.3	68.0	1.46	26.5	43.9	1.34
35	13.9	72.4	1.50	19.6	54.4	1.41
45	25.7	57.2	1.43	31.5	45.3	1.37
55	28.2	57.5	1.44	29.1	48.4	1.40
65	16.6	73.9	1.53	21.4	49.8	1.41
75	22.2	54.9	1.45	17.1	53.8	1.44

†B is bulk density.

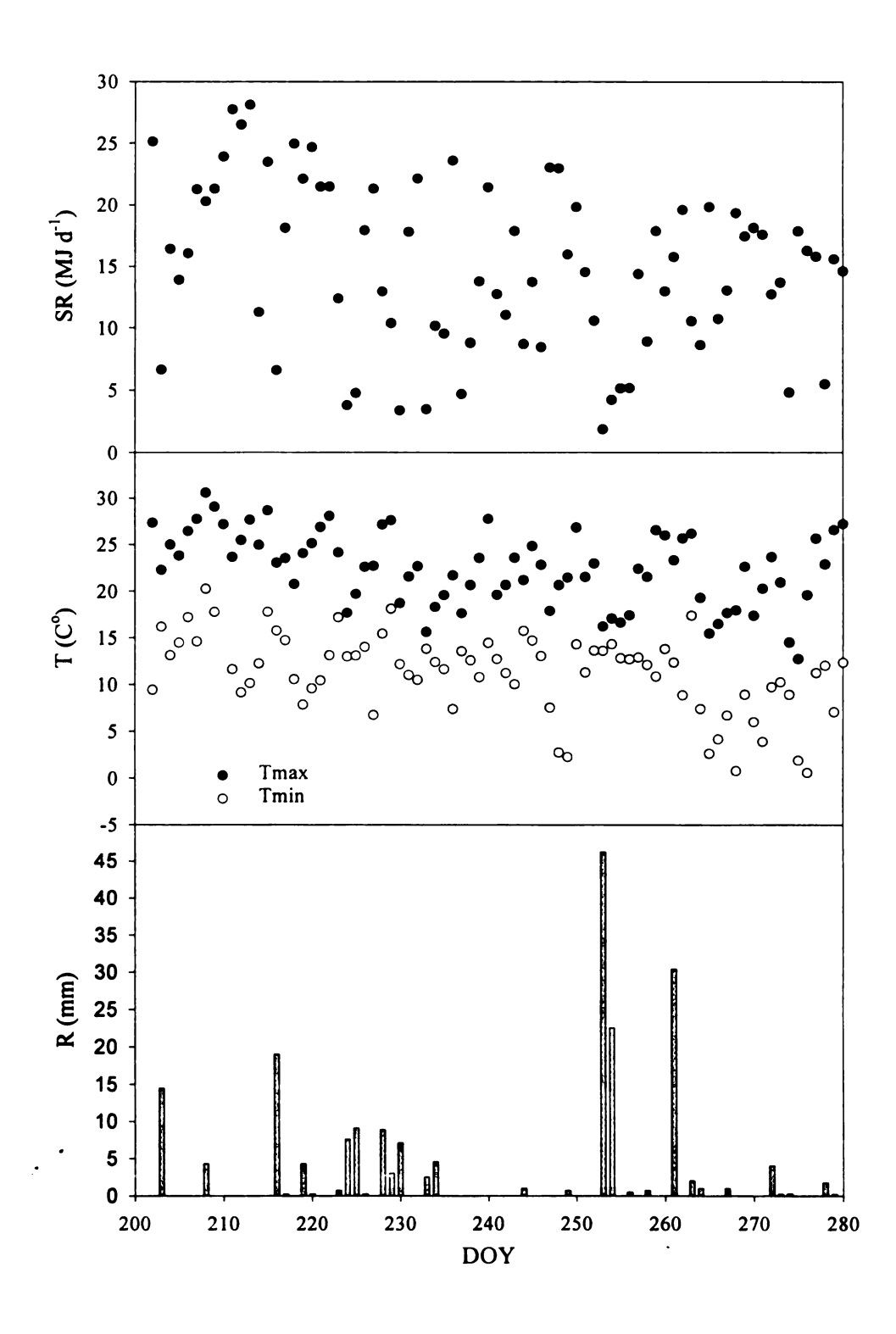


Figure 1.1. Daily solar radiation (SR), maximum (Tmax) and minimum (Tmin) temperatures, and rainfall (R) from DOY 200 to 280 in 1997.

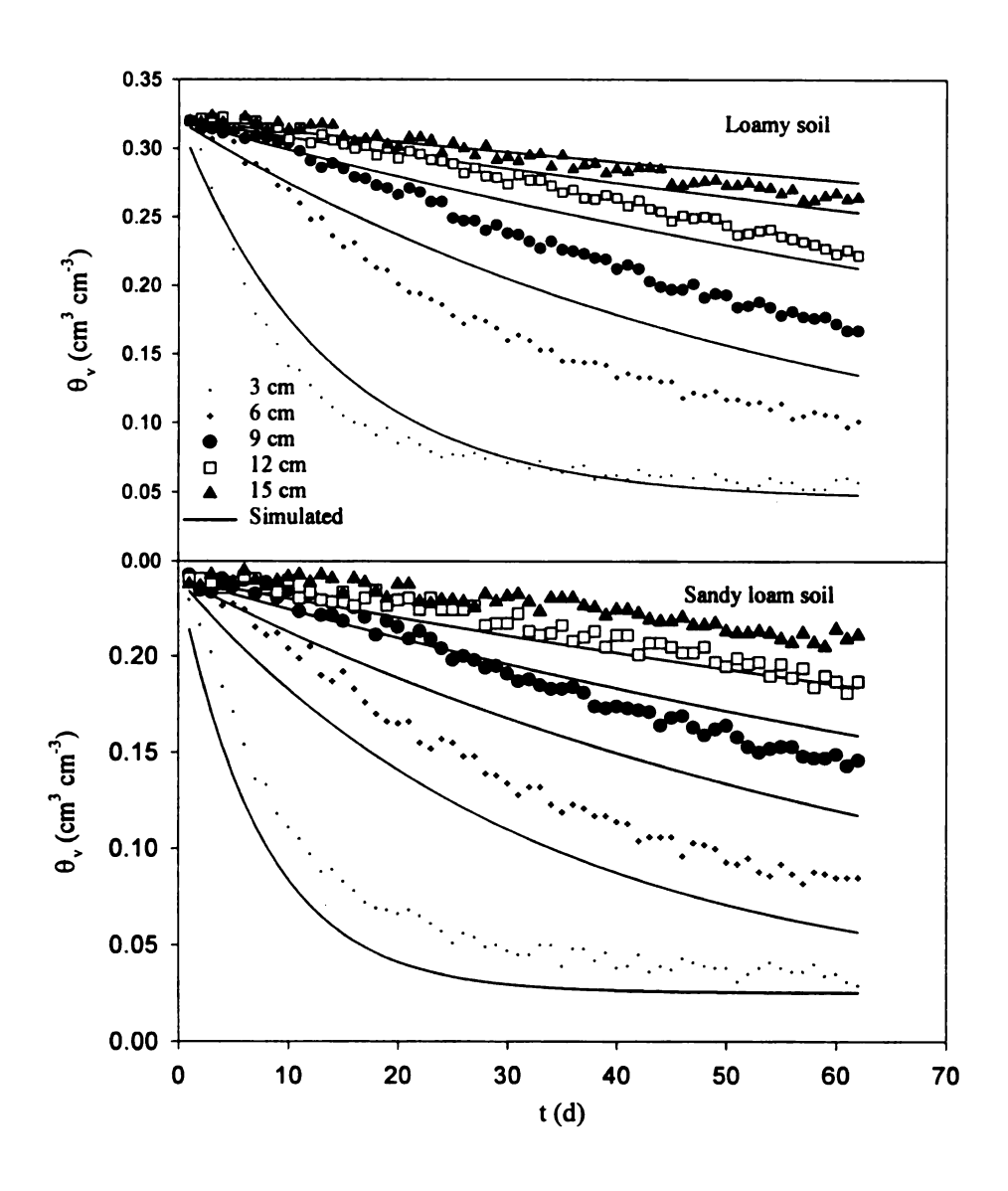


Figure 1.2. Measured and simulated soil water content profiles of 60-cm columns of loam and sandy loam soils drying during second stage evaporation.

Results and Discussion

Laboratory Results

Soil water content distribution under the second stage of evaporation was function of depth and time (Figure 1.2). The change of soil water content decreased with increasing depth and time (Figure 1.2). Soil water content went from θ_{dul} toward θ_{ad} . The volumetric drained upper limit soil water content was about 0.32 cm³ cm⁻³ for loamy soil and about 0.24 cm³ cm⁻³ for sandy loam soil. The volumetric air dry soil water content was about 0.05 cm³ cm⁻³ for loamy soil and about 0.03 cm³ cm⁻³ for sandy loam soil (Figure 1.2).

The simulated soil water contents, using the water balance of CERES, were higher than measured ones for loamy soil and lower than measured values for sandy loam soil at all depths (Figure 1.2). The simulated water contents had trend similar to the trend found in the measured soil water contents. The simulated water contents were function of time and depth and the change of simulated soil water contents decreased with increasing depth and time (Figure 1.2).

Using value of n constant equal to -1.94 instead of -2, produced simulated water content close to the measured soil water contents for loamy soil (Figure 1.3). Similarly, using value of n equal to -2.2 instead of -2, produced simulated water content close to the measured soil water contents for sandy loam soil (Figure 1.3). This suggested that n was soil specific, and was related to θ_{dul} , and α was related to θ_{dul} .

The relationship between θ_{dul} and α was investigated and demonstrated in Figure 1.4. As explained in the theory, α can be obtained by solving Eq. [5]. Numerical solutions were obtained for the loam and sandy loam soils, and the six different soils from D.A.

Figu loan

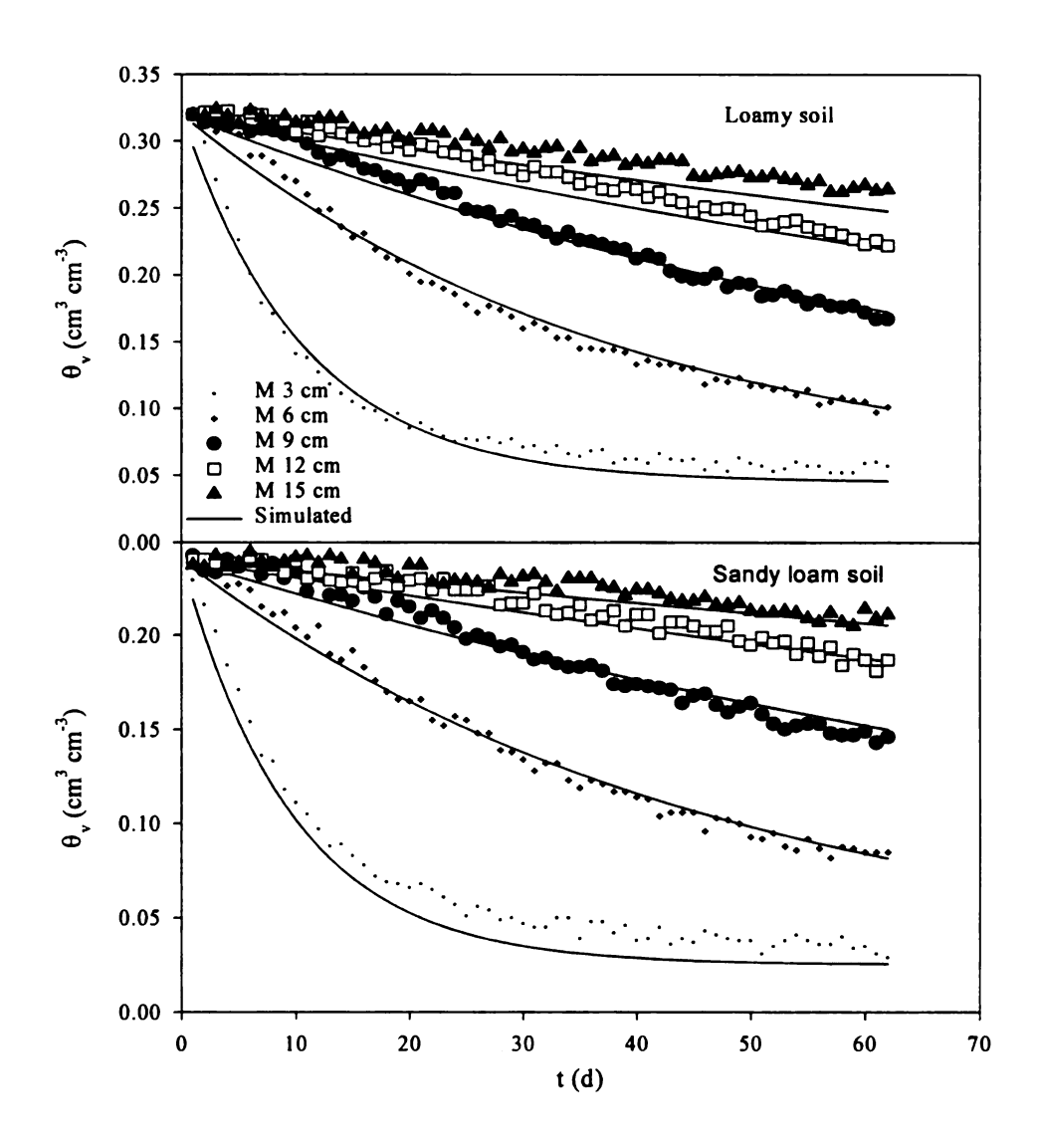


Figure 1.3. Measured and simulated soil water content profiles of 60-cm columns of loamy and sandy loam soils drying during second stage evaporation.

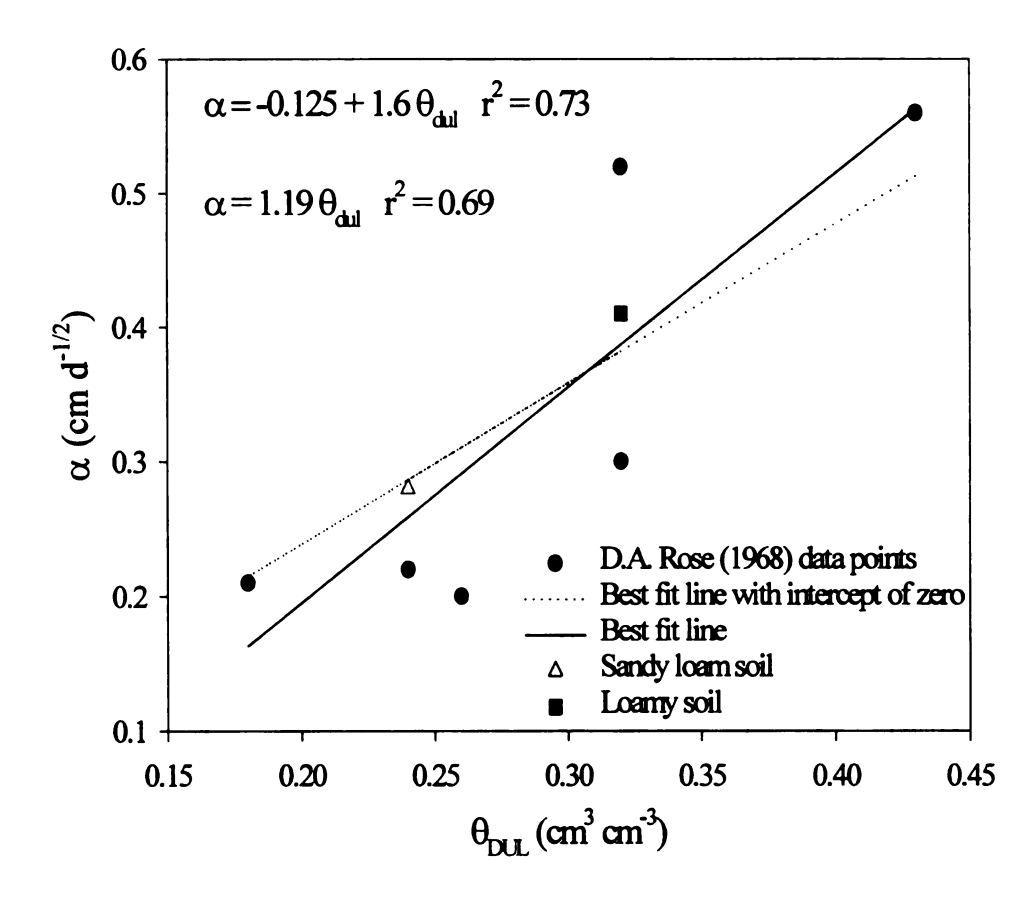


Figure 1.4. Relationship between α and θ_{dul} of 8 soils: Loamy and Sandy loam soils from Michigan and 6 soils from D.A. Rose (1968).

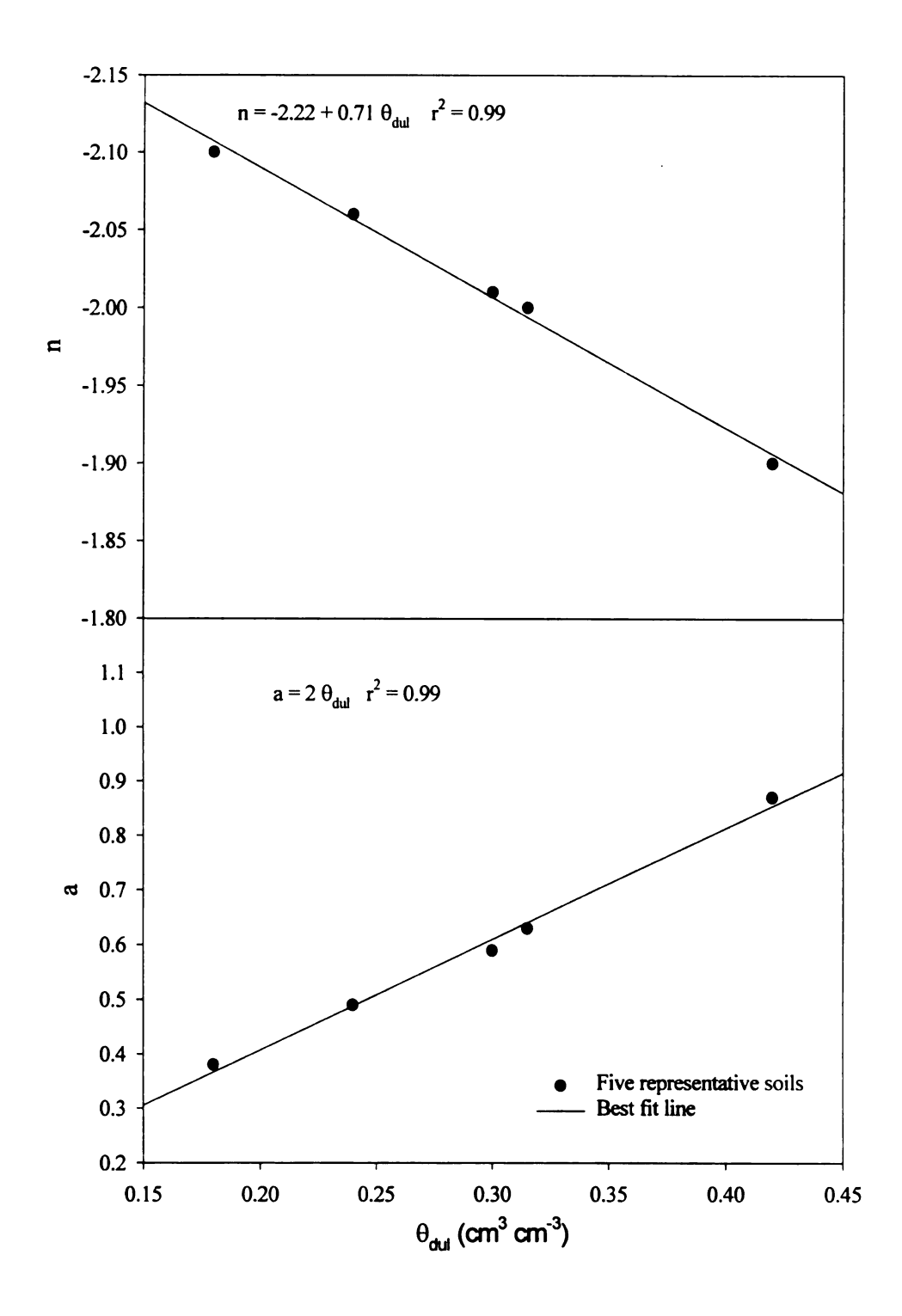


Figure 1.5. Relationships between drained upper limit soil water content (θ_{dul}) and constants n and a.

Rose (1968). A linear relationship was found between α and θ_{dul} with r^2 =0.73 for the best fit line and 0.69 for best fit line with zero intercept (Figure 1.4). Because no soil would have negative α , best fit line with zero intercept is more realistic. By definition, α is proportional to E_c and equal to E_c at the end of first day of evaporation under second stage evaporation. This led us to conclude that, E_c is site specific too.

The developed relationship with zero intercept between α and θ_{dul} was used to obtain simulated values to n corresponding to five different θ_{dul} . Trial and error was used to produce n values. A value of n was accepted if the simulated E_c was equal to E_c that was calculated from the developed relationship between α and θ_{dul} . A linear relationship was found between n and θ_{dul} with r^2 =0.99 (Figure 1.5). The developed relationship between n and θ_{dul} can be used to improve the simulated E_c .

It was noticed that any alteration of n should be accompanied with change of a to preserve the diffusivity theory and keep a linear relationship between E_c and $t^{1/2}$. It was found, that a linear relationship existed between a and θ_{dul} with r^2 =0.99 as shown in (Figure 1.5). When n was equal to -2, a was equal to 0.63 at θ_{dul} of 0.305 cm³ cm⁻³ (Figure 1.5). The value of a was inversely related to n (Figure 1.5). The relationships of n with θ_{dul} and a with θ_{dul} were evaluated and validated for values of θ_{dul} ranged from 0.15 to 0.45 cm³ cm⁻³.

Loamy soil evaporated more water than sandy loam soil (Figure 1.6). At day 1, measured E_c in Figure 6 was too low because the change of soil water content below 2 cm was not included in computing E_c since the closest TDR probe to surface was at 3 cm. The relationship between E_c and $t^{1/2}$ was linear (Figure 1.6). The simulated E_c that was obtained by using modified values for n and a was accurate (Figure 1.6).

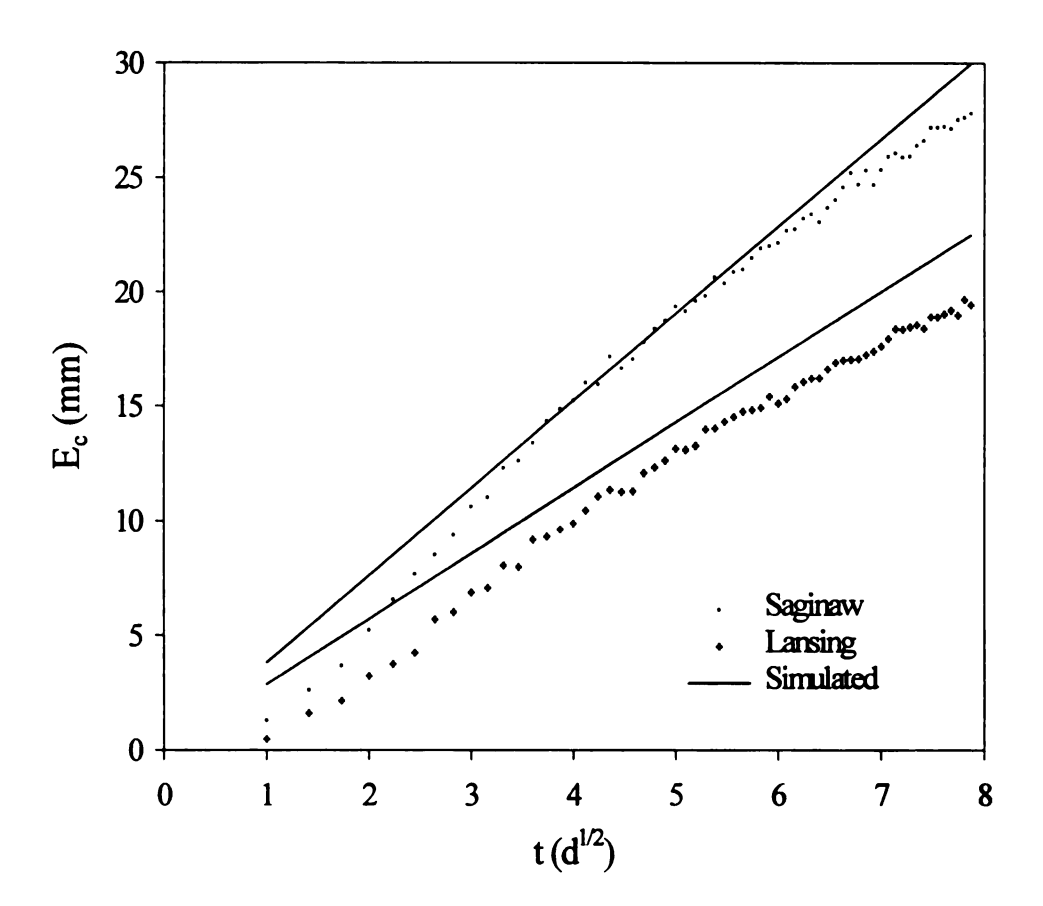


Figure 1.6. Measured and simulated cumulative evaporation (E_c) of loam and sandy loam soil during second stage evaporation.

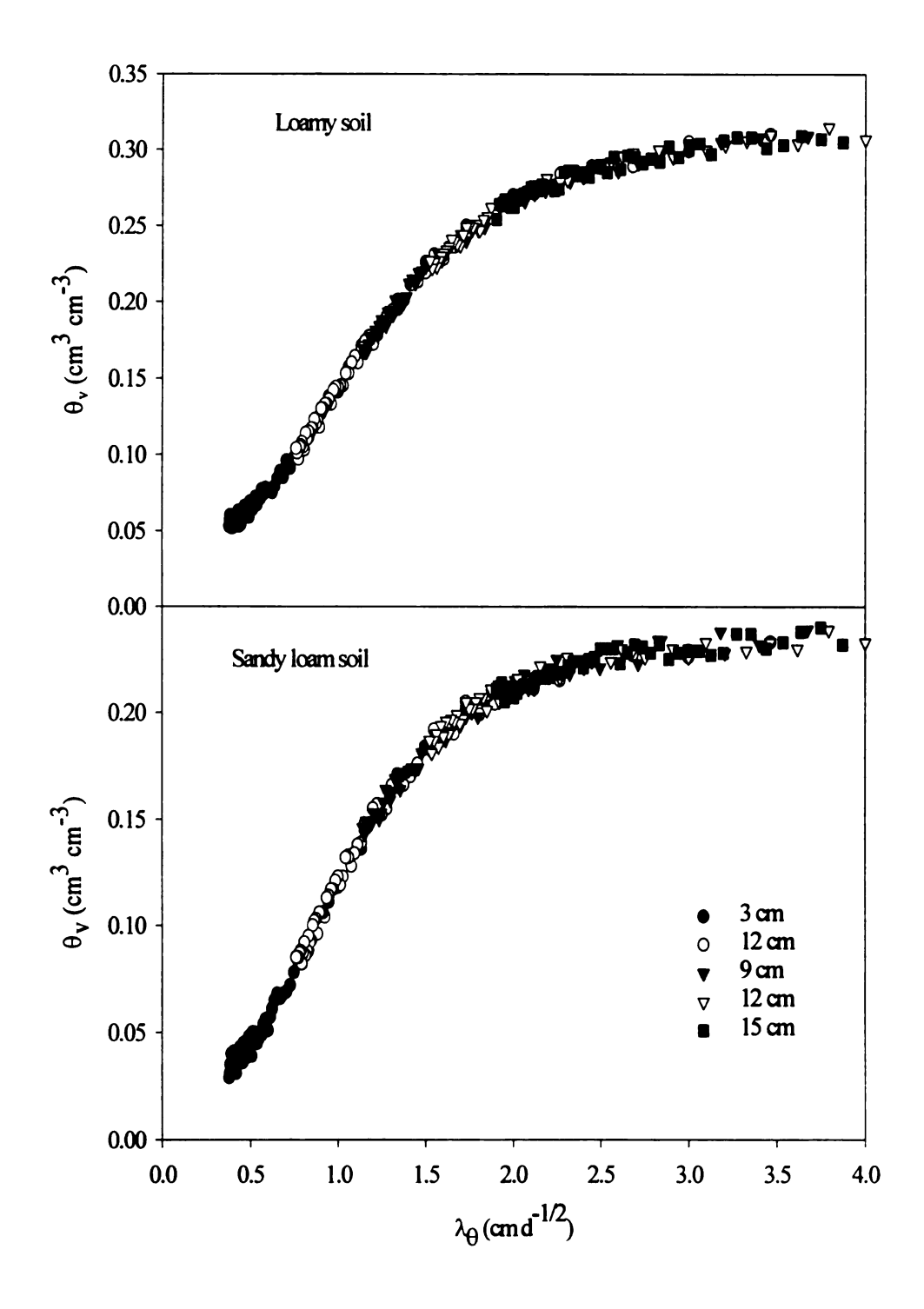


Figure 1.7. Soil water content profiles of 60-cm columns of loamy and sandy loam soils versus Boltzmann transform under second stage evaporation.

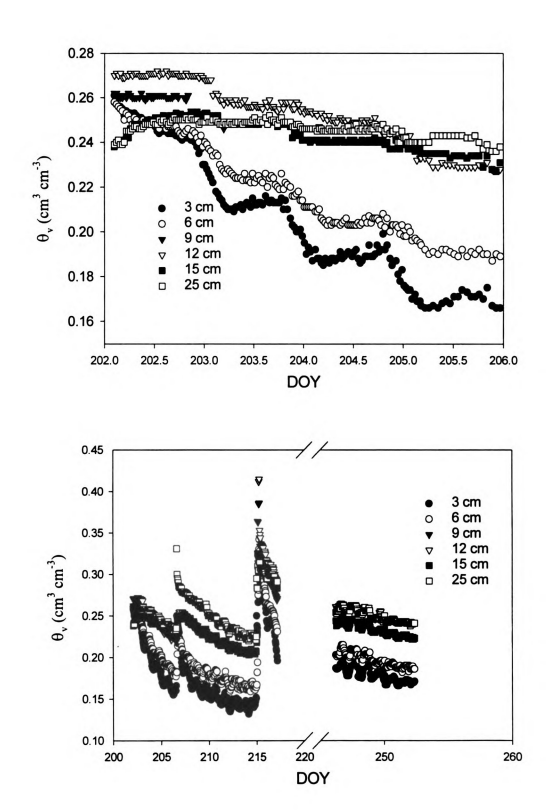


Figure 1.8. Soil water content profiles at six depths of sandy loam soil profile in 1997.

Volumetric water contents at 3, 6, 9, 12, and 15 cm depths had the same relationship with λ_{θ} for loam and sandy loam soils for about 62 days (Figure 1.7). This is a proof that diffusivity theory is valid for heterogenous but uniform and isotropic soil drying under second stage evaporation and this is in agreement with D.A. Rose (1968). Soil physical characteristic play an important role in defining the movement of soil water. Significant change of soil water content started at about 2.5 cm d^{-1/2} for loamy soil and at about 2 cm d^{-1/2} for sandy loam soil (Figure 1.7).

Field Results

Field data, in addition to the laboratory data, were used to evaluate the second stage evaporation module of water balance of CERES. Soil water content profiles were shown at six depths (Figure 1.8). A 4-day close-up, on which daily solar radiation was > 15 MJ d⁻¹, average temperature was about 20 C°, and rainfall was 0, was selected plotted in Figure 1.8 to show the fluctuation of soil water content between day and night. It was clear that soil water content at 3 cm depth and to less extend at 6 cm increased at night (Figure 1.8) as result of upward soil water flow at a time of zero evaporation. The driving force of such movement is the soil hydraulic gradient.

Simulated soil water contents in the field showed good agreement with the measurements (Figure 1.9). The root mean square error (RMSE, cm³ cm⁻³) was 0.013, 0.013, 0.005, 0.01, 0.011 at 3, 6, 9, 12 and 15 cm depths, respectively, using Eq. [8] with n = -2 and a=0.63. Whereas, RMSE (cm³ cm⁻³) was 0.014, 0.014, 0.005, 0.01, 0.012 at 3, 6, 9, 12 and 15 cm depths, respectively, using Eq. [8] with n=-2.09 and a=0.47. The RMSE values showed that the modification of n and a values had no improvement on the prediction of soil water content distribution under second stage evaporation. However,

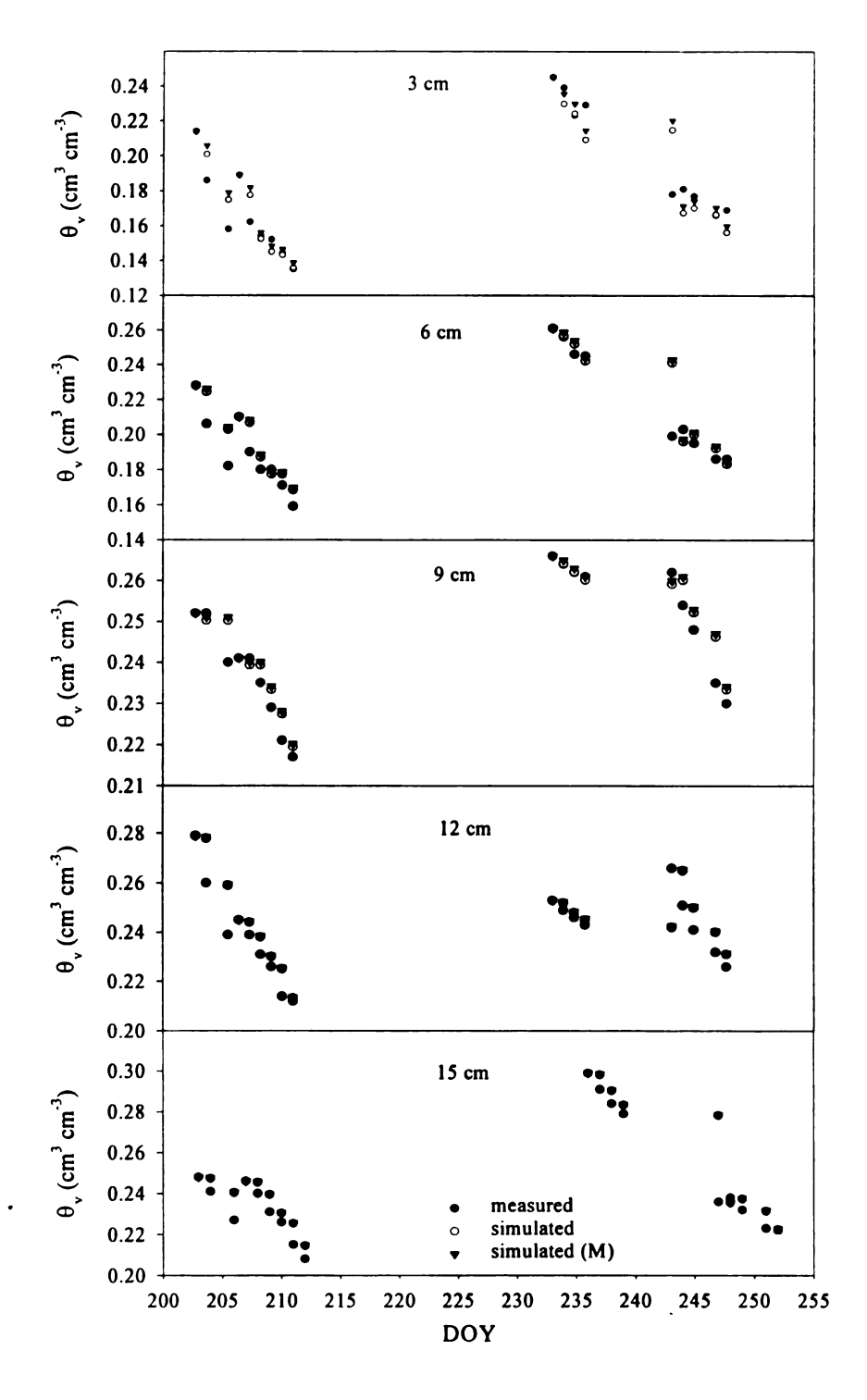


Figure 1.9. Measured, simulated (using Eq. [8] with n=-2 and a=0.63), simulated (M) (using Eq. [8] with n=2.09 and a=0.47) soil water content of a bare soil in Lansing field in 1997 at six different depths.

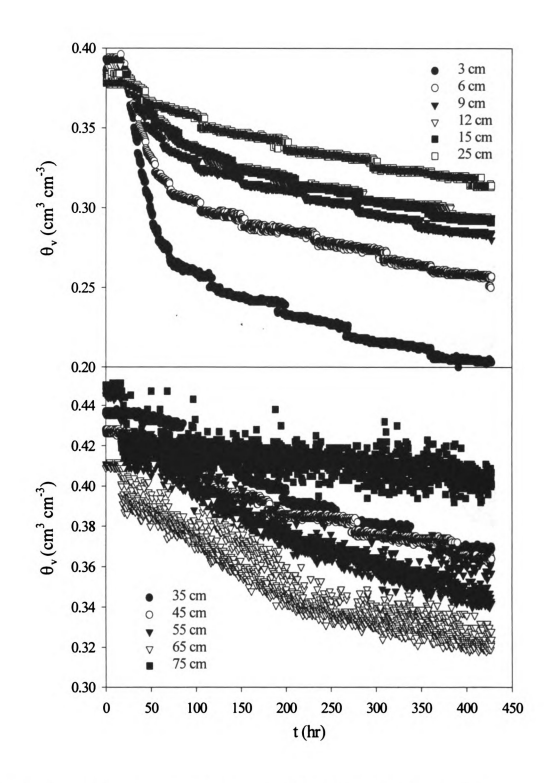


Figure 1.10. Soil water content profiles of 150-cm columns of loamy soil drying during second stage evaporation.

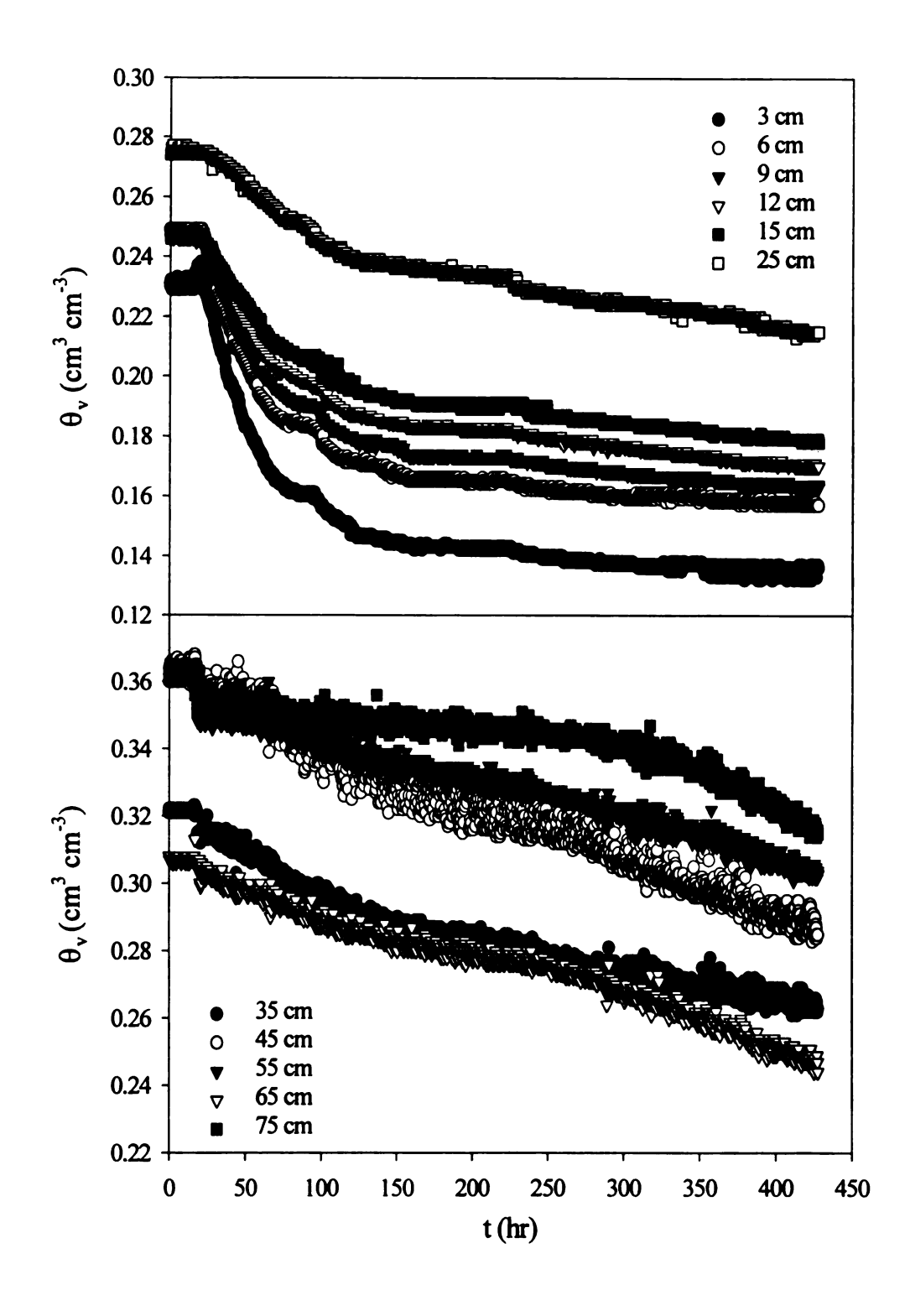


Figure 1.11. Soil water content profiles of 150-cm columns of sandy loam soil drying during second stage evaporation.

the modified version of second stage evaporation model can be used since it was produced under ideal second stage evaporation initial and boundary conditions.

Effect of Water Table

If one or more of the boundary conditions of second stage evaporation was violated, the above relationships may not be applicable. For instance, having a shallow water table may violate the boundary condition of semi-infinite soils. Because a shallow water table is evident in many agricultural fields, in this research the impact of a shallow water table on the diffusivity theory under second stage evaporation was investigated.

Figure 1.10 and Figure 1.11 show volumetric soil water content at 11 depths under evaporation for loam and sandy loam soils. The soil initial soil water content was not uniform but rather increased from θ_{dul} at 3 cm to about saturation at 75 cm for loamy soil (Figure 1.10) and increased from θ_{dul} at 3 cm to about saturation at 45 cm for sandy loam soil (Figure 1.11). Soil water content under evaporation was function of depth and time and the change of soil water content decreased with depth and time (Figure 1.10 and 1.11).

To test the validity of diffusivity theory under such conditions, volumetric soil water content was plotted against λ_{θ} as shown in (Figure 1.12). It was found that soil water content at any depth for loam and sandy loam soils was going from its initial value toward a certain soil water content higher than θ_{ad} . That soil water content was about 0.19 cm³ cm⁻³ for loamy soil and about 0.12 cm³ cm⁻³ for sandy loam soil. Soil water content had different relationship with λ_{θ} at each depth when $\lambda_{\theta} \geq 2$ cm $d^{-1/2}$ (Figure 1.12) since initial soil water was different at different depths(Figures 1.10 and 1.11). It was

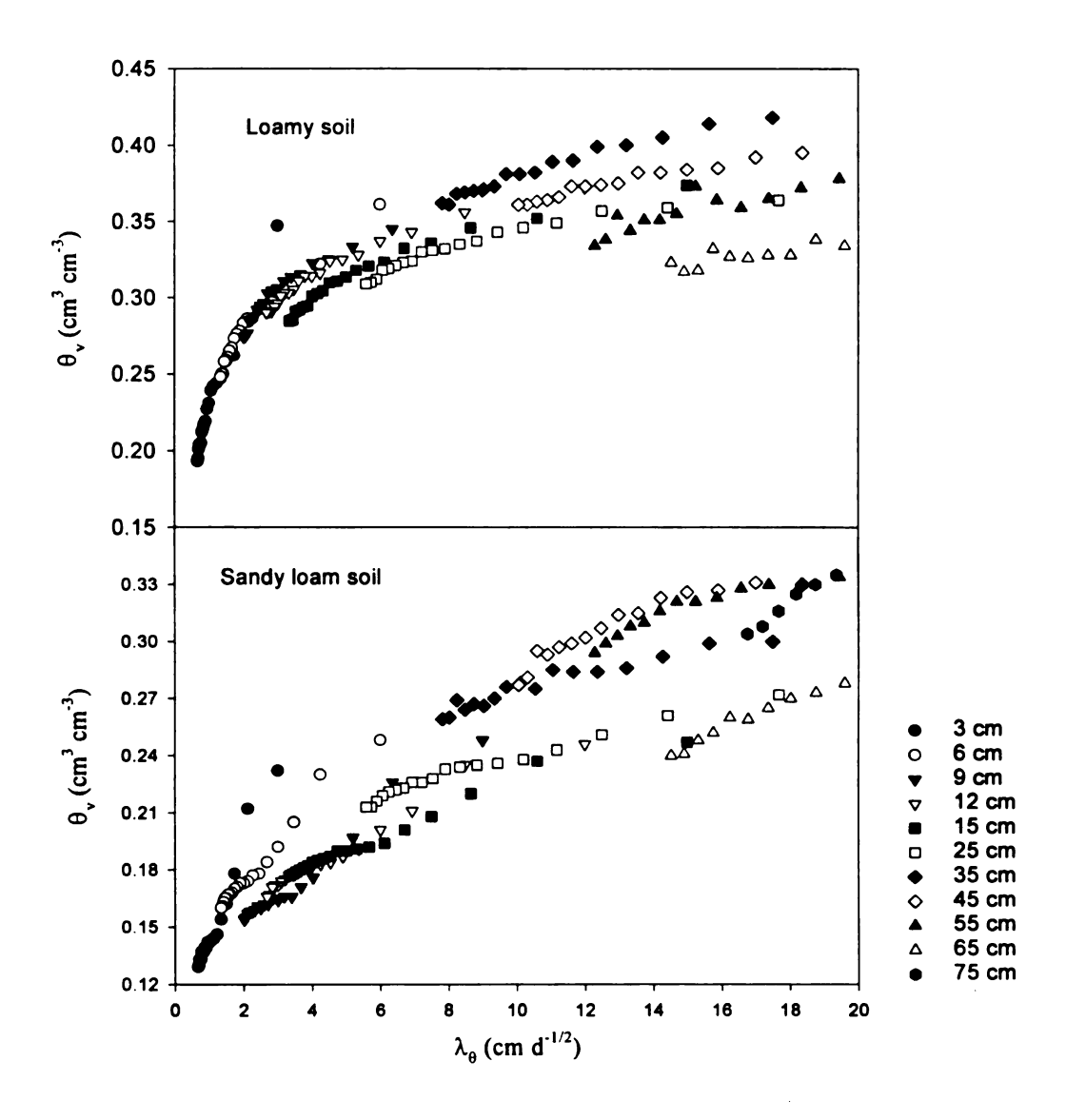


Figure 1.12. Soil water content profiles of 150-cm columns of loamy and sandy loam soils versus Boltzmann transform during second stage evaporation.

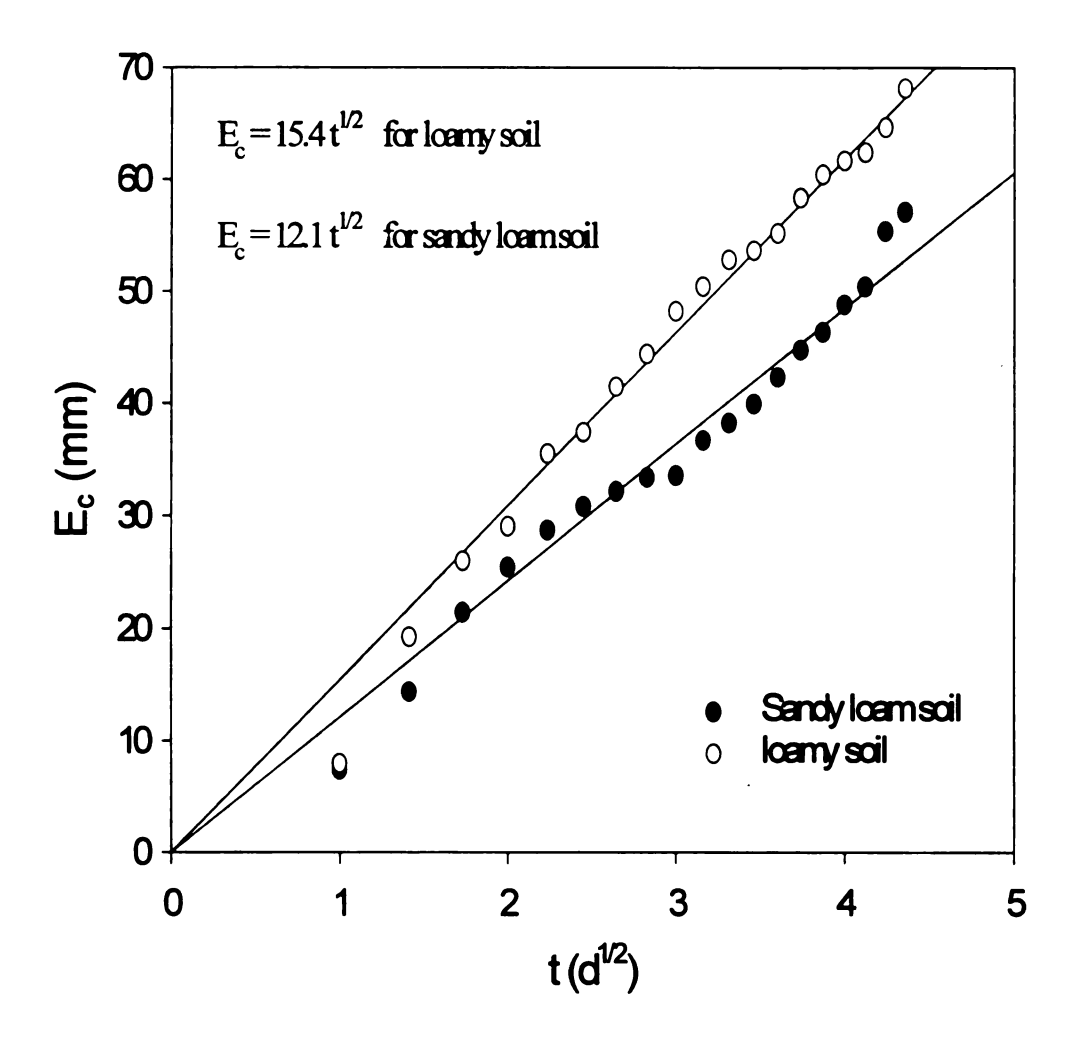


Figure 1.13. Cumulative evaporation of 150-cm column of loamy and sandy loam soils during second stage evaporation.

concluded, that Boltzmann transform cannot be used since there was no single-valued function between soil water content and λ_{θ} .

A linear relationship was found between E_c and $t^{1/2}$ for loam and sandy loam soils (Figure 1.13). This suggested that soil evaporation was limited by soil water content and soil characteristics. Evaporation from loamy soil was higher than that from sandy loam soil (Figure 1.13). The slope of the best fit line was 15.4 mm $d^{-1/2}$ for loamy soil and 12.1 mm $d^{-1/2}$ for sandy loam soil (Figure 13). The slope of the best fit line should be close to α . Hence, α for soils affected by shallow soil water table was about 4 time greater than α for semi-infinite soils under second stage evaporation. This led us to conclude, that the relationships that developed for semi-infinite soils were not applicable for soils affected by shallow water table.

Conclusions

The second stage evaporation model in the water balance of CERES was evaluated. The two constants (n and a) that used in the model were found to be soil specific since α was soil specific. However, they did not vary much and were highly correlated to θ_{dul} . New linear relationships between α , n, and a with θ_{dul} were developed. These relationships enabled the second stage evaporation model in the water balance of CERES to better simulate soil water distribution and soil water evaporation for diverse soils.

It was found that the impact of water table on second stage evaporation could not be captured by second stage evaporation theory because soil water contents at different depths had different relationships with Boltzmann transform. Further studies should be conducted on modeling evaporation from soils that have shallow water table.

Refer Black

Evet

Fara

Fed

Gab

Gar

Har

Hil

Las

Mc

Nor

Phil

Ritch

Ritchi

References

- Black, T.A., W.R. Gardner, and G.W. Thurtell. 1969. The prediction of evaporation, drainage, and soil water storage for a bare soil. Soil Sci. Soc. Am. J. 33:655-660.
- Evett, S.R, and R.J. Lascano. 1993. ENWATBAL.BAS: a mechanistic evapotranspiration model written in compiled basic. Agron. J. 85(3):763-772.
- Farahani, H.J., and L.R. Ahuja. 1996. Evapotranspiration modeling of partial canopy/residue covered fields. Trans. ASAE. Vol. 39(6):2051-2064.
- Feddes, R.A., P.J. Kowalik, and H. Zaradny. 1978. Simulation of field water use and crop yield. PUDOC, Wageningen, Netherlands.
- Gabrielle, B., S. Menasseri, and S. Houot. 1995. Analysis and field evaluation of the CERES models water balance component. Soil Sci. Soc. Am. J. 59:1403-1412.
- Gardner, H.R., and W.R. Gardner. 1969. Relation of water application to evaporation and storage of soil water. Soil Sci. Soc. Am. Proc. 33:192-196.
- Hanks, R.J. 1991. Soil evaporation and transpiration. ASA-CSSA-SSSA, 677 S. Regoe Rd., Madison, WI 53711, USA. Modeling plant and soil systems-Agronomy Monograph no. 31.
- Hillel, D., and H. Talpaz. 1977. Simulation of soil water dynamics in layered soils. Soil Sci. 123:54-62.
- Lascano, R.J., and J.L. Hatfield. 1992. Spatial variability of evaporation along two transects of a bare soil. Soil Sci. Soc. Am. J. 56:341-346.
- Mcllroy, I.C. 1984. Terminology and concepts in natural evaporation. Elsevier Science Publishers B.V., Amsterdam, Agricultural Water Management, 8:77-98.
- Norman, J.M., and G.C. Campbell. 1983. Application of a plant-environment model to problems in irrigation. p. 155-188. *In* D. Hillel (ed.) Advances in irrigation. Vol. 2. Academic Press, New York.
- Philip, J.R. 1957. Numerical solution of equations of the diffusion type with diffusivity concentration-dependent. II. Aust. J. Phys., 10:29-42.
- Ritchie, J.T. 1972. Model for predicting evaporation from a row crop with incomplete cover. Water Resour. Res. 8:1204-1213.
- Ritchie, J.T., and B.S. Johnson. 1990. Soil and plant factors affecting evaporation. ASA-CSSA-SSSA, 677 South Segoe, Madison, WI 53711, USA. Irrigation of Agricultural Crops-Agronomy Monograph no. 30:363-390.

- Rose, C. W. 1968. Evaporation from bare soil under high radiation conditions. Trans. Int. Congr. Soil Sci. 9th, Adelaide. I:57-66.
- Rose, D.A. 1968. Water movement in porous materials III. Evaporation of water from soil. Brit. J. Phys., Ser 2, Vol. 1:1779-1791.
- Van Bavel, C.H.M., and D. Hillel. 1976. Calculating potential and actual evaporation from a bare soil surface by simulation of concurrent flow of water and heat. Agric. Meteorol. 17:453-476.

CHAPTER TWO

ASSESSING AND MODELING VERTICAL SOIL WATER DRAINAGE

Introduction

According to Corwin et al. (1991), groundwater is a major source of drinking, industrial, and agricultural water. Groundwater supplies will become even more important resource as world demands for water grow. Acute and chronic health affects resulting from contaminants in drinking water has brought the degradation of ground water to public attention. Groundwater quality is a concern for health reasons, and because of the decrease in crop productivity, which can often accompanied by the use of poor quality irrigation water. Suitable mathematical models and appropriate values for downward soil water flow are needed to assess the impact of surface-applied agrochemicals on the subsurface environment (Vanderborght et al., 1997) and groundwater (Corwin et al., 1991).

The ability of a soil to drain water could be critical for crop yield. Fast drainage would be desirable to avoid long-term saturation conditions. On the other hand, water can be taken by plants while drainage out of the root zone is occurring. Many productive agricultural soils drain slowly, providing a potentially significant quantity of water for plant use before gravity induced drainage stops (Ritchie, 1998). So accurate modeling of soil water drainage is needed for prediction of crop yield as well as for water use efficiency.

Preferential flow paths are formed in soils by biological, chemical and physical

processes and their interactions. Their influence is usually reflected in reduced travel time through the soil, increased solute concentrations in drainage water, or deeper penetration of chemicals into the soil profile, than predicted by conventional flow theory. Preferential flow maybe considered the main contributor to solute transport (Montas et al., 1997). Corwin et al. (1991) developed a functional model to account for the bypass flow. Such model is beyond our scope in this work since total daily drainage is the main concern of this study and preferential flow makes more difference when the time step is minutes or hours.

It was found that the drainage model in CERES has to be calibrated in order to give good estimates of soil water drainage (Gabrielle et al., 1995; Gerakis and Ritchie, 1998). Although a procedure was introduced to determine the drainage coefficient (the fraction of drainable soil water that can be drained in a day) that is used in CERES drainage model based on soil porosity (Ritchie et al., 1986), Gerakis and Ritchie (1998) and Ritchie (1998) suggested that the drainage coefficient can be assumed constant for different soils in the drainage model.

A theoretical basis for the drainage coefficient was lacking in the literature. An effort has been made to fill that gap by introducing a theoretical basis for the drainage coefficient. A theory was introduced on the basis of Darcy's Law, the assumption of a unit gradient for a drainage cycle, and the validity of Brooks and Corey (1964) equation for unsaturated hydraulic conductivity estimation. Two new methods were developed to estimate the drainage coefficient from drained upper limit and saturated water content. The link between the drainage coefficient and soil physical properties enables the drainage model to take into account the spatial variability of the drainage coefficient.

The objective of this study was to link the downward soil water flow dynamics and drainage model in the water balance of the CERES family models to the vertical drainage theory and establish a relationship between the drainage coefficient and drained upper limit soil water content. Ritchie et al. (1999) demonstrated that drained upper limit soil water content can be estimated reasonably well from texture and bulk density.

Theory

Darcy's equation works well in describing soil water flow during drainage for homogenous soils with uniform initial soil water content (Youngs, 1957a,b). It can be written as follows (Philip, 1957):

$$q = K(\theta) \left(\frac{\partial h}{\partial z} \right) \tag{1}$$

where q is the soil water flux (cm d⁻¹), $K(\theta)$ is soil water hydraulic conductivity (cm d⁻¹), θ is soil water content, and $\partial h/\partial z$ is the hydraulic gradient. The hydraulic gradient maybe assumed 1 for saturated soil water flow or for soil water flow in drainage cycle. Based on such assumption, the soil water flow can be described as follows (Black et al., 1969; Gabrielle et al., 1995):

$$q = K(\theta)$$

(2)

When a layer of soil of 1 cm thickness, initially at a uniform water content θ_s , has its surface covered, the initial and boundary conditions governing flow rate are

$$\begin{aligned} E_s &= 0 & t \geq 0 \\ \theta &= \theta_s & z \geq 0 & t = 0 \\ \theta_s &> \theta > \theta_{dul} & z \geq 0 & t > 0 \end{aligned}$$

where z is depth, t is time, and E_s is soil evaporation.

The change of soil water content in 1 day $(d\theta)$ under the above initial and boundary conditions can be described as:

$$d\theta \frac{dz}{dt} = C_1 \left(\theta_s - \theta_{dul}\right) \frac{dz}{dt} \tag{3}$$

where C_1 is the fraction of drainable soil water that can be drained from the soil layer in the first day (d^{-1}).

By combining Eq. [2] and Eq. [3] C_1 can be described as follows:

$$C_1 = \frac{K_1(\theta)}{\left(\theta_s - \theta_{dul}\right)} \tag{4}$$

where $K_1(\theta)$ is the 1st day hydraulic conductivity. A harmonic mean can be used to estimate $K_1(\theta)$ as follows:

$$K_1(\theta) = \frac{2K(\theta_1)K_s}{K(\theta_1) + K_s} \tag{5}$$

where θ_1 is soil water content after 1 day of drainage and K_s is saturated hydraulic conductivity.

The unsaturated hydraulic conductivity at any θ can be estimated using the

following equation (Brooks and Corey, 1964; Brutsaert, 1967; Corey, 1977; Corey et al., 1965; Mualem, 1976; Mualem, 1978; Schuh and Cline, 1990):

$$K(\theta) = K_s \left(\frac{\theta - \theta_r}{\theta_s - \theta_r}\right)^n \tag{6}$$

where θ_r is residual soil water content and can be assumed equal to θ_{dul} in drainage cycle (Suleiman and Ritchie, 1999; Ahuja et al., 1984; Ahuja et al., 1993), and n is a constant that depends on the soil pores distribution (Corey et al., 1965) and the amount of work per unit volume of soil required to drain a saturated soil to the wilting point (Mualem, 1978) (the lower limit for drainage cycle is drained upper limit and not the wilting point, and the energy needed to drain saturated soil to the wilting point is substantially greater than to drain saturated soil to drained upper limit soil water content). According to Suleiman and Ritchie (1999), K_s can be estimated as follows:

$$K_s = 37 \left(\frac{\theta_s - \theta_{dul}}{\theta_{dul}} \right)^2 \tag{7}$$

By combining Eq. [4], Eq. [5], Eq. [6], and Eq. [7], C₁ can be calculated as follows:

$$C_{1} = \alpha \frac{\left(1 - C_{1}\right)^{n}}{1 + \left(1 - C_{1}\right)^{n}} \tag{8}$$

where α can be written as:

$$\alpha = 74 \left(\frac{\theta_s - \theta_{dul}}{\theta_{dul}^2} \right) \tag{9}$$

Using the same procedure, C_2 (the fraction of drainable soil water that can be drained from the soil layer in the second day) can be calculated as follows:

$$C_{2} = \alpha \frac{\left(1 - C_{1}\right)^{n-1} \left(1 - C_{1} - C_{2}\left(1 - C_{1}\right)\right)^{n}}{\left(1 - C_{1}\right)^{n} + \left(1 - C_{1} - C_{2}\left(1 - C_{1}\right)\right)^{n}}$$
(10)

Estimating n from other soil properties would be helpful since it is impossible to determine its value or even its range from purely theoretical basis (Mualem, 1978). Schuh and Cline (1990) showed that n can be estimated from percent of sand (ps) as follows:

$$n = 47.61 \exp\left(-0.026 ps\right)$$

(11)

Eq. [11] gives high values of n and such high values of n is only found when measurements are taken at low saturation with a capillary tension of several atmosphere (Mualem, 1978). What is relevant for drainage cycle of n values are those measured when soil matric potential is between 0 and -50 kPa since that would cover any drainage cycle. It was noticed that n values that are measured at low saturation with a capillary tension of several atmosphere is about 4 times greater than that for those measured at the drainage range on data published in Mualem (1978). Eq. [11] was used to estimate n for all the soils of Ratliff et al. (1983) data set and then the estimated n values were divided by 4 to

estimate n values relevant to a drainage cycle. Then, a linear relationship between n and θ_{dul} was developed as follows:

$$n = 3 + 20.2\theta_{dul} \tag{12}$$

The initial water content can vary in the field and it may never be equal to θ_s . It is clear from Eq. [8] and Eq. [10] that C (drainage coefficient) is dependent on initial soil water content. An average C for each soil can be introduced to be used at any initial soil water content. The C can be calculated from C_1 and C_2 in the condition that the soil water content at the end of day 2 is identical whether C_1 was used for day 1 drainage and C_2 for day 2 drainage or that C was used for day 1 and day 2. Assuming the initial soil water content, θ_s , soil water content after 2 d of drainage, θ_2 , and drained upper limit soil water content, θ_{dul} , C can be calculated as follows:

$$\theta_1 = \theta_s - C \times \left(\theta_s - \theta_{dul}\right) \tag{13}$$

where θ_1 is soil water content after 1 day of drainage.

$$\theta_2 = \theta_1 - C \times \left(\theta_1 - \theta_{dul}\right) \tag{14}$$

By substituting Eq. [13] in Eq. [14] θ_2 can be described using θ_s as follows:

$$\theta_2 = \theta_s - 2 \times C \times (\theta_s - \theta_{dul}) + C^2 \times (\theta_s - \theta_{dul})$$

(15)

C can be calculated using the quadratic formula as follows:

$$C = \frac{-\left(2 \times \left(\theta_{dul} - \theta_{s}\right)\right) - \sqrt{\left(2\left(\theta_{dul} - \theta_{s}\right)\right)^{2} - 4\left(\theta_{s} - \theta_{2}\right)\left(\theta_{s} - \theta_{dul}\right)}}{2\left(\theta_{s} - \theta_{dul}\right)}$$
(16)

Drainage Model in CERES Water Balance

According to Ritchie (1998), redistribution of water in the soil profile and drainage out of the root zone are calculated using a functional model developed from field drainage information. For soil water redistribution during infiltration water is moved downward from the top soil layer to lower layers in a cascading approach. Drainage from a layer takes place only when θ (soil water content) is between θ_{sat} (0.92 of saturated soil water content) and θ_{dul} (drained upper limit soil water content).

The change of volumetric soil water content in a day at any depth under drainage is calculated as follows:

$$\Delta \theta = C(\theta - \theta_{dul}) \tag{17}$$

where C is a constant equal to 0.55 (Ritchie, 1998).

Materials and Methods

Laboratory and field experiments were conducted to study the downward soil water flow and drainage during a drainage cycle. In addition to the laboratory and field experiments, data from Reichardt and Nielsen (1984) were used to evaluate the drainage coefficient in the drainage model in the water balance of CERES. Their data set include a dozen soils of diverse taxonomy, from Belgium, Brazil, Chile, Cyprus, Japan, Madagascar, Niger, Palestine, Senegal, Syria, and Thailand (Reichardt and Nielsen, 1984). Although complete drainage cycles were done on these soils, only saturated soil water content, initial soil water content, final soil water content (drained upper limit soil water content), and soil water content after 2 days of drainage were available. These soil

water contents were needed to estimate the drainage coefficient for each soil. Data from Ratliff et al. (1983) were used to produce a relationship between n (defined in the theory) and θ_{dul} . Sand content (ranges from 0.9 to 97.5 cm³ cm⁻³) and drained upper limit soil water content (ranges from 0.068 to 0.45 cm³ cm⁻³) were available for each of the 388 soils in Ratliff et al. (1983) data set. Drained upper limit, for these soils, was measured in the field after drainage a cycle.

Laboratory Experiments

Two different soils were used to study the soil water distribution under a drainage cycle. One of the soils was obtained from Saginaw area, Michigan and it was loamy soil (25.4 % clay and 43 % sand). The second one was obtained from Lansing area, Michigan and it was sandy loam soil (9.4 % clay and 65.4 % sand). The two soils were air dried, sieved through 2 mm screen, and then assembled into PVC columns with height of 150 cm and diameter of 30 cm. Twenty cm time domain reflectometry probes (TDR) were installed horizontally at depths of 3, 6, 9, 12, 15, 25, 35, 45, 55, 65, and 75 cm. The soils were saturated from the bottom using a constant head of 150 cm. The soils were allowed to drain for 10 days while the soil surface was covered to prevent evaporation from the soil surface. Soil water content was monitored at all depths every 20 minutes during the drainage cycle.

Field Experiment

Two sets of 20-cm TDR probes were installed horizontally at depths of 3, 6, 9, 12, 15, 25, 35, 45, 55, 65, and 75 cm from the surface in a bare soil in the Lansing area on July 10, 1997. The two sets were 3 m apart. The soil was saturated using ponding and

then the soil surface was covered for 15 days on August 15, 1997. The soil water content was monitored at all depths every 20 min during the drainage cycle.

Results and Discussion

Trial and error procedure was used to solve Eq. [8] and Eq. [10] in order to find C_1 and C_2 at representative combination of θ_s and θ_{dul} . These values of C_1 and C_2 were used then to solve for C using Eq. [13] through Eq. [16]. Linear Relationships between C_1 , C_2 , and C with $(\ln \alpha)^{1/n}$ were developed (Figure 2.1). These relationships (Eq. [18], Eq. [19], and Eq. [20]) can be used to estimate C_1 , C_2 , and C directly from θ_s and θ_{dul} instead of using trial and error to solve for them. All of C_1 , C_2 , and C are dependent on θ_s and to greater extent on θ_{dul} because α is function of both θ_s and θ_{dul} , whereas, n is function of θ_{dul} . The reason that C_2 is lower than C_1 is that average soil water hydraulic conductivity during the 2nd day of drainage is lower than that during the 1st day of drainage. The drainage coefficient, C is greater than arithmetic mean of C₁ and C₂ as can be seen in Figure 2.1. The ratio of C to C_1 was 68% for soils with θ_{dul} equal to 0.07 cm³ cm⁻³, and 0.83 for soils with θ_{dul} equal to 0.42 cm³ cm⁻³. An average ratio of C to C_1 was about 0.75. The root mean square error (RMSE) of the estimation of C using Eq. [20] was 0.144 while it was 0.253 assuming a constant value of 0.55 (Ritchie, 1998) for the international soils (Figure 2.2). The international C values showed clear dependence on the independent variable, $(\ln \alpha)^{1/n}$, (Figure 2.2). Some of the error was due error measurement and some resulted from using Eq. [12] to estimate n because Eq. [12] estimates an average value of n at each θ_{dul} . Overall, Eq. [20] is a better estimate of C instead of using a constant of 0.55 for different soils.

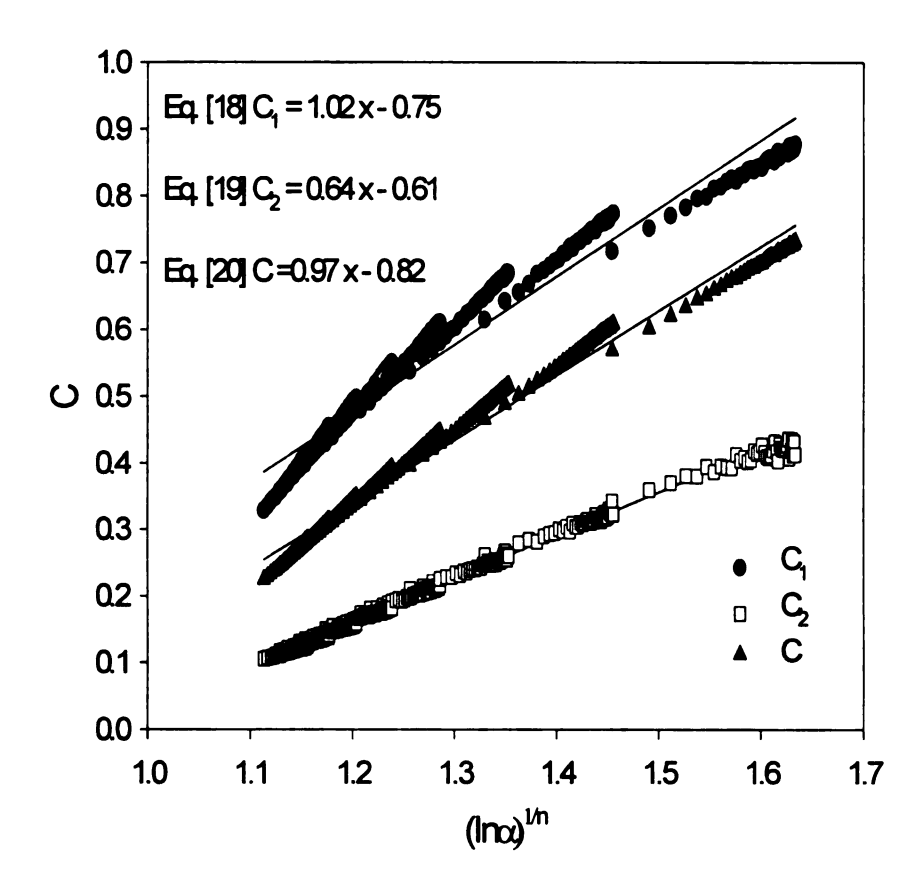


Figure 2.1. Relationships between C_1 , C_2 , and C with $(ln\alpha)^{1/n}$ for any realistic possible combination of θ_s and θ_{dul} .

It is possible to approximate C from θ_{dul} only since C is highly dependent on θ_{dul} (Figure 2.3). A quadratic polynomial relationship was developed to estimate C from θ_{dul} (Figure 2.3). The deviation of points from Eq. [21] line is due to the difference between θ_s and θ_{dul} . The deviation from Eq. [21] line is greater at lower θ_{dul} and minimum at high θ_{dul} . However, maximum deviation from the line is about 10% at any θ_{dul} . The advantage of using Eq. [21] over Eq. [20] in modeling soil water drainage is that the independent variable in Eq. [21] (θ_{dul}) is available while the independent variable in Eq. [20] (Ln α)^{1/n} is to be calculated from θ_s and θ_{dul} .

The RMSE of the estimation of C using Eq. [21] for the international soils was 0.136 (Figure 2.4). The 0.55 line overestimated all the points of soils that have θ_{dul} of 0.22 cm³ cm⁻³ or greater. For instance a heavy soil with θ_{dul} of 0.4 would drain on average 20-25% of its drainable water not 55% in a day (Figure 2.4). On the other hand, a light soil with θ_{dul} of 0.05 would drain on average 70-75% of its drainable water not 55% in a day (Figure 2.4). Although Eq. [21] it was developed to simplify the estimation of C, Eq. [21] outperformed Eq. [20] in the case of international data soils. This led us to conclude that Eq. [21] can also be used to estimate C for different soils in the water balance of CERES instead of assuming constant value of C of 0.55. To account for the impact of incoming water flow (Q_i) on the change of soil water content of a certain layer during drainage, a generic relationship between C and Q_i can be introduced as follow:

$$C = a + b \ln(Q_i + \phi_e) \tag{22}$$

where ϕ_{ϵ} (cm³ cm⁻³) is soil effective porosity and equal to θ_{s} - θ_{dul} . Having in mind that (1) when $Q_{i} = 0$, C has to be equal to the original C and (2) when $Q_{i} = K_{s}$, C is 0, a and b

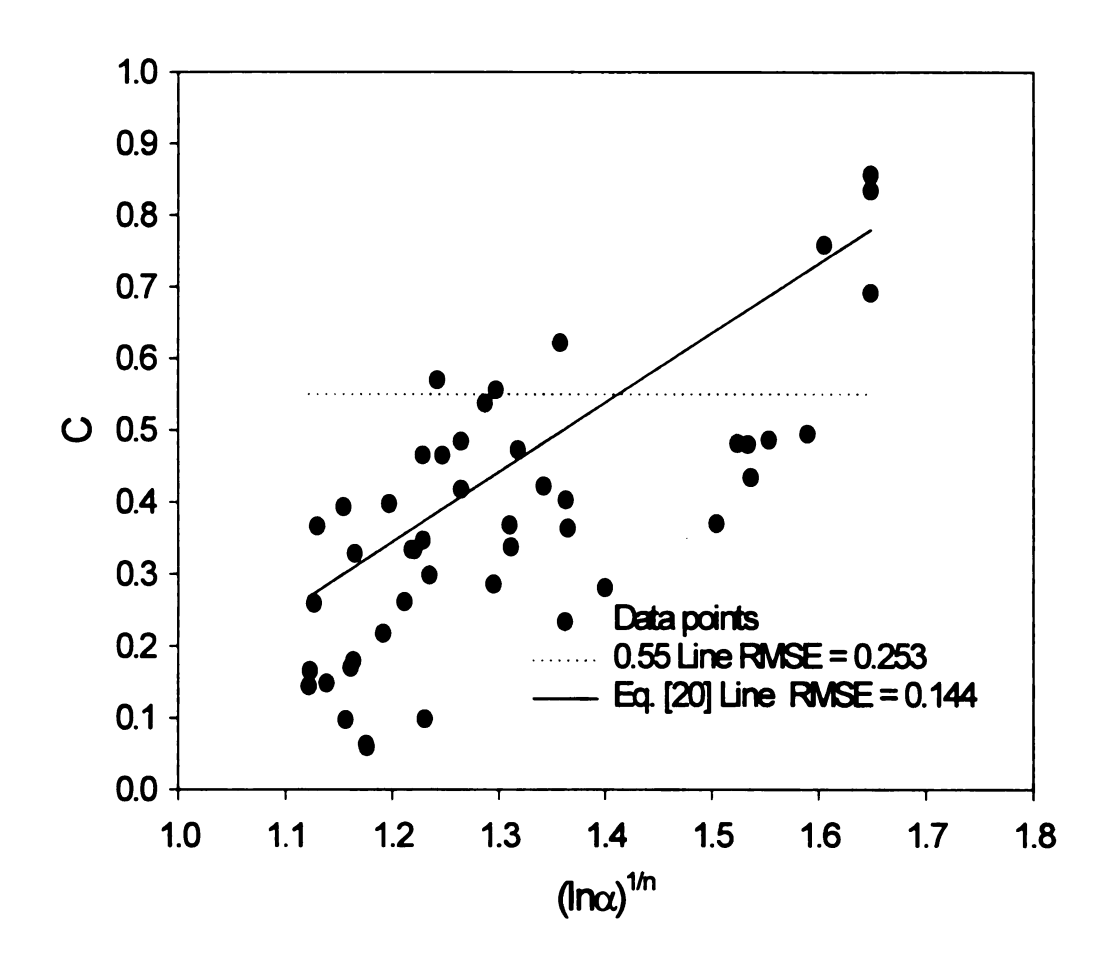
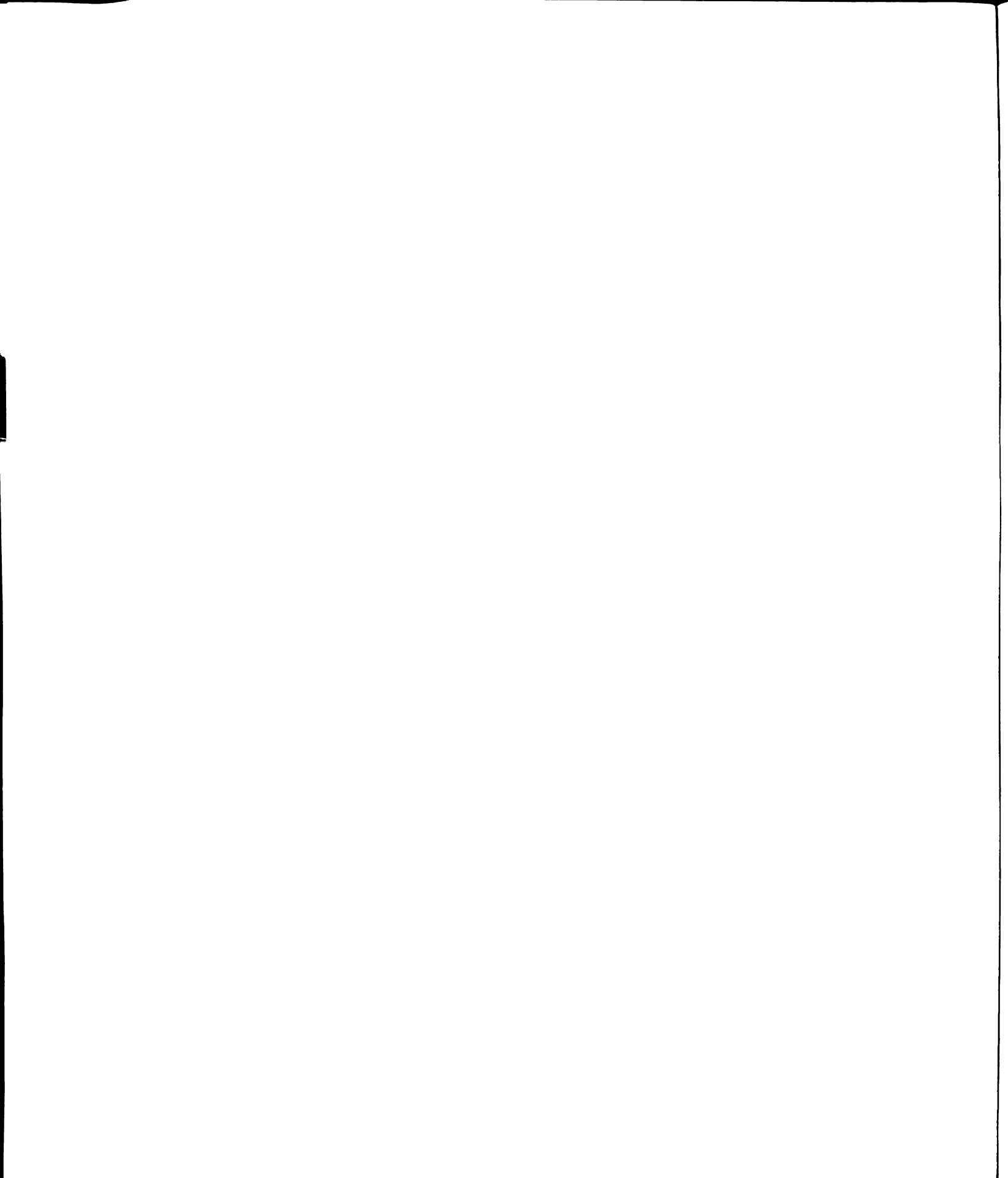


Figure 2.2. Measured and estimated C using Eq. [20] of the international soils versus $(\ln \alpha)^{1/n}$.



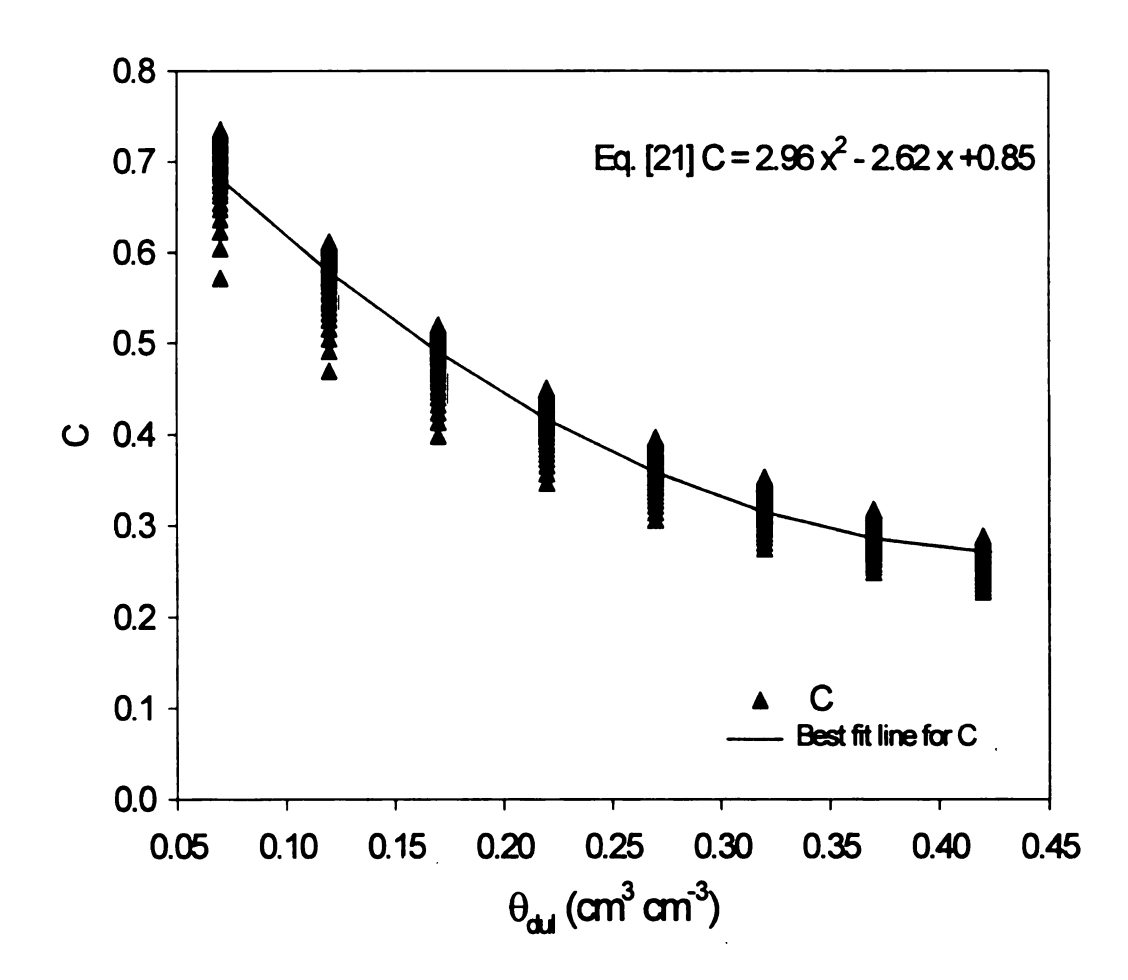


Figure 2.3. Relationship between C and θ_{dul} for any possible realistic combination of θ_s and θ_{dul} .

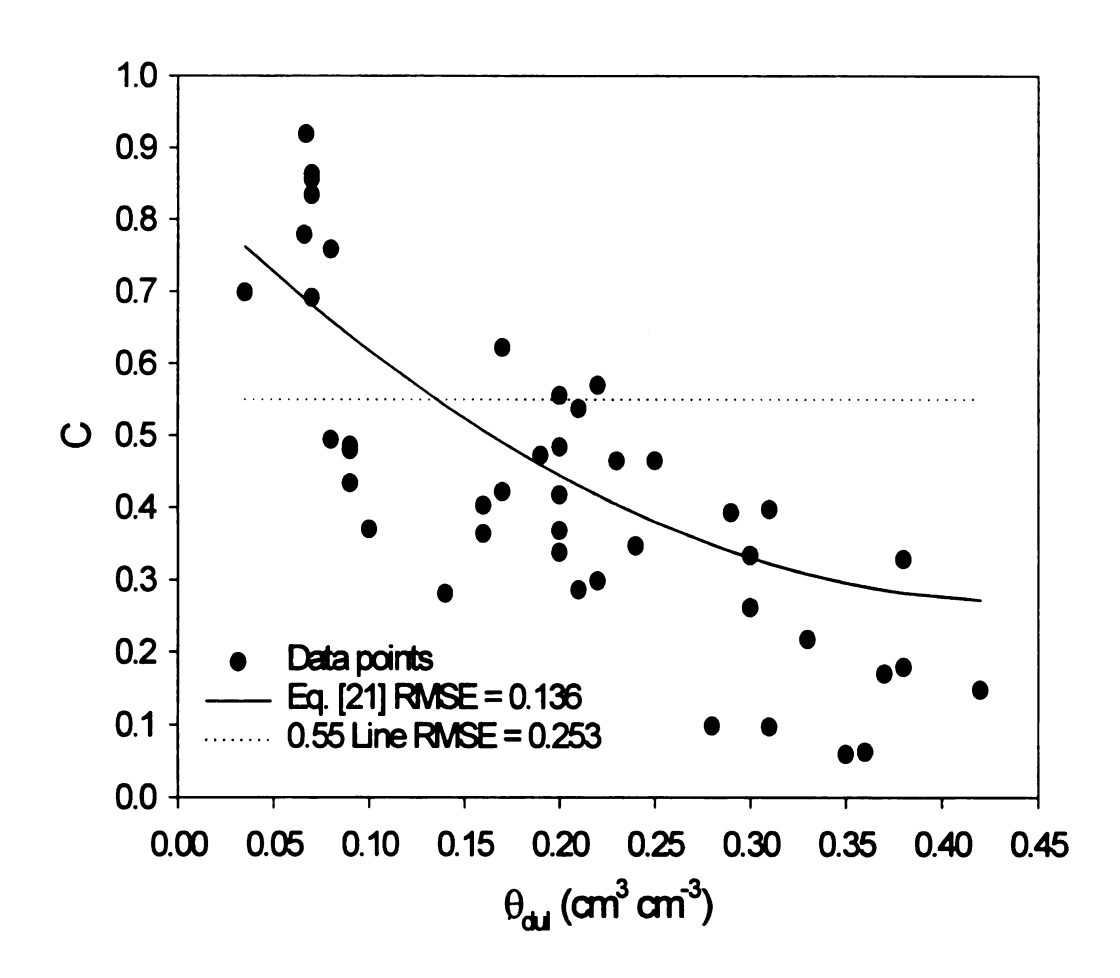


Figure 2.4. Measured and estimated C using Eq. [21] of the international soil versus θ_{dul} .

can be defined as follows:

$$a = -b \ln(K_s)$$
and
$$b = \frac{C}{\ln(\phi_e) - \ln(K_s)}$$
(23)

To explain Eq. [22] and Eq. [23], let us assume that a saturated soil layer has $\theta_s = 0.4 \text{ cm}^3 \text{ cm}^{-3}$ and $\theta_{dul} = 0.2 \text{ cm}^3 \text{ cm}^{-3}$. Using Eq. [21], C was found to be 0.44 and using Eq. [23], a was found to be 0.324 and b was found to be -0.075. Assuming that Q_i ranged from 0 cm d^{-1} to 100 cm d^{-1} , applying Eq. [22] C against Q_i was plotted and shown in Figure 2.5. It was clear that C was equal to the original C when Qi was 0 and C was equal to 0 when Qi was equal to K_s (37 cm d^{-1}). When Qi was greater than K_s (37 cm d^{-1}) C is assumed to be 0 and only K_s (37 cm d^{-1}) of water can pass through the soil layer.

Laboratory Results

A revision of the definition of drainable soil water had to be done to explain the laboratory results. Defining the drainable soil water as the difference between θ_i (initial soil water content) and θ_{dul} (as in Eq. [17]) is correct if the final soil water content (θ_f) after a drainage cycle is equal to θ_{dul} . However, if θ_f after drainage cycle is greater than θ_{dul} , the drainable soil water content has to be defined as the difference between θ_i and θ_f and not the difference between θ_i and θ_{dul} . The deviation of θ_f from θ_{dul} for a soil layer usually happens when that layer is affected by a water table. Zacharias and Bohne (1997)

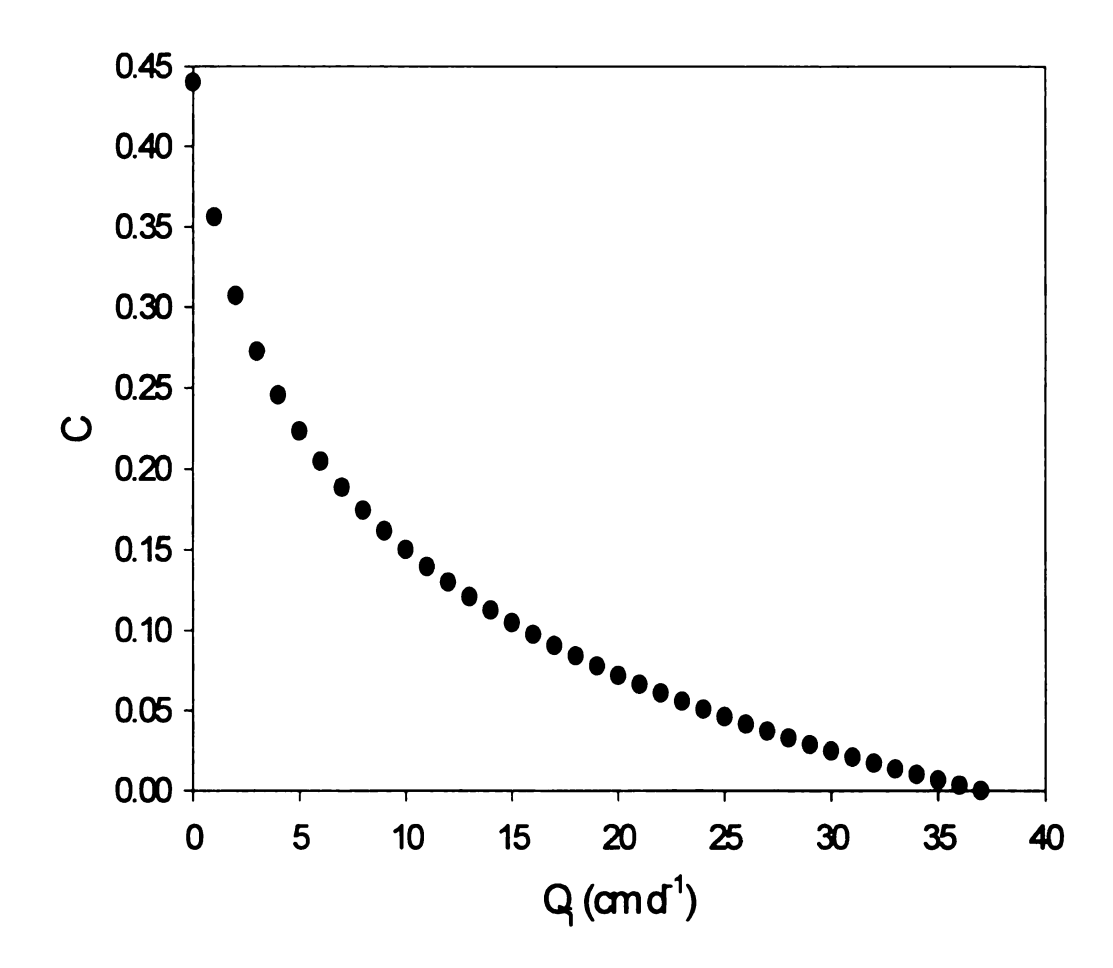


Figure 2.5. Relationship between C and Q_i for a soil of $\theta_s=0.4$ cm³ cm⁻³ and $\theta_{dul}=0.4$ cm³ cm

introduced a procedure to determine θ_f in such a case. In this study, the actual measured θ_f was used at each soil depth instead of θ_{dul} in defining the drainable soil water. Final soil water content at 3, 6, 9, 12, 15, and 25 cm depths of loamy soil and sandy loam soil could be considered equal to θ_{dul} (Figure 2.6.a, Figure 2.6.b, Figure 2.7.a, and Figure 2.7.b). Whereas, θ_f at 35, 45, 55, 65, and 75 cm depths of loamy soil and sandy loam soil were greater than θ_{dul} assuming that both soils were uniform and each soil had only one θ_{dul} for all depths (Figure 2.6.a, Figure 2.6.b, Figure 2.7.a, and Figure 2.7.b).

When θ_f is greater than θ_{dul} , using Eq. [4] to define C and Eq. [20] or Eq. [21] to estimate C is irrelevant because the change of hydraulic conductivity in a day will be less than if θ_f was equal to θ_{dul} . An approximation was developed to estimate C at any θ_f as follows:

$$C = C + (0.85 - C)(1 - H)$$
(24)

where H ranges from 0 to 1 and can be defined as follows:

$$H = \frac{\left(\theta_s - \theta_f\right)}{\left(\theta_s - \theta_d\right)} \tag{25}$$

Using Eq. [21] and Eq. [24], C was 0.57, 0.51, 0.62, 0.39, and 0.51at depths of 35, 45, 55, 65, and 75 cm, respectively, for loamy soil and it was 0.66, 0.79, 0.79, 0.72, and 0.79 at depths of 35, 45, 55, 65, and 75 cm, respectively, for sandy loam soil. There was no significant improvement in estimating the daily soil water contents during drainage cycle of loam and sandy loam soils by using these values of C for loamy soil

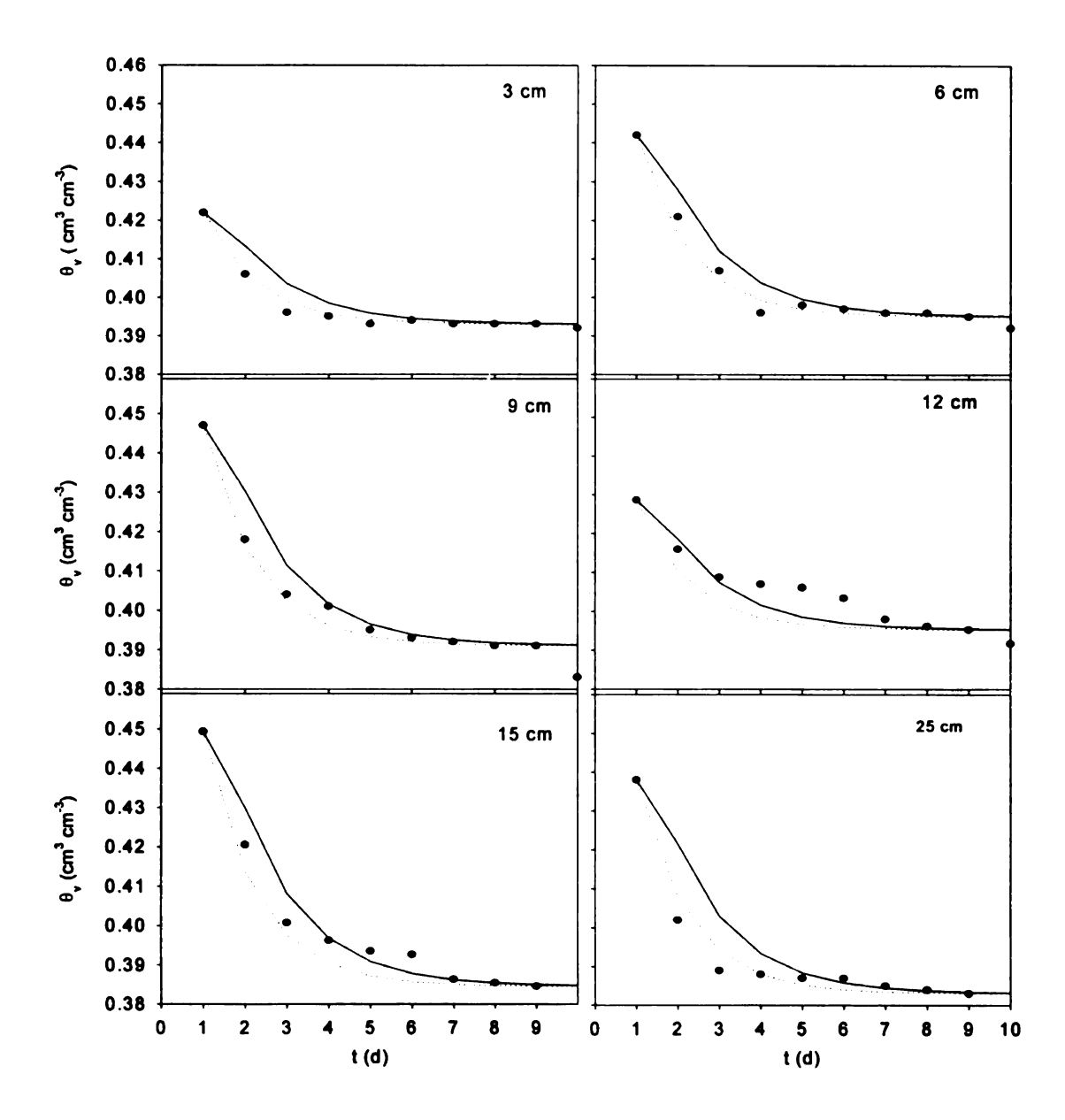


Figure 2.6.a. Soil water content profiles for a 150-cm column of loamy soil during drainage cycle at 3, 6, 9, 12, 15 and 25 cm depths.

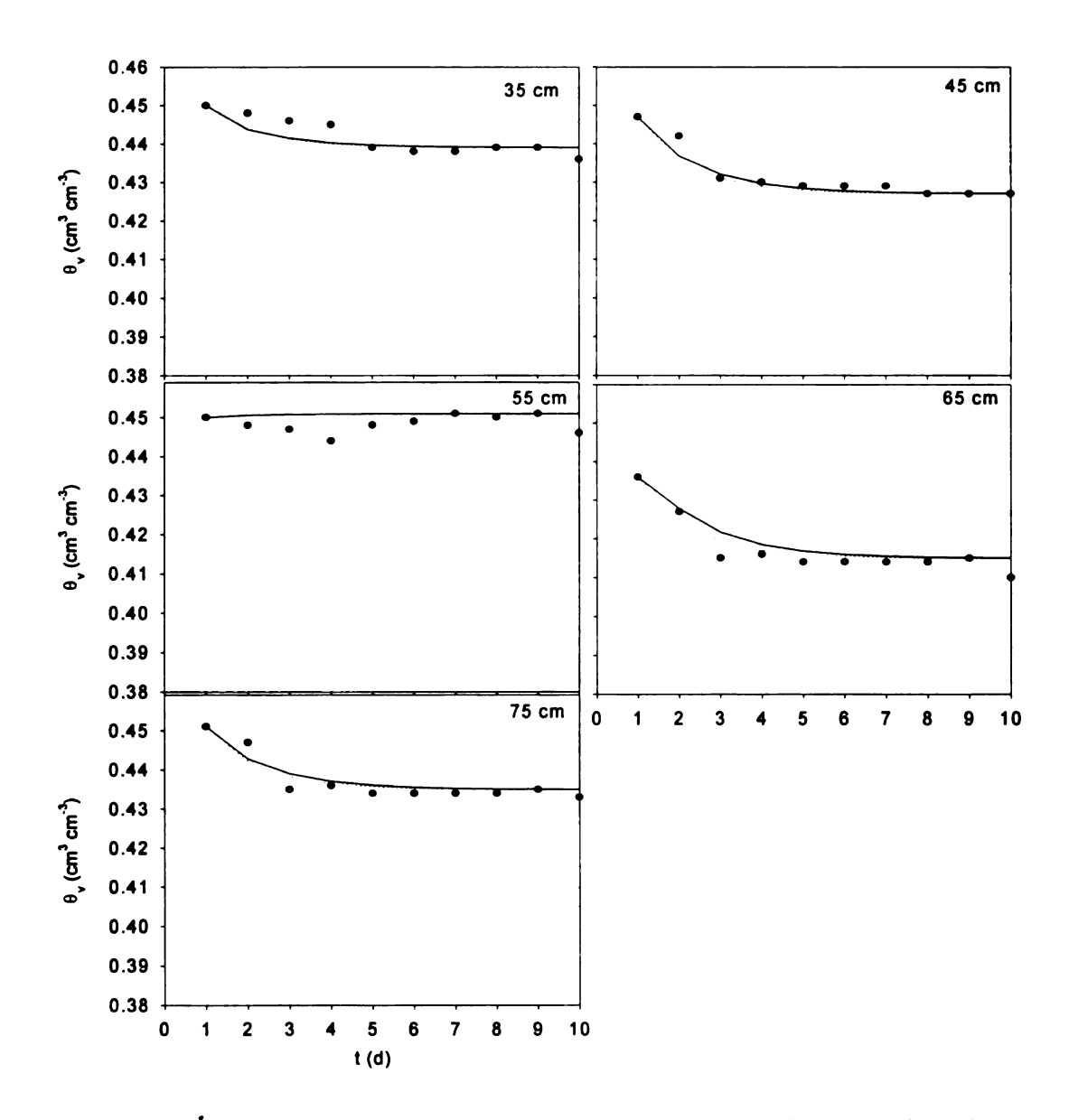


Figure 2.6.b. Soil water content profiles for a 150-cm column of loamy soil during drainage cycle at 35, 45, 55, 65, and 75 cm depths.

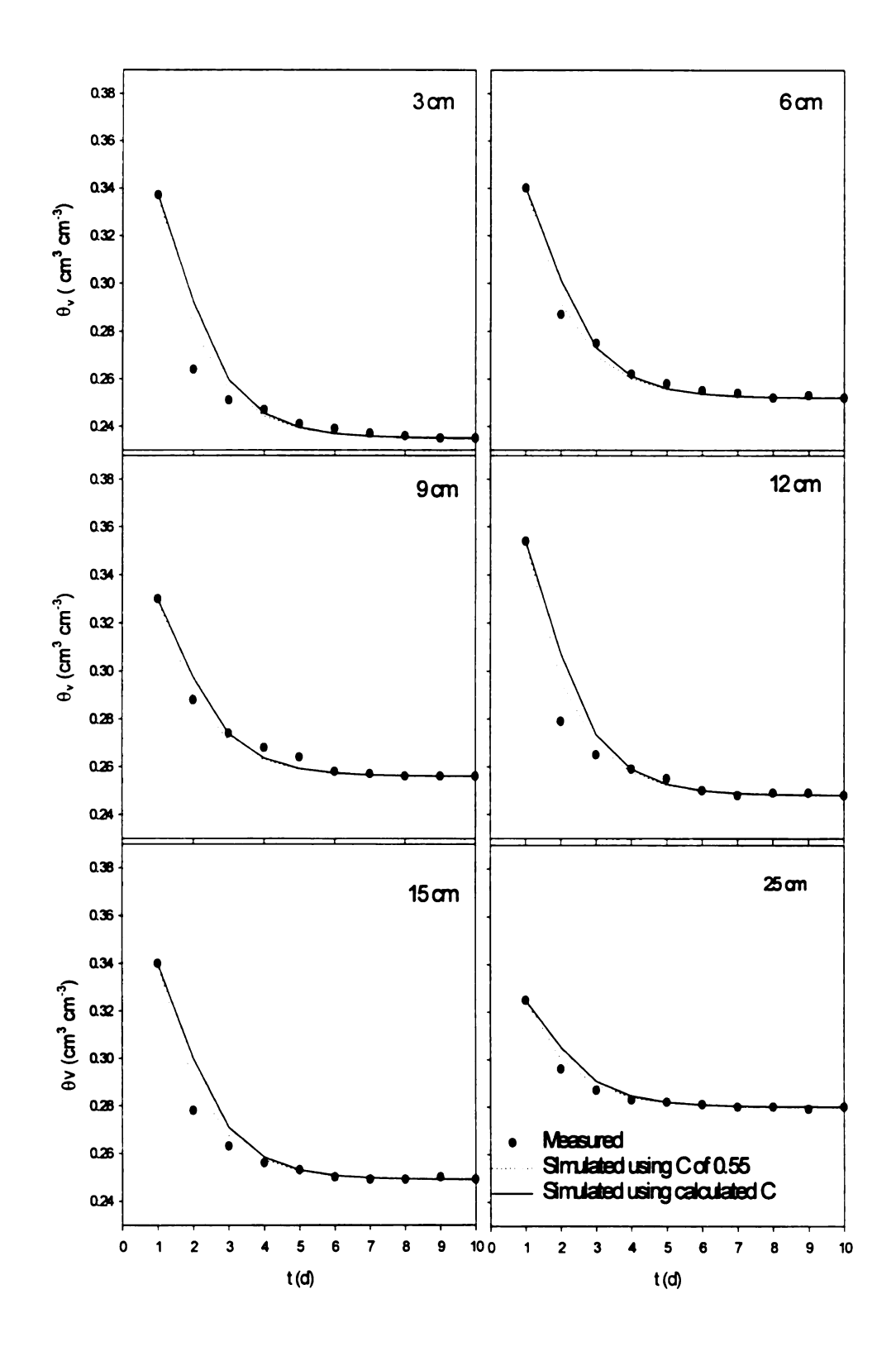


Figure 2.7.a. Soil water content profiles for a 150-cm column of sandy loam soil during drainage cycle at 3, 6, 9, 12, 15 and 25 cm depths.

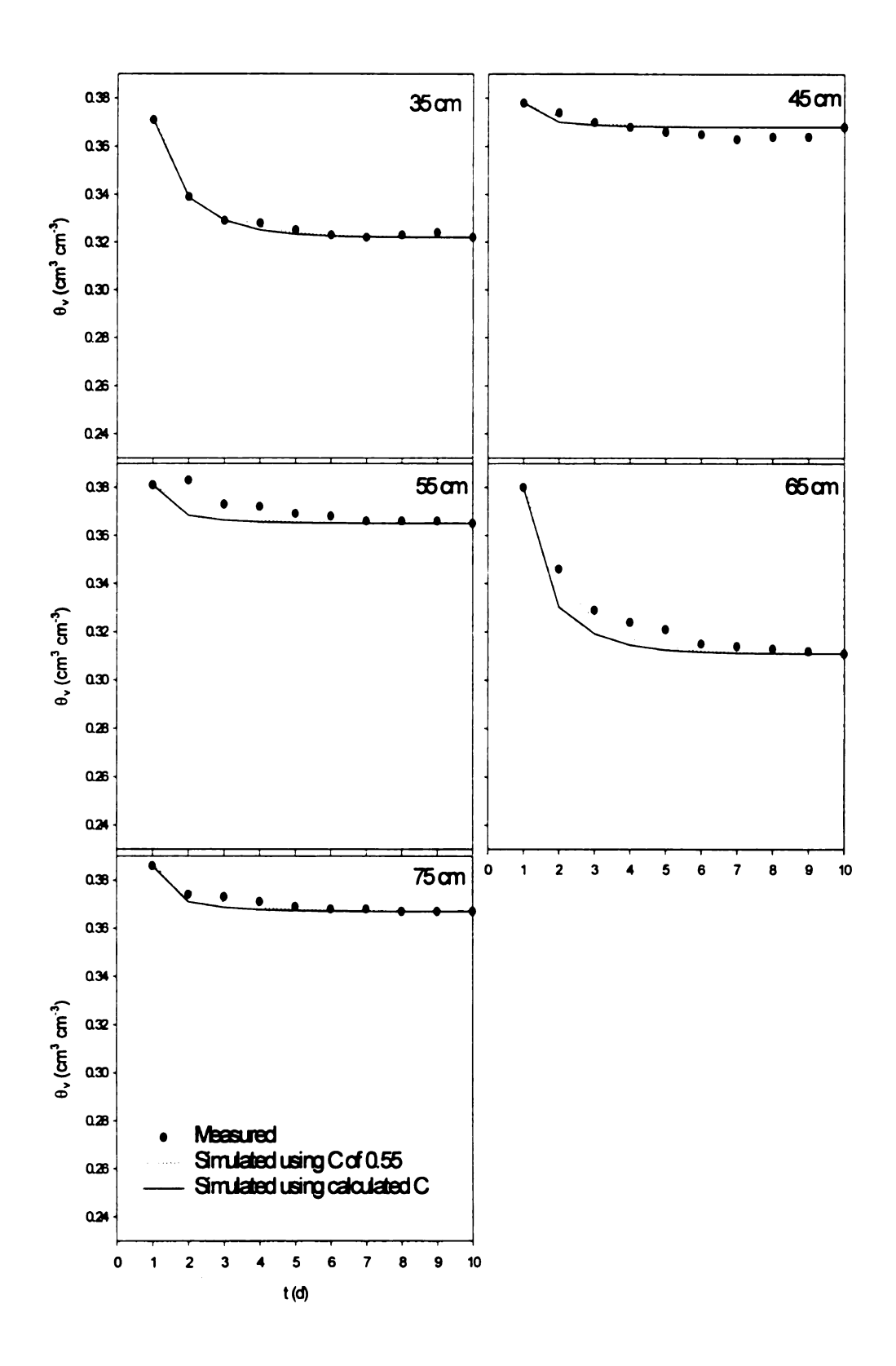


Figure 2.7.b. Soil water content profiles for a 150-cm column of sandy loam soil during drainage cycle at 35, 45, 55, 65, and 75 cm depths.

and sandy loam soil over using C of 0.55 for both soils (Figure 2.6.a, Fig.2.6.b, Figure 2.7.a, and Figure 2.7.b).

Using the calculated C for loamy and sandy loam soils gave better estimates of 1st day drainage rate than using C of 0.55 (Figure 2.8). The measured 1st day drainage rate was about 10 mm d⁻¹ for loamy soil and about 22 mm d⁻¹ for sandy loam soil (Figure 2.8). The measured 1st day drainage rate for sandy loam soil was about double of that for loamy soil partially because C was higher for sandy loam soil than that for loamy soil and mainly because the drainable soil water for sandy loam soil was about twice that for loamy soil. There were no significant differences in estimating the drainage rate of loam and sandy loam soils on other days between the different models (Figure 2.8). The over all estimate of the drainage rate was reasonably accurate on all days of the drainage cycle for the different models.

Measured and simulated cumulative soil water drainage at the end of a drainage cycle was about 20 mm for loamy soil and 36 mm for sandy loam soil (Figure 2.9). Measured and estimated cumulative soil water drainage at the end of a drainage cycle for loam and sandy loam soils was essentially equal regardless of what C was used, because measured and estimated cumulative soil water drainage at the end of a drainage cycle was equal to the drainable soil water. Knowing and using the right θ_f was important in defining the drainable soil water and as result in estimating the cumulative soil water drainage.

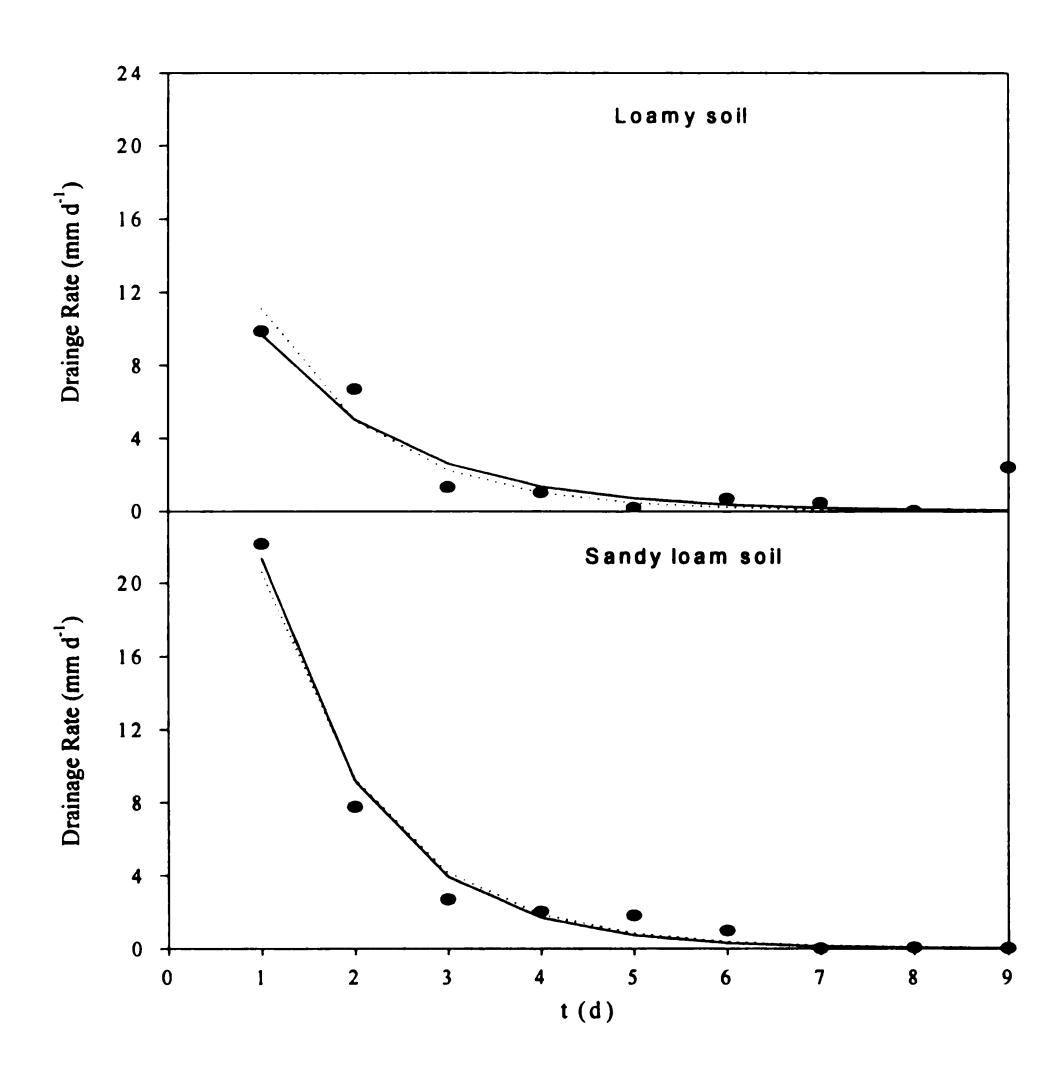


Figure 2.8. Daily drainage rate of a 150-cm column of loamy soil and a 150-cm column of sandy loam soil.

Field Results

Equation[20] was used to estimate C of profile 1 and profile 2 in Lansing area. The calculated C was 0.48. The daily soil water contents were estimated better for profile 1 using C of 0.48 than using C of 0.55 at 6, 9, 15, 25, 35, 45, 55, and 65 cm depths (Figure 2.10.a, Figure 2.10.b). The daily soil water contents were estimated better for profile 2 using C of 0.48 than using C of 0.55 at 3, 6, 15, 25, 35, 45, 55, 65, and 75 cm depths (Figure 2.11.a, Figure 2.11.b). These results showed that using 0.55 underestimated the soil water contents. The maximum negative difference between simulated and measured soil water content was about 0.02 cm³ cm⁻³.

Using C of 0.48 for profile 1 and profile 2 gave better estimate of 1st day drainage rate than using C of 0.55 (Figure 2.12). There was no significant difference in estimating the drainage rate of profile 1 and profile 2 on other days between the different models (Figure 2.12). The over all estimate of the drainage rate was reasonably accurate on all days of the drainage cycle for the different models. Measured and simulated cumulative soil water drainage at the end of a drainage cycle was about 104 mm for profile 1 and about 99 mm for profile 2 (Figure 2.13). Measured and estimated cumulative soil water drainage at the end of a drainage cycle for profile 1 and profile 2 was essentially equal regardless of what value was used of C because measured and estimated cumulative soil water drainage at the end of a drainage cycle was equal to the drainable soil water. Using C of 0.55 overestimated the cumulative soil water drainage during the first 4 days during a drainage cycle (Figure 2.13).

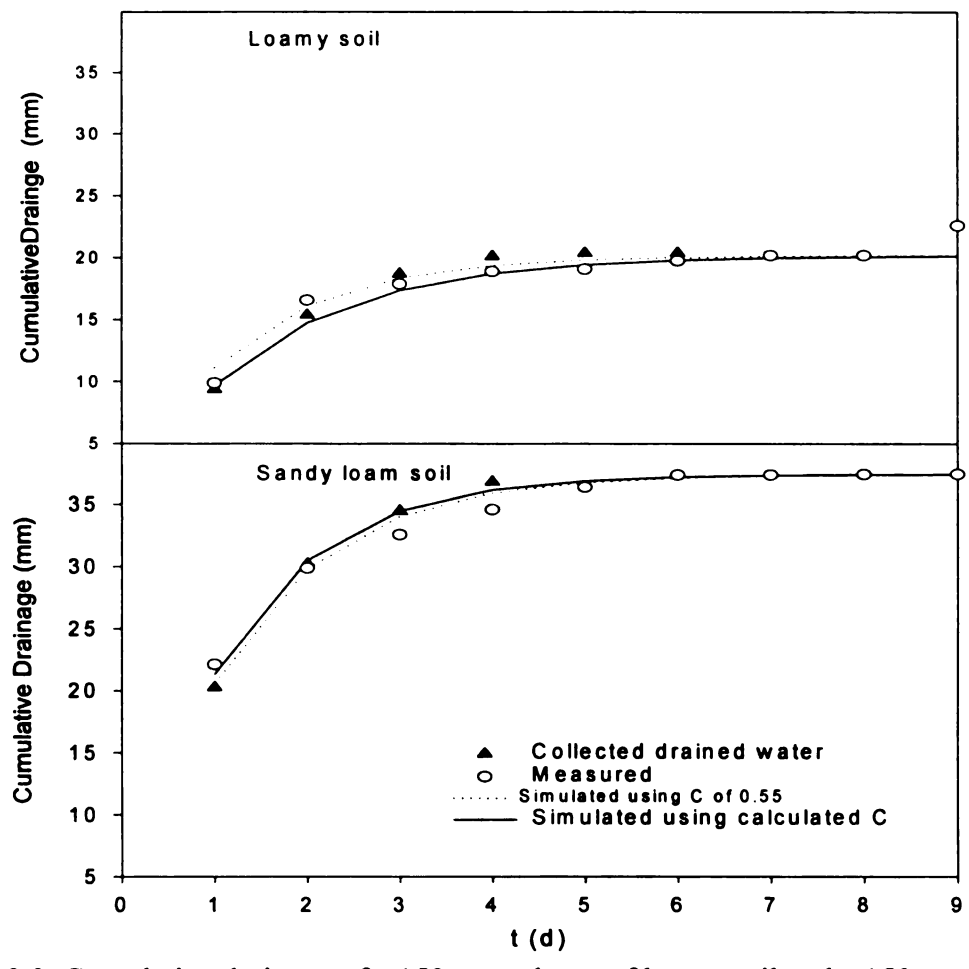


Figure 2.9. Cumulative drainage of a 150-cm column of loamy soil and a 150-cm column of sandy loam soil.

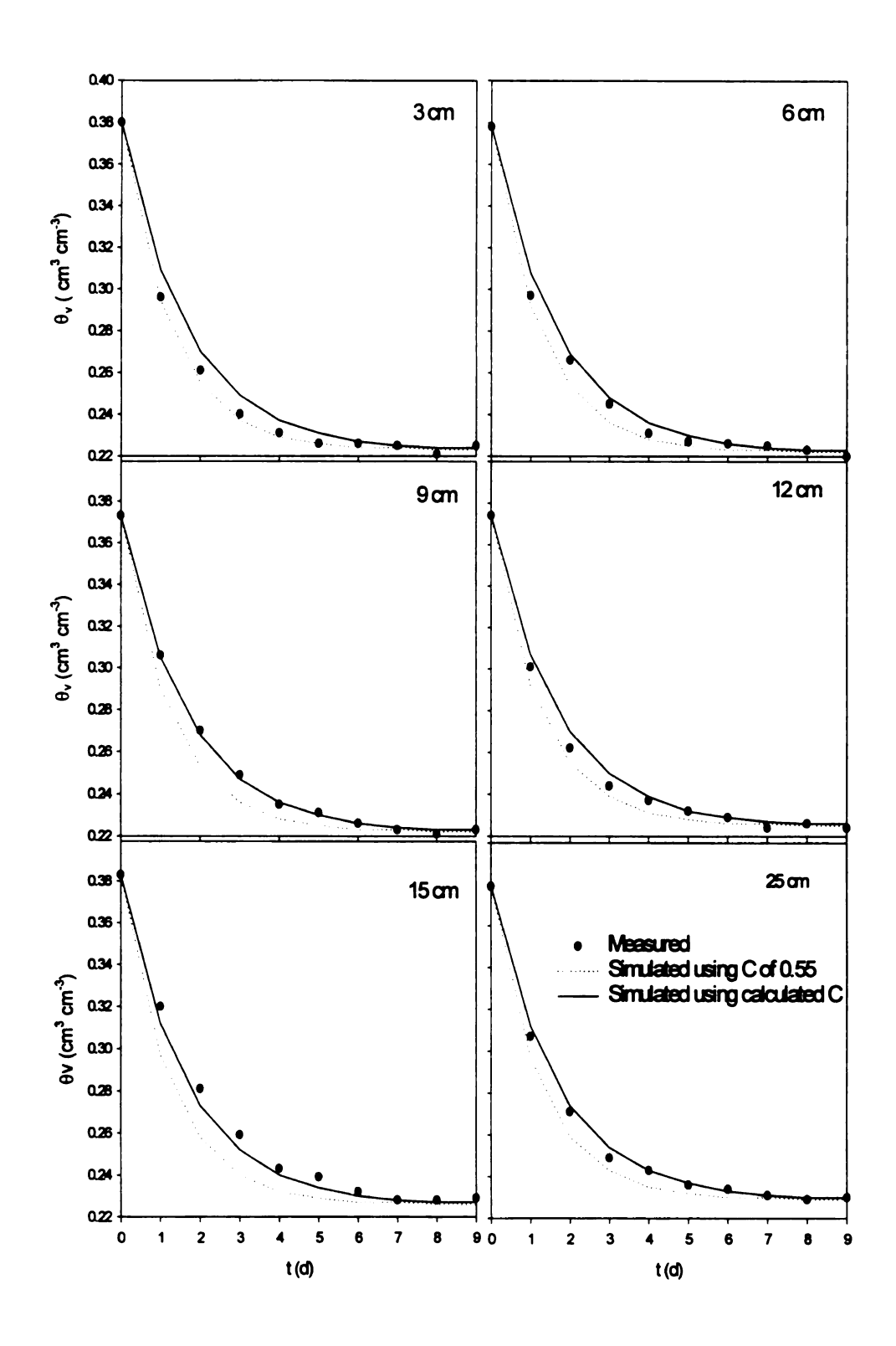


Figure 2.10.a. Soil water content profiles for profile 1 of sandy loam soil during drainage cycle at 3, 6, 9, 12, 15, and 25 cm depths.

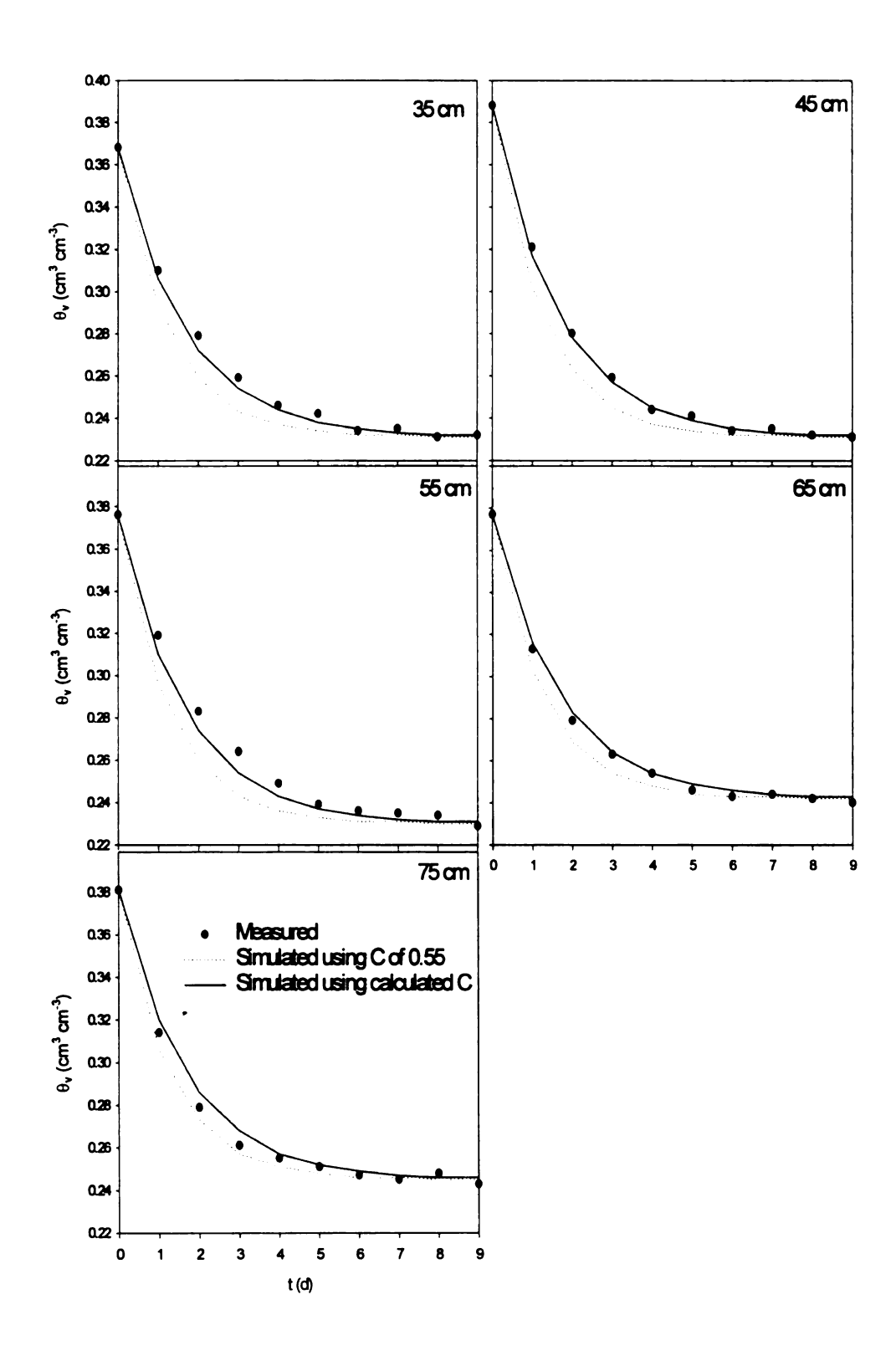


Figure 2.10.b. Soil water content profiles of profile 1 of sandy loam soil during drainage cycle at 35, 45, 55, 65, and 75 cm depths.

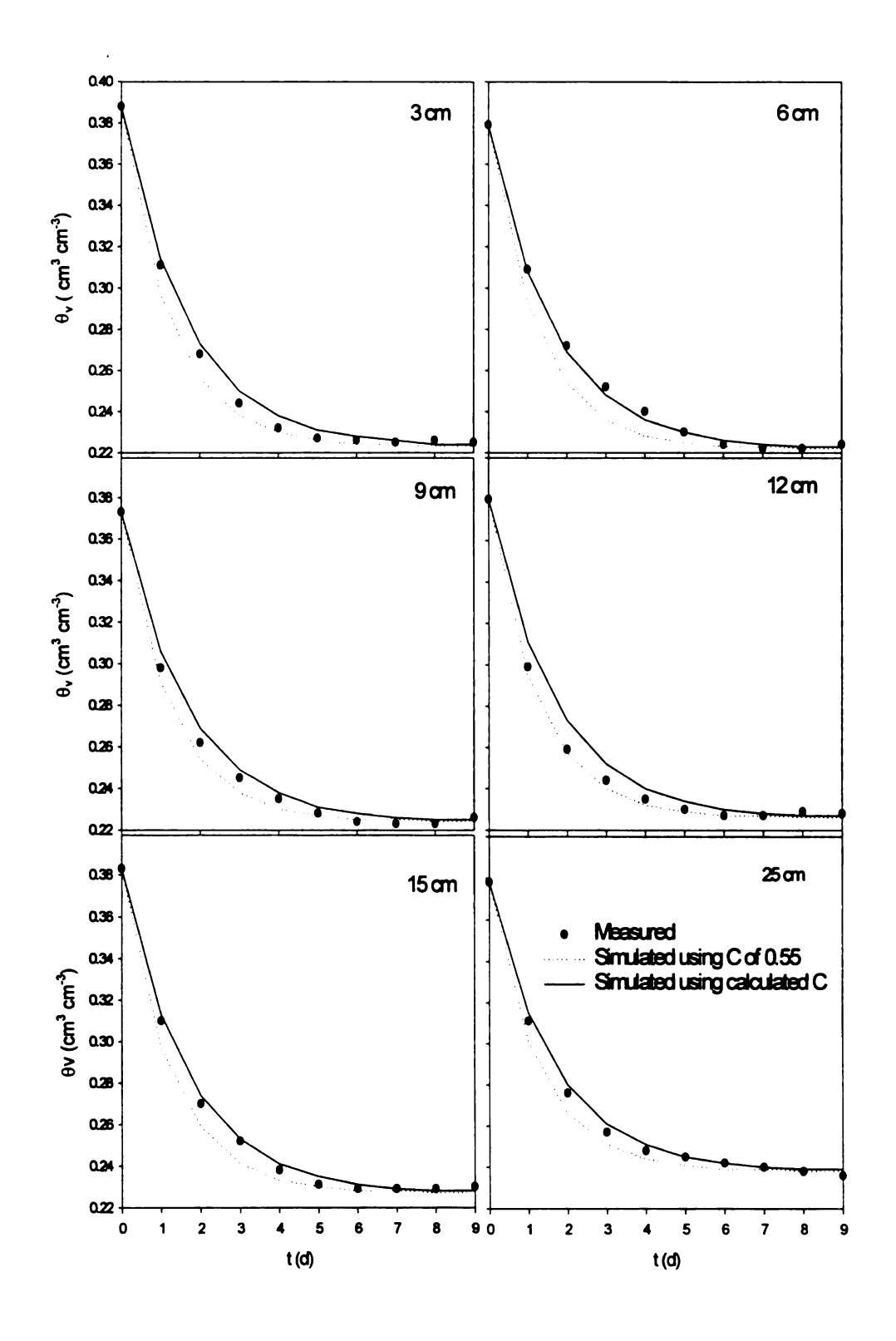


Figure 2.11.a. Soil water content profiles for profile 2 of sandy loam soil during drainage cycle at 3, 6, 9, 12, 15, and 25 cm depths.

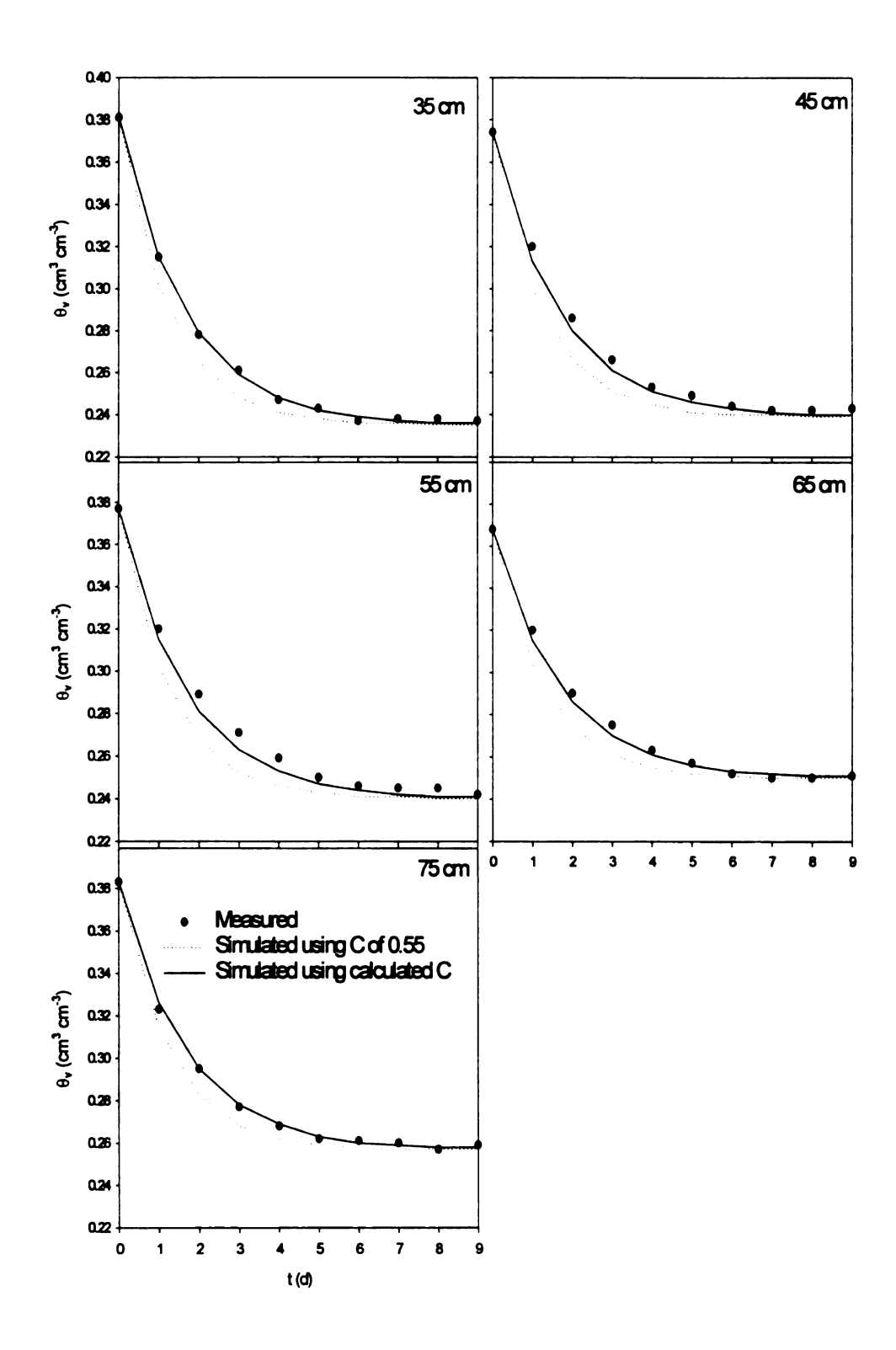


Figure 2.11.b. Soil water content profiles for profile 2 of sandy loam soil during drainage cycle at 35, 45, 55, 65, and 75 cm depths.

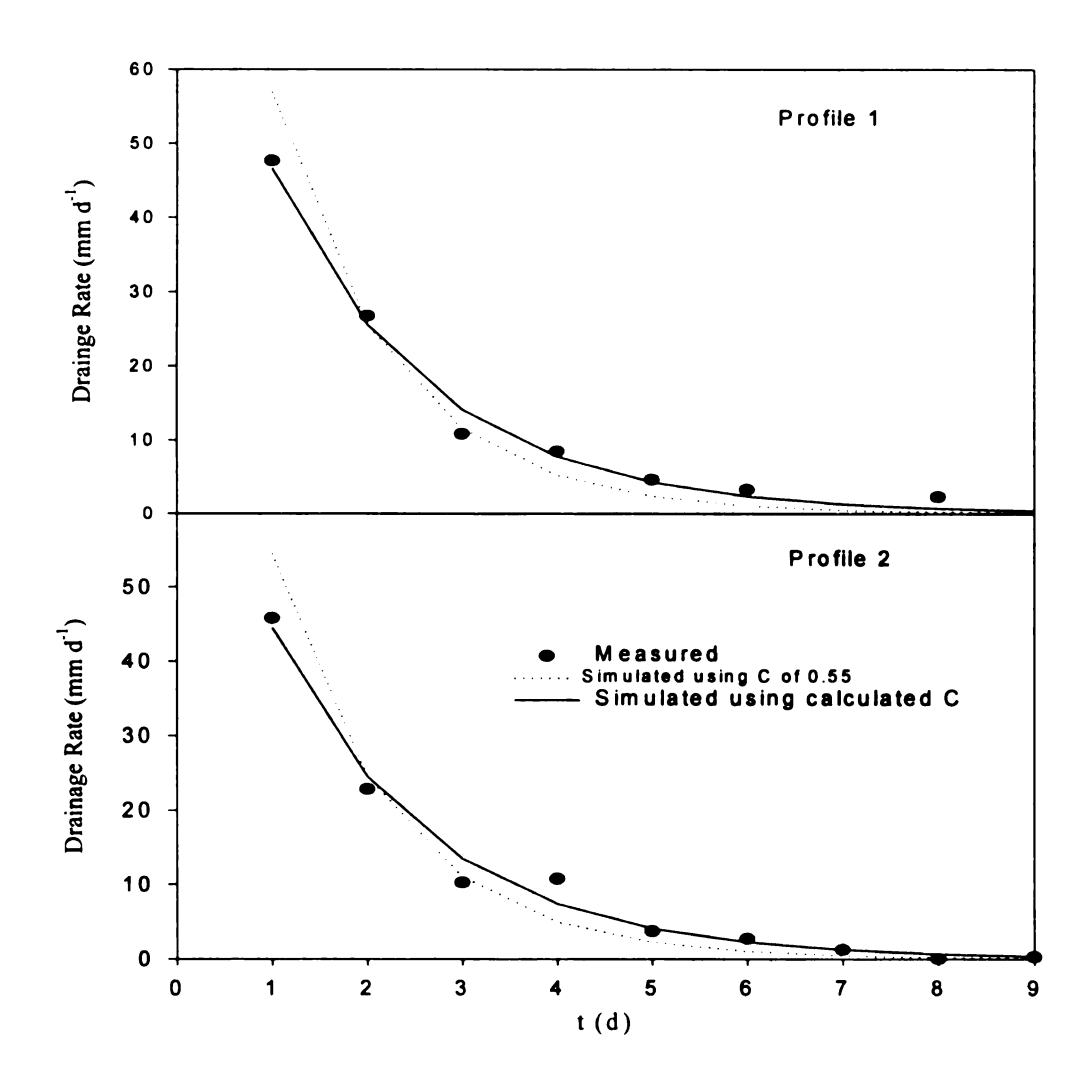


Figure 2.12. Daily drainage rate of profile 1 and profile 2 of sandy loam soil.

Conclusions

A theoretical basis to explain the drainage coefficient that is used in the water balance of CERES family models was introduced. It was found that the drainage coefficient is soil dependent. It was clear that the drainage coefficient depends on the initial soil water content. However, using a sole value of the drainage coefficient for each soil is reasonable and simplifies soil water drainage modeling. Two models were developed to estimate the drainage coefficient from drained upper limit water content and saturated water content. The new models gave good estimates of the drainage coefficient. Therefore, Eq. [21] is recommend to be used in the water balance of CERES instead of a constant value of 0.55. A generic relationship between C and Q_i was developed to account for the effect of incoming flow on the change of soil water content of a certain soil layer.

A new definition to the drainable soil water was introduced. The new definition made the drainage model in the water balance of CERES applicable under shallow soil water table conditions. More studies are needed on the estimation of the final soil water content of a soil layer when that layer is affected by shallow water table. Estimating the final soil water content accurately would result in accurate predictions of soil water contents during drainage cycle, drainage rate, and cumulative soil water drainage.

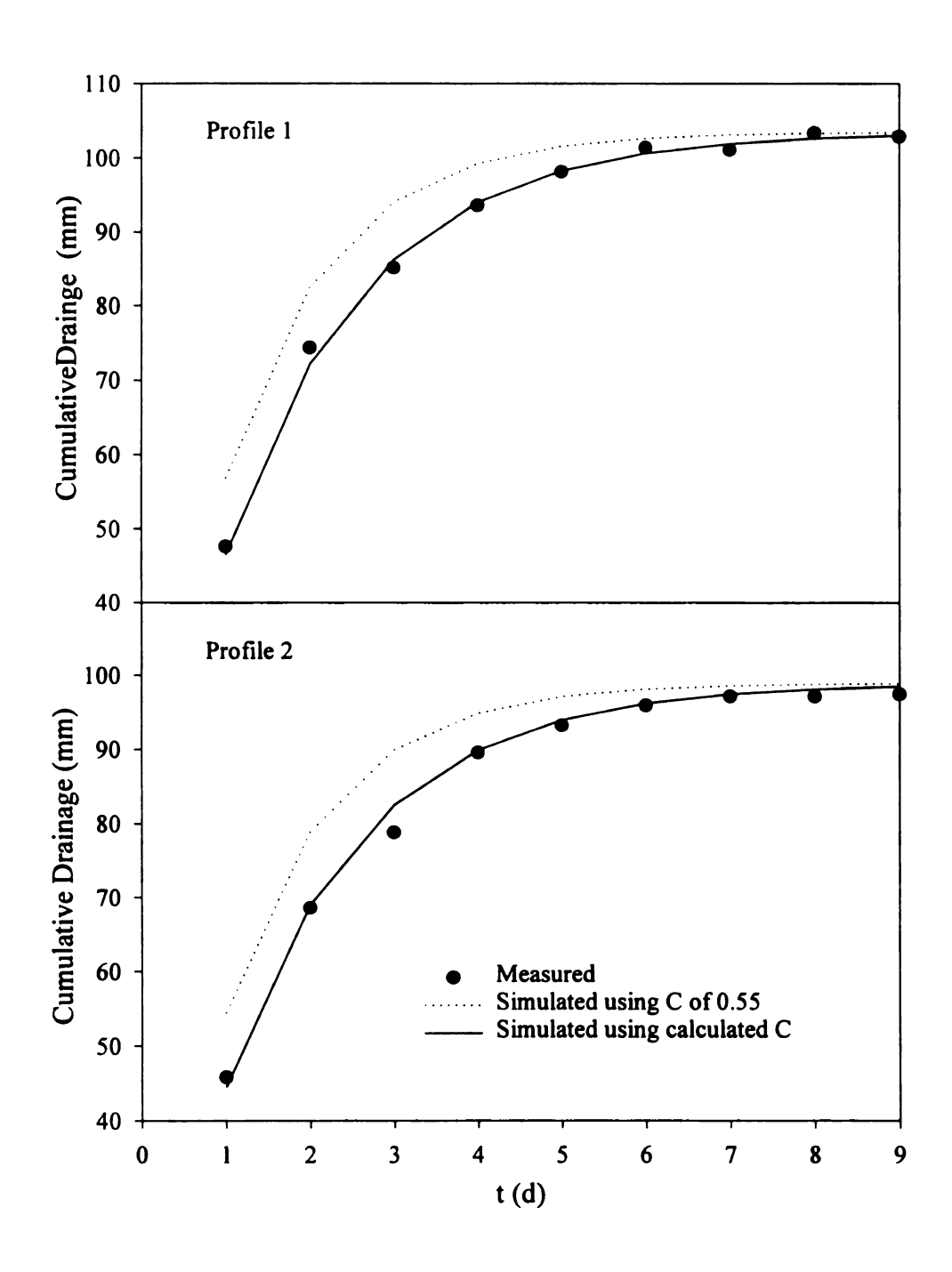


Figure 2.13. Cumulative drainage of profile 1 and profile 2 of sandy loam soil versus time.

References

- Ahuja, L.R., J.W. Naney, R.E. Green, and D.R. Nielsen. 1984. Macroporosity to characterize spatial variability of hydraulic conductivity and effects of land management. Soil Sci Soc Am. J. 48:699-702.
- Ahuja, L.R., O. Wendroth, and D.R. Nielsen. 1993. Relationship between initial drainage of surface soil and average profile saturated conductivity. Soil Sci. Soc. Am. J. 57:19-25.
- Black, T.A., W.R. Gardner, and G.W. Thurtell. 1969. The prediction of evaporation, drainage, and soil water storage for a bare soil. Soil Sci. Soc. Am. J. 33:655-660.
- Brooks, R.H. and A.T. Corey. 1964. Hydraulic properties of porous media. Hydrology Paper 3. Colorado State Univ., Fort Collins.
- Brutsaert, W. 1967. Some methods of calculating unsaturated permeability. Trans. of ASAE. 400-404.
- Corey, A.T. 1977. Mechanics of heterogeneous fluids in porous media. Water Resour. Pub., Fort Collins, CO.
- Corey, G.L., A.T. Corey, and R.H Brooks. 1965. Similitude for non-steady drainage of partially saturated soils. Hydrology Paper 9. Colorado State Univ., Fort Collins.
- Corwin, D.L., B.L. Waggoner, and J.D. Rhoades. 1991. A functional Model of solute transport that accounts for bypass. J. Environ. Qual. 20:647-658.
- Gabrielle, B., S. Menasseri, and S. Houot. 1995. Analysis and field evaluation of the CERES models water balance component. Soil Sci. Soc. Am. J. 59:1403-1412.
- Gerakis, A., and J.T. Ritchie. 1998. Simulation of atrazine leaching in relation to water table management using CERES model. J. Env. Management 52:241-258.
- Mualem, Y. 1976. A new model for predicting the hydraulic conductivity of unsaturated porous media. Water Resour. Res. 12(3):513-522.
- Mualem, Y. 1978. Hydraulic conductivity of unsaturated porous media: generalized macroscopic approach. Water Resour. Res. 14(2):325-334.
- Montas, H.J., J.D. Eigel, B.A. Engel, and K. Haghighi. 1997. Deterministic modeling of solute transport in soils with preferential flow pathways-Part 1. Model development. Trans. ASAE. 40:1245-1256.
- Philip, J.R. 1957. Numerical solution of equations of the diffusion type with diffusivity concentration-dependent. II. Aust. J. Phys. 10:29-42.

- Ratliff, L. F., J. T. Ritchie, and D. K. Cassel. 1983. Field-measured limits of soil water as related to laboratory-measured properties. Soil Sci. Soc. Am. J. 47:770-775.
- Reichardt, K., and D.R. Nielsen. 1984. Field soil-water properties measured through radiation techniques. IAEA-TECDOC-312. Joint FAO/IAEA Div. Isotope Radiat. Appl. Atomic Energy Food Agric. Dev. Vienna.
- Ritchie, J.T. 1998. Soil Water Balance and Plant Water Stress. p. 45-58. In Tsuji Y., Gordon Y.Tsuji, Gerrit Hoogenboom, Philip K. Thornton (Ed.) Understanding Options for Agricultural Production. Kluwer Academic Publishers, Dordrecht. ISBN 0-7923-4833-8.
- Ritchie, J.T., A. Gerakis, and A.A. Suleiman. 1999. Simple Model to Estimate Field-Measured Soil Water Limits. Trans. ASAE. (Accepted).
- Ritchie, J.T., J.R. Kiniry, C.A. Jones, and P.T. Dyke. 1986. Model inputs. pp. 37-48. *In* C.A. Jones and J.R. Kiniry (Ed.) CERES-Maize: A simulation model of maize growth and development. Texas A&M Press, College Station, TX.
- Schuh, W.M., and R.L. Cline. 1990. Effect of soil properties on unsaturated hydraulic conductivity pore-interaction factors. Soil Sci. AM. J. 54:1509-1519.
- Suleiman, A.A., and J.T. Ritchie. 1999. Estimating saturated hydraulic conductivity from drained upper limit water content and bulk density. Trans. ASAE. (In review).
- Vanderborght, J., C. Gonzalez, M. Vanclooster, D. Mallants, and J. Feyen. 1997. Effect of soil type and water flux on solute transport. Soil. Sci. Soc. Am. J. 61:372-389.
- Youngs, E.G. 1957a. Redistribution of moisture in porous materials after infiltration:1. Agricultural Res. Council of Soil Physics. 117-125.
- Youngs, E.G. 1957b. Redistribution of moisture in porous materials after infiltration:2. Agricultural Res. Council of Soil Physics. 202-207.
- Zacharias, S., and K. Bohne. 1997. Replacing the field capacity concept by an internal drainage approach -- A method for homogeneous soil profiles. SCIENCES of SOILS, Rel. 2, 1997 http://www.hintze-online.com/sos/1997/Articles/Art2.

CHAPTER THREE

ASSESSING AND MODELING DOWNSLOPE LATERAL SOIL WATER FLOW ALONG A SLOPING LANDSCAPE

Introduction

Water is the medium in which biological and chemical transformations of nutrients occur and in which different nutrient forms move and are transported in the soil profile, either to plant roots or out of the profile and eventually into the ground water (Nielsen et al., 1973). Within a sloping landscape, soil water may move laterally from one soil profile to another carrying nutrients with it. Such movement of soil solution could be a main reason behind the spatial variability of crop yield within sloping landscapes. Effective management of soil water within agricultural landscape requires a solid understanding of the mechanisms that regulate soil-water-landscape interaction. Soil physical properties and the amount of soil water within a sloping landscape are largely determined by landscape position (Rosek, 1995).

Lateral downslope saturated and unsaturated soil water flow in the root zone of a hillslope with homogeneous and heterogeneous soils has been observed (Beven, 1982; Jackson, 1992; McCord et al., 1991; and Tsuboyama et al., 1994). McCord and Stephens (1987) conducted a tracer study that showed a strong lateral downslope component in vadose flow in sand dunes with surface slope of 23° (Jackson, 1992). That led them to conclude that even in permeable sandy locations, where the soil profile is uniform and deep, water will flow laterally downslope on the hillside. McCord et al. (1991) showed that for all conditions except high constant anisotropy, significant lateral downslope flow occurred only during drainage. The lateral downslope flow can become more significant

when the soil has highly permeable layers, cracks, or cavities (Wallach and Zaslavsky, 1991).

Many scientists have attempted to model the lateral downslope soil water flow using a mechanistic approach. Most of these models are numerical such as Beven (1982), Bouraoui et al. (1997), Hillel (1977), Nieber and Walter (1981), and Smith and Hebbert (1983). Few have tried to find analytical models for simplified cases such as Philip (1991), Stagnitti et al. (1986), and Warrick et al. (1997). On the other hand, no attempt has been made to produce functional models to simulate lateral downslope soil water flow.

The water balance of the CERES family soil-water-crop-atmosphere simulation models lack a lateral downslope flow component since it was built to simulate soil water redistribution in the vertical dimension. Although lateral downslope flow is not considered in CERES model, runoff is considered and simulated using time-to-ponding concept (Gerakis and Ritchie, 1998). Modeling the lateral downslope flow and incorporating it into the water balance of the CERES model will enable the model to account for both surface and subsurface downslope flow and to simulate the spatial variability of crop yield more accurately.

The objective of this study was to develop a simple functional model to simulate lateral downslope soil water flow and incorporate such a model within the water balance of CERES model. To do so, the new functional lateral downslope model has to be simple, accurate, and not required additional inputs more than those required by the CERES models as a minimum data set.

Theory

To study the lateral downslope drainage flow along a sloping landscape, a layer of isotropic homogeneous soil is considered along a planar hillslope. The slope angle is γ . Cartesian rectangular space coordinates x and z, with x taken positive in the horizontal downslope direction and z positive in the downward vertical direction are introduced. Rotated co-ordinates $(x_{\bullet}, z_{\bullet})$ are introduced and defined by (Figure 3.1).

$$x_* = x \cos \gamma + z \sin \gamma$$

$$z_* = -x \sin \gamma + z \cos \gamma$$
(1)

The lateral downslope flow $(q, cm d^{-1})$ (flux in x. direction) subject to the following initial and boundary conditions

$$\theta = \theta_{s} \qquad t = 0 \quad z_{\bullet} \ge 0$$

$$\theta < \theta_{s} \qquad t > 0 \quad z_{\bullet} \ge 0 \quad x_{\bullet} = 0$$
(2)

can be described by:

$$q = K(\theta)\sin\gamma \tag{3}$$

where $K(\theta)$ is soil water hydraulic conductivity (cm d⁻¹), θ is soil water content cm³ cm⁻³, t is time (d), z is distance (cm), and sin γ is the slope and it is equal to the hydraulic

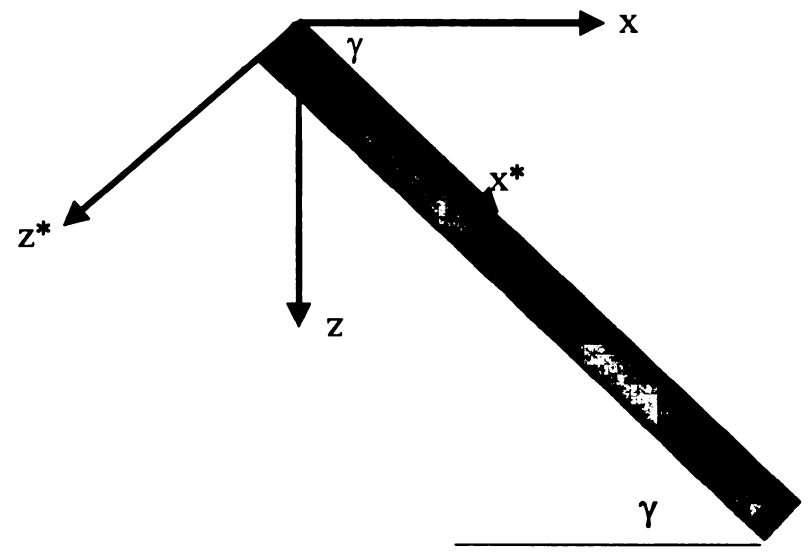


Figure 3.1. Cartesian rectangular space coordinate x and z and rotated coordinates x. and z.

gradient $(\partial h/\partial x)$. If for some reason (e.g., irregular slope) $\partial h/\partial x$ is not equal to $\sin \gamma$, $\partial h/\partial x$ has to be used in Eq. [3] instead of $\sin \gamma$. At t = 0, the equipotential lines are horizontal which results in flow in the z direction only. At t > 0, equipotential lines perpendicular to the downslope surface will be formed resulting in a downslope flow component. Many scientists have found that Eq. [3] can be used to describe lateral downslope flow under different initial and boundary conditions (Jackson, 1992; Philip, 1991; Stagnitti et al., 1992).

The change of soil water content in 1 day ($\Delta\theta$) subject to (2) can be described as:

$$\Delta \theta = C(\theta_s - \theta_{dul}) \sin \gamma \Delta t \, \Delta z \tag{4}$$

where $C \sin \gamma$ is the fraction of soil water content that can be drained from the soil layer in a day.

Using the theory of vertical drainage as introduced in the previous chapter, C can be calculated as follows:

$$C = \alpha \frac{\left(1 - C\sin\gamma\right)^n}{1 + \left(1 - C\sin\gamma\right)^n} \tag{5}$$

where α can be written as:

$$\alpha = 150 \left(\frac{\theta_s - \theta_{dul}}{\theta_{dul}^2} \right) \tag{6}$$

and *n* can be described as:

$$n = 0.8 + 29.3\theta_{dul} \tag{7}$$

In case of infiltration, the infiltrated water can be assumed to flow vertically (z direction) only (Jackson, 1992; 1993). In case of an isotropic homogeneous soil overlaying an impervious layer, the vertical flow component will stop on the interface between the soil and the impervious layer and a lateral downslope flow component will start parallel to the impervious layer. A maximum lateral downslope flux (q_s, cm d⁻¹), in this case, occurs when the soil is saturated and the infiltration rate is equal to q_s. Saturated hydraulic conductivity (K_s) has to be used in Eq. [3] instead of K(θ) to describe the saturated lateral downslope flow. According to Suleiman and Ritchie (1999), K_s (cm d⁻¹) can be estimated as follows:

$$K_s = 75 \left(\frac{\theta_s - \theta_{dul}}{\theta_{dul}} \right)^2 \tag{8}$$

where θ_s and θ_{dul} are saturated and drained upper limit soil water contents, respectively.

In general, soils on a real hillslope are never isotropic. Both saturated hydraulic conductivities and porosities tend to decrease with depth into the soil profile, sometimes with significant layering or other irregularities (Beven, 1982). Quite so often, impervious layer may exist within the root zone or close to it causing significant lateral flow.

Anisotropy and layering could result in significant lateral downslope flow during drainage (McCord et al., 1991) since they would give more time for the drainable soil water to move laterally downslope than if the soil was isotropic and homogeneous.

Dividing a soil profile into many layers as in CERES-WHEAT water balance and

assuming that each of them has homogenous and isotropic soil facilitates using the above theory in field situation.

The water table depth (WT, cm) due to lateral downslope soil water flow assuming that (1) there is no water loss during vertical drainage out of the profile because of an impervious layer, (2) water loss due to evapotranspiration does not affect the WT, and (3) infiltration is zero, can be described as follows:

$$WT_L = WT_i (1 - C\sin\gamma)^{L-1} \tag{9}$$

where WT_i is initial water table depth (cm), L is an integer equal to 1 at day 1, then 2 at day 2 and so on.

Material and Methods

Data Collection

A field experiment was conducted to study the lateral downslope water flow along a sloping landscape in East Lansing, MI. A 100 m x 600 m field was planted to AC Ron (described in Teich et al., 1992) winter wheat variety on October 19, 1997 and harvested on July 11, 1998. In order to monitor the soil water content at different landscape positions along the slope, fifteen 150-cm access tubes were installed 20-m apart after planting along a transect perpendicular to the contour lines (Figure 3.2). To label the locations in which access tubes installed, the further north location was labeled as L1, the second further north was labeled as L2, and so on until L15. A neutron probe reading was taken in November 15. 1997. Other neutron probe readings were taken from April 15, to harvest in 1998, once a

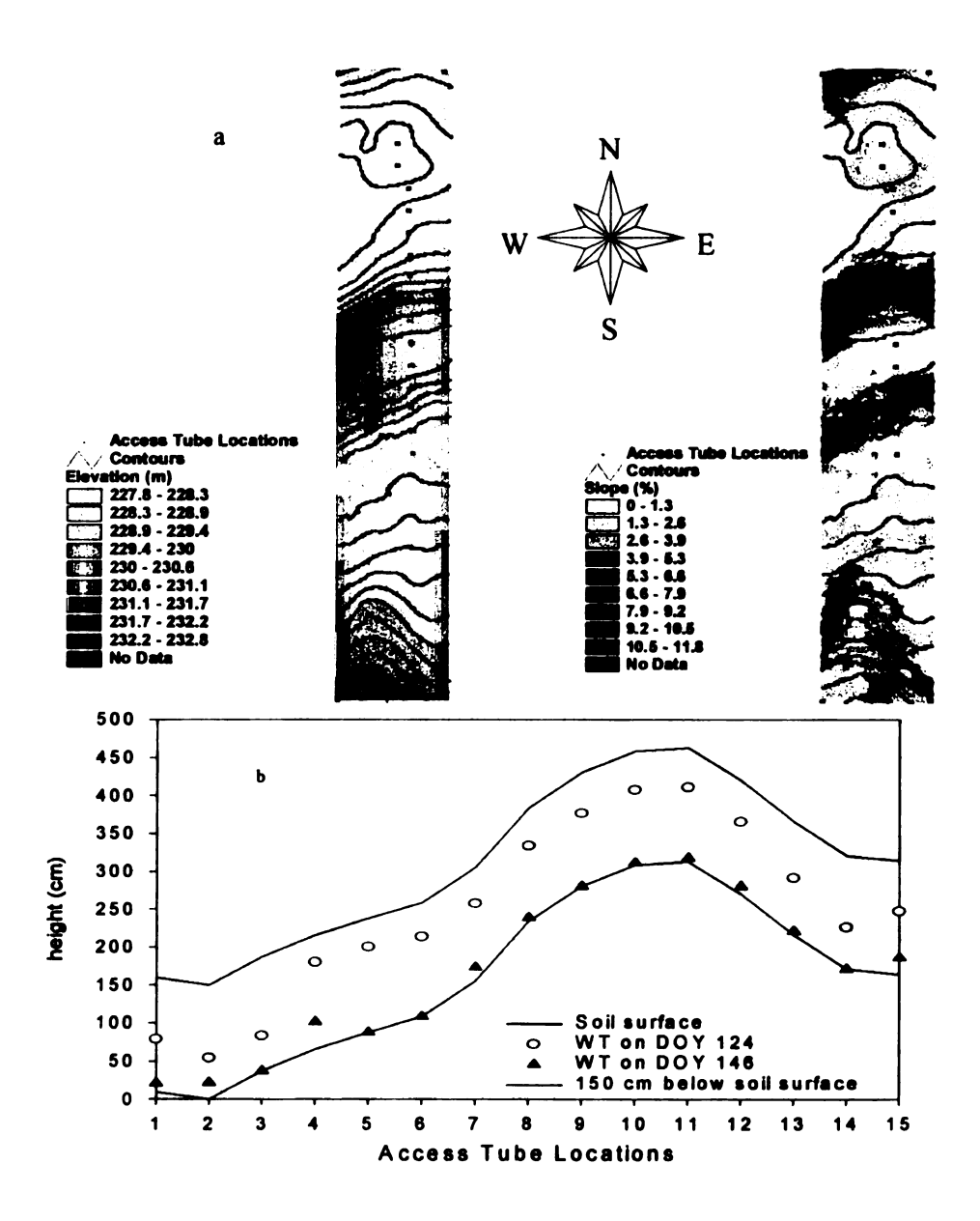


Figure 3.2. (a) Elevation, slope, and access tube locations within the field. (b) relative soil surface height, water table (WT) height, and the restricted layer (at 150 cm depth).

week and after rain events at 15, 30, 45, 60, 90, 120, and 150 cm depths. Three sets of time-domain reflectometry (TDR), 50-m apart, were installed on May 1, 1998 at the top of the hill (L10), in the middle of the southern hillside (between L12 and L13), and on the bottom of the southern slope (L15) along a transect parallel to the access tube transect to capture the detailed change of soil water content at different landscape positions. Automated readings of the TDR probes were taken bi-hourly until the harvest. Fifteen 150-cm observation wells were installed along a transect parallel to the access tube transect to monitor the water table level. Manual readings for the water table levels were taken at the same dates neutron probe readings were taken from the date of installation (April 28) to June 3, 1998 (on which water table was below 150 cm depth). A weather station was installed on the top of the hill (L10) to record hourly temperature, solar radiation, and rainfall. Daily maximum and minimum temperature, solar radiation, and rainfall are shown in Figure 3.3. Three other rain gages 150-m apart were installed along a transect parallel to the access tubes transect to assess the spatial variability of rainfall. Manual measurement of these rain gages were done after rain events. Along the transect of access tubes, leaf area index (LAI) was measured near each of the access tubes about weekly from April 15 until anthesis date (June 4) using LAI-2000. Leaf area index (LAI) is needed to estimate crop transpiration (Ritchie, 1972). CERES-WHEAT was run to estimate LAI during the entire season assuming there were neither water nor nitrogen stresses. Then, the measured LAI using LAI-2000 was used to produce more accurate LAI at each location during the growing season.

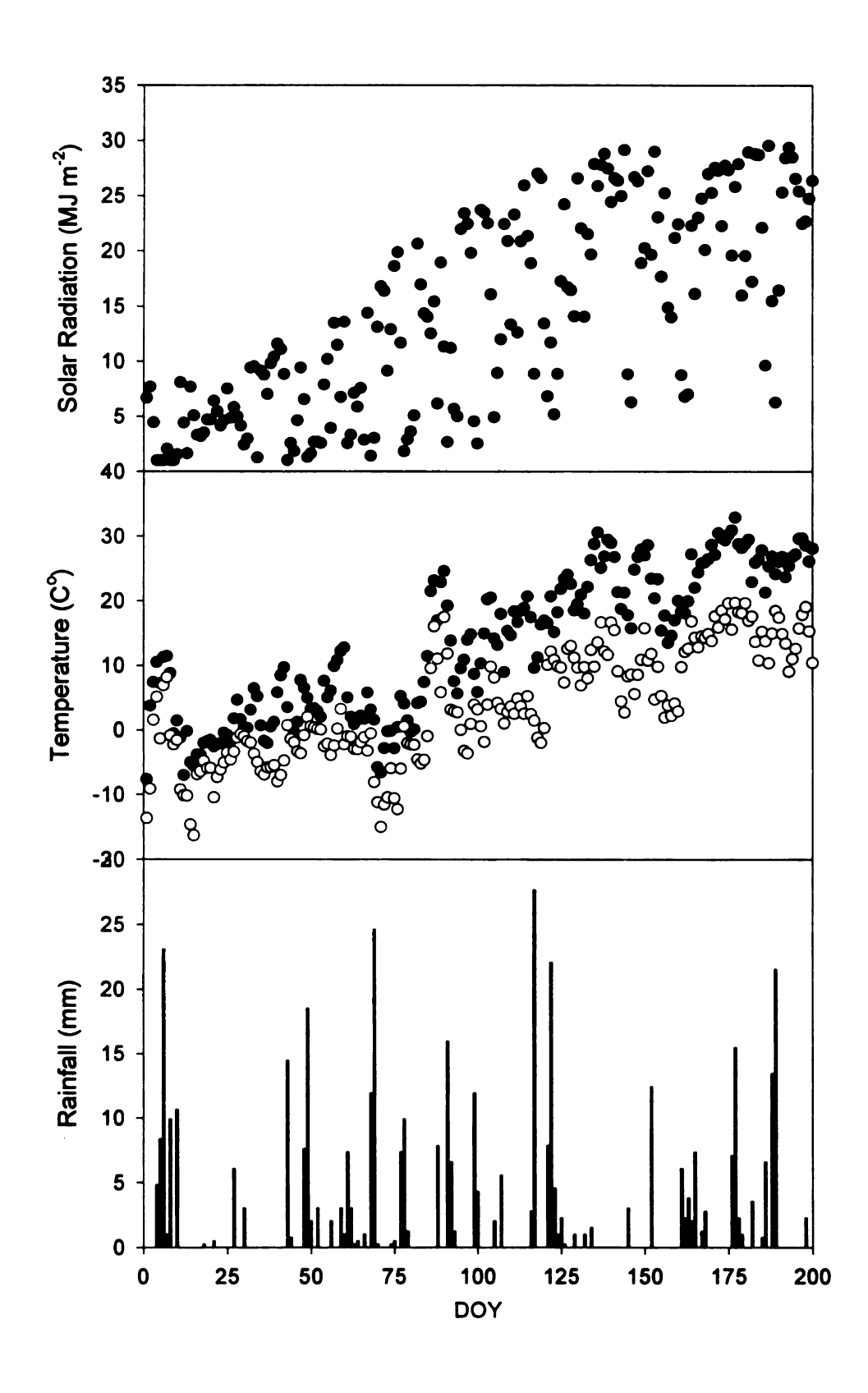


Figure 3.3. Daily solar radiation (MJ m⁻²), temperature (C°), and rainfall (mm) from DOY 1 through DOY 200 in 1998.

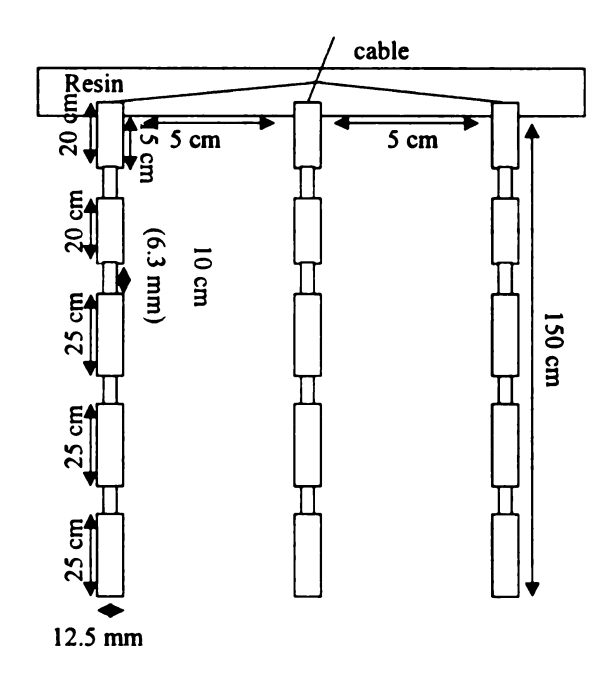
Site Description

The soil of the 6 ha field is classified as Capac series. According to soil survey, a Capac series consists of somewhat less poorly drained, moderately and moderately slow permeable soils on till plains and moraines. These soils formed in medium and moderately fine textured deposits. While installing the access tubes, disturbed soil samples were taken from 0-15, 15-30, 30-60, 60-90, 90-120, and 120-150 cm from each profile. Clay, sand, total nitrogen, and organic matter contents were determined for each soil sample and are shown in appendix A. The soil water limits were estimated using a procedure described in Ritchie et al. (1999). The elevation was measured at about 300 representative locations in the field using a theodolite. The elevation ranged from about 91 to 97 m and the slope ranged approximately from 0 % to12 % (Figure 3.2).

TDR Description

Regular continuous and discontinuous 3-rod TDR probes were used to monitor the soil moisture during the growing season (Top and Davis, 1985; Baker and Allmaras, 1990) (Figure 3.4). A 20-cm regular continuous TDR (TDR20) and 15-cm regular continuous TDR (TDR15) were used to measure soil moisture at soil surface.

Discontinuous TDR probes of 150-cm (DTDR150) were used to measure soil water profile. As it is shown in Figure 3.4, each rod of DTDR150 consists of 5 parts (15, 20, 25, 25, and 25 cm, respectively) of 12.5 mm in diameter and 4 parts (10 cm each) of 6.3 mm in diameter. All the parts of 6.3 mm in diameter were coated with resin to make their diameter equal to 12.5 mm. Resin was chosen since it is a dielectric material. Each one of these discontinuities was used to separate two 12.5 mm parts. A typical wave for DTDR150 is shown in Fig.3.4.



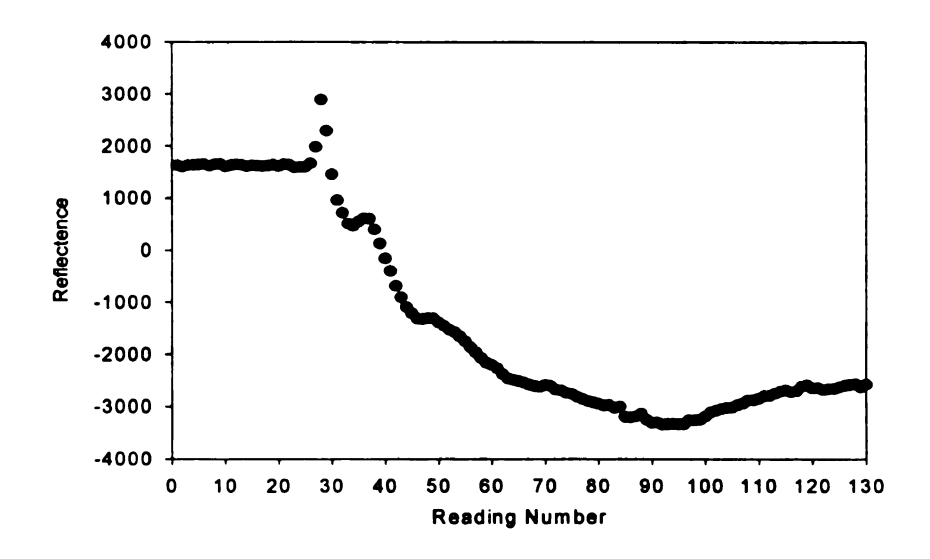


Figure 3.4. A discontinuous TDR probe (DTDR150) and a typical wave.

Each set of TDRs consisted of 5 TDR20, 1 TDR15, and 1 DTDR150 except the one that was located between L12 and L13 where only 4 of TDR20 were used. The 5 TDR20 were installed horizontally at 3, 6, 9, 12, and 15 cm depths to capture the dynamic and fast change of soil surface layer water content, while TDR15 and DTDR150 were installed vertically. The TDR15 was used to integrate the soil water content of the surface layer. The DTDR150 was used to measure the average soil water content from 0-15, 25-45, 55-80, 90-115, and 125-150 cm.

Data Analysis

The lateral downslope soil water flow (L, mm) was calculated as follows:

$$L = I - E_t - \Delta S - D$$

(10)

where I is infiltration (mm), E_t is total evaporation and it is equal to soil and plant evaporation (mm), ΔS is the change of soil water storage (mm), and D is vertical drainage (mm). Infiltration and E_t were estimated using CERES-WHEAT. The change of soil water storage was calculated from the difference between soil water content measurements. Vertical drainage was assumed zero because an impervious layer was preventing soil water to flow vertically out of the profile.

Results and Discussion

Trial and error procedure was used to solve Eq. [6] to find C at representative combinations of θ_s , θ_{dul} , and $\sin \gamma$. A power function relationship between C, $\sin \gamma$ and θ_{dul} was shown in Figure 3.5. This relation can be described as:

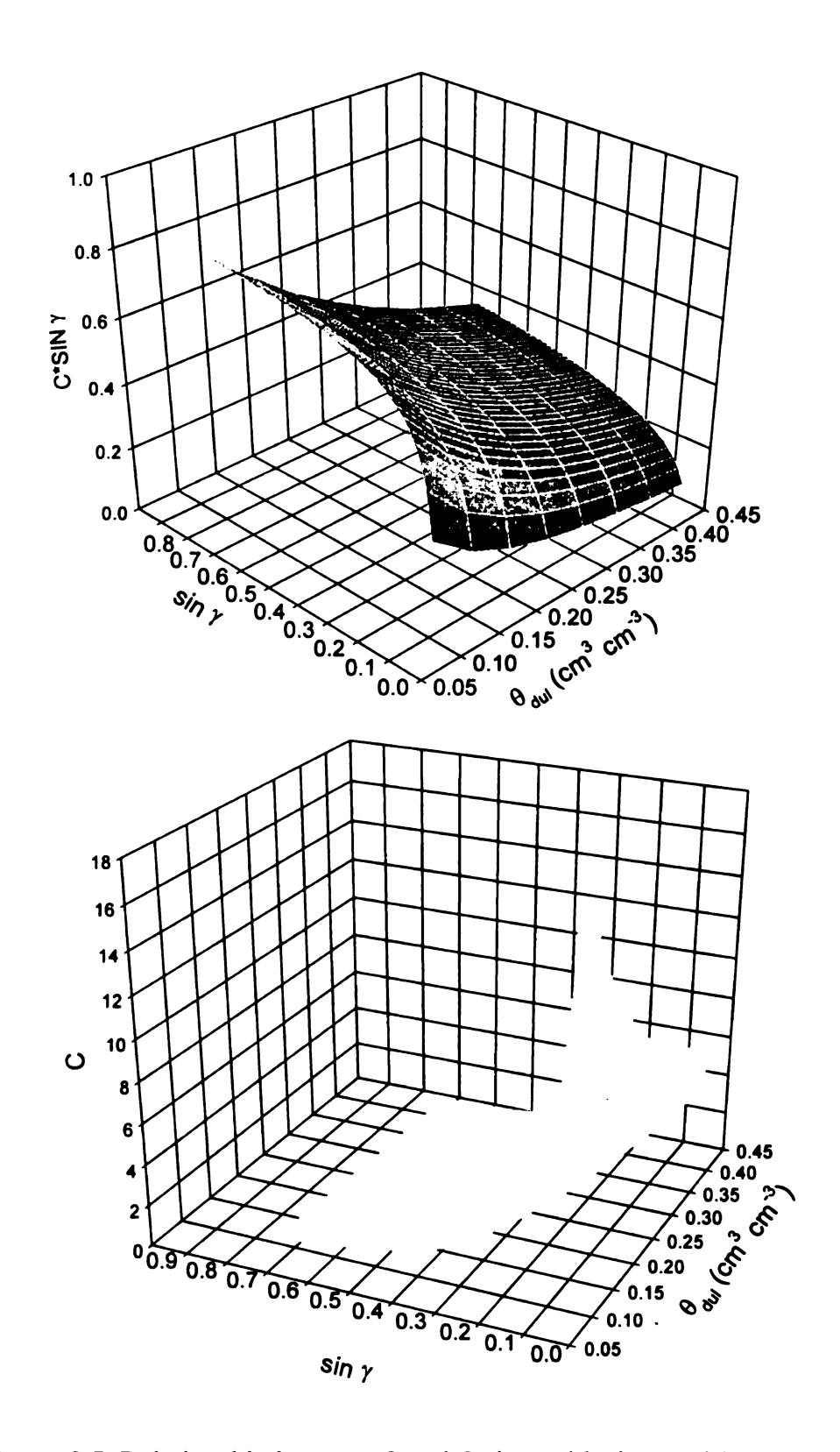


Figure 3.5. Relationship between C and C sin γ with sin γ and θ_{dul} at representative combinations of θ_{dul} and sin γ .

$$C = a_1 (\sin \gamma)^{b_1} \tag{11}$$

where a_1 and b_1 are functions of θ_{dul} and can be calculated as follows:

$$a_1 = -1.41\theta_{dul} + 1.02$$

and
 $b_1 = -1.27\theta_{dul}^2 + 0.99\theta_{dul} - 0.88$ (12)

The developed relationship can be used to estimate C directly from θ_{dul} and $\sin \gamma$ instead of using trial and error to solve for it. As it is shown in Figure 3.5 and Eq. [11] and Eq. [12], C is dependent on both $\sin \gamma$ (slope) and θ_{dul} . The higher $\sin \gamma$ and greater θ_{dul} the lower C and vise versa. Although C can be greater than 1, C $\sin \gamma$ must be less than 1 because C $\sin \gamma$ is ratio between the soil water that may drain in a day and total drainable water.

Numerical solution was used to investigate the impact of x_{\bullet} on the daily change of soil water content (0) of 1 cm thick by 200 cm long isotropic homogeneous layer of soil of uniform slope overlaying an impervious soil layer during lateral downslope soil water flow subject to (2) for 1 day. A time increment of 1 min and distance increment of 1 cm were used assuming that the hydraulic conductivity is constant during a time step of 1 min at any x_{\bullet} , 0 is uniform within a distance step of 1 cm at any time, and $\sin \gamma$ is the hydraulic gradient during the 1 day drainage. Representative combination of θ_s , θ_{dul} , and $\sin \gamma$ were used in the numerical solutions to find a relationship between C_{\bullet} (the fraction of soil water content that can be drained from the soil layer in a day at x_{\bullet}) with C and x_{\bullet} (cm). A logarithmic relationship between C_{\bullet} and x_{\bullet} and a linear relationship between C_{\bullet}

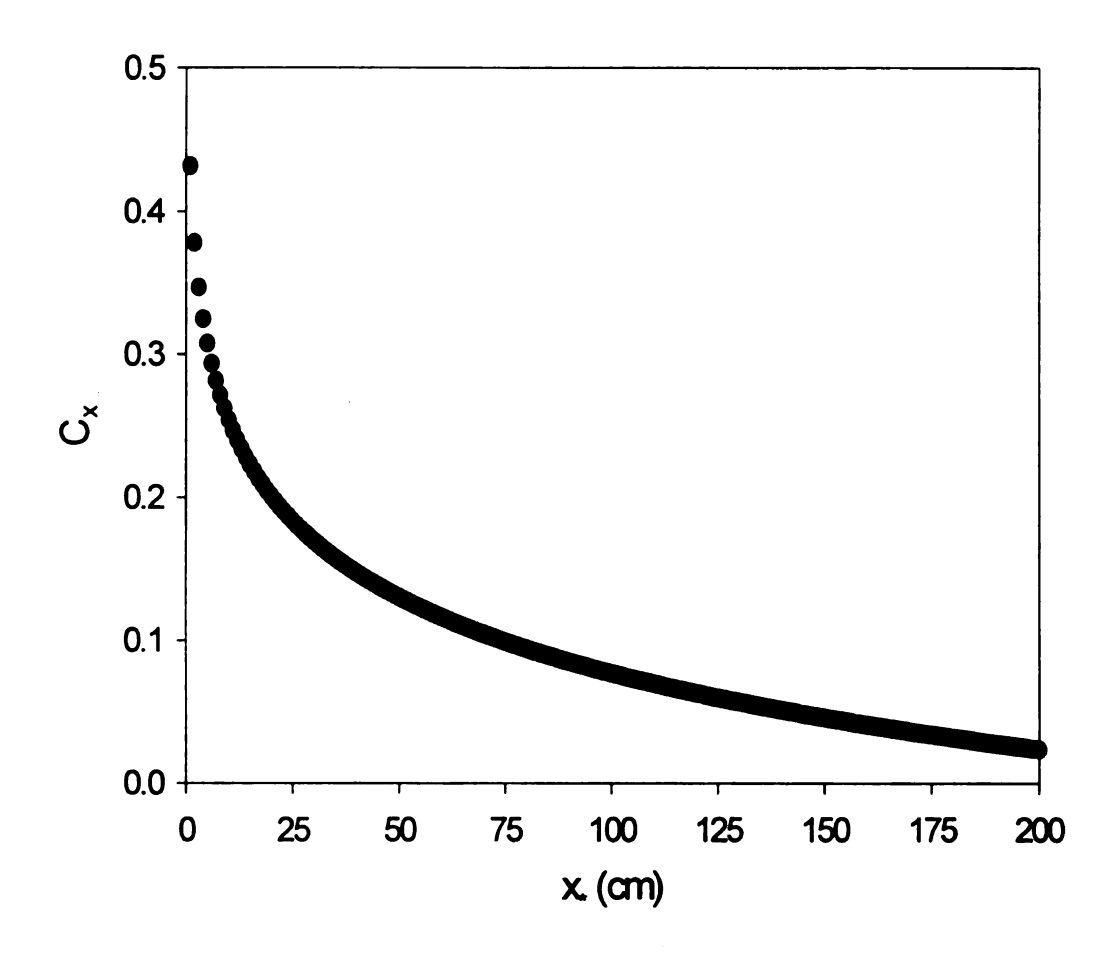


Figure 3.6. Example of a typical relationship between C_x and x. for a soil.

and C were found and they are shown in Figure 3.6. Using these relationships, C. can be obtained as follows:

$$C_* \sin \gamma = 1.13C \sin \gamma - 0.077 \ln(x_*) - 0.03 \tag{13}$$

if the calculated C_{\bullet} sin γ is less than 0 then it is assumed 0.

Using Eq. [11] and Eq. [13] suffices to describe lateral downslope drainage subject to (2). In many cases, non uniform slope and two dimensional lateral downslope soil water flow may complicate the use of Eq. [13]. An assumption can be made that x. has no impact on q. Parlange et al. (1986), Stagnitti et al. (1992), and Wallach and Zaslavsky (1991) have implemented similar assumption. Such an assumption maybe reasonable for watershed hydrology to estimate total drainage but to determine soil water content at any position within a field, such an assumption may decrease the accuracy of estimation. Another way of dealing with this problem is to study the relationship between incoming flux (Q_i, cm d⁻¹)) and C to a profile. Such relationship will remove the confusion of determining x. and its impact on C. More importantly, it will make it possible to combine the lateral downslope soil water flow model with a geographical information system (GIS) framework.

A generic relationship between $C_p \sin \gamma$ (C $\sin \gamma$ at any landscape position) and Q_i can be introduced as follow:

$$C_{p}\sin\gamma = a + b\ln(Q_{i} + \phi_{e}) \tag{14}$$

where Φ_e (cm³ cm⁻³) is soil effective porosity and equal to θ_s - θ_{dul} . Having in mind that (1) when $Q_i = 0$, C_p has to be equal to C and (2) when $Q_i = K_s \sin \gamma$, C_p is 0, a and b can

be defined as follows:

$$a = -b \ln(K_s \sin \gamma)$$
and
$$b = \frac{C \sin \gamma}{\ln(\phi_e) - \ln(K_s \sin \gamma)}$$
(15)

To explain Eq. [14] and Eq. [15], let us assume that a soil layer overlaying an impervious soil layer was located within a sloping landscape. The following were known: $\theta_s = 0.4 \text{ cm}^3 \text{ cm}^{-3}$, $\theta_{dul} = 0.2 \text{ cm}^3 \text{ cm}^{-3}$, and $\sin \gamma = 0.5$. The initial and boundary conditions are similar to (2). Using Eq. [11] and Eq. [12], C $\sin \gamma$ was found to be 0.32. Using Eq. [15], a was found to be 0.221 and b was found to be -0.061. Now, assuming that Q_i ranged from 0 cm d⁻¹ to 50 cm d⁻¹, applying Eq. [14] $C_p \sin \gamma$ against Q_i was plotted and shown in Fig.3.7. It was clear that $C_p \sin \gamma$ was equal to C $\sin \gamma$ when Q_i was $Q_i \cos Q_i \cos Q_j \cos$

In case of a profile that has both unsaturated layer on the top of a saturated soil layer that is overlaying an impervious layer, only vertical drainage is assumed to occur in the unsaturated layer.

Water table

A shallow water table was evident at all the observation well locations from April

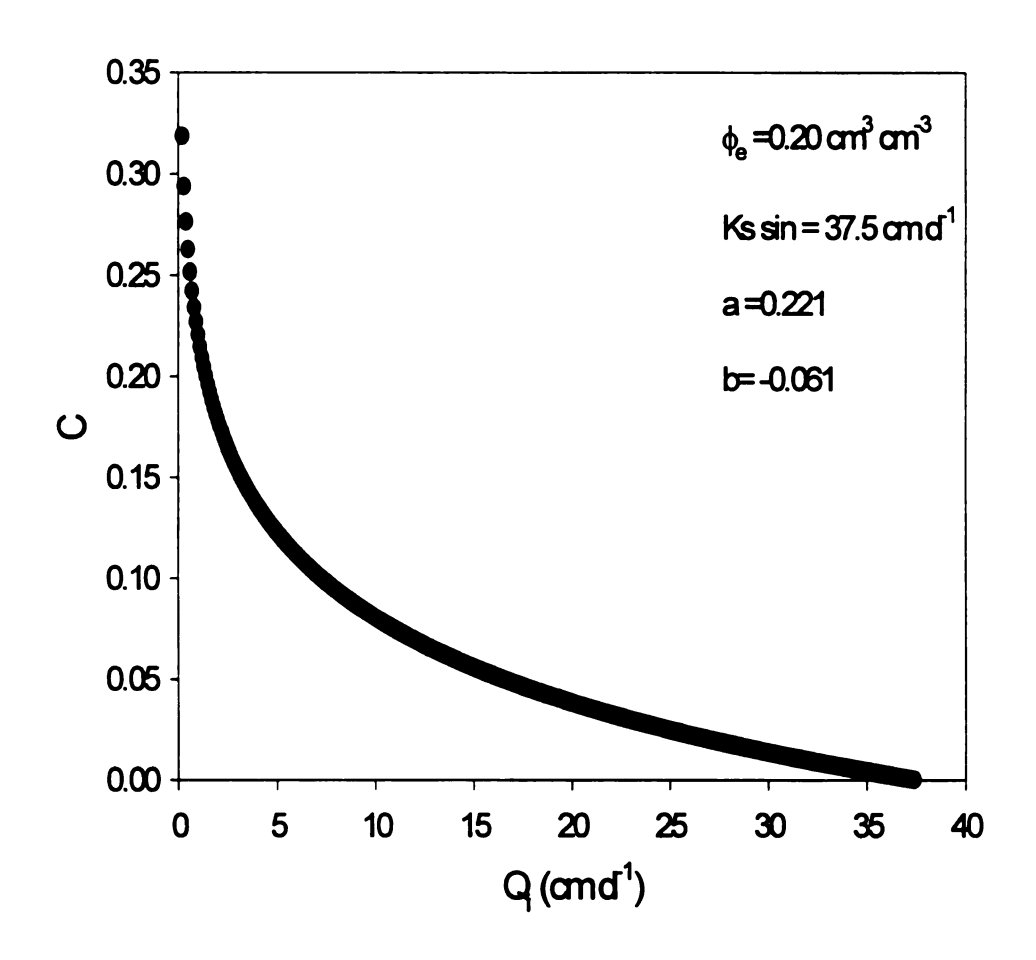


Figure 3.7. Example of a typical relationship between $C_{\mathfrak{p}}$ and $Q_{\mathfrak{i}}$ for a soil.

28 through May 22. On May 26, the water table level was below 150-cm for most of the observation wells (Figure 3.2). Existence of a water table in a sloping landscape is a sufficient proof of a lateral downslope soil water flow and depending on the slope such lateral downslope soil water flow can be significant since part of the soil profile is saturated. The shallower a water table level is, the greater lateral downslope soil water flow is, since more of the soil profile would be saturated and hence would contribute more significantly to the lateral downslope soil water flow.

The change of a water table level at a certain location depends on E_t, I, incoming and outgoing lateral downslope soil water flow, vertical drainage from upper soil layers, depth of the impervious layer and its effectiveness (depending on its K_s). The simulated (using Eq. [9]) and measured change of water table from DOY 124 to 146 was in good agreement at most access tube locations (Figure 3.8). The root mean square error (RMSE) was 2.84 cm during 22 days (from DOY 124 to 146). The maximum water table depth change was about 120 cm at L5 and the lowest was about 50 cm at L2.

Leaf Area Index

A significant growth of wheat and increase of LAI occurred on about DOY 105 and continued through DOY 130 (Figure 3.9.a and 3.9.b). A slow decrease of LAI started on about DOY 130 until about DOY 160, after which a rapid reduction of LAI took place until DOY 185 at all locations. Some variation of LAI at different location was noticed as early as DOY 115. Maximum LAI varied within these locations and ranged from 1.7 at L5 to 3.3 at L15. The standard deviation of LAI was greatest when the mean LAI was highest on about DOY 133.

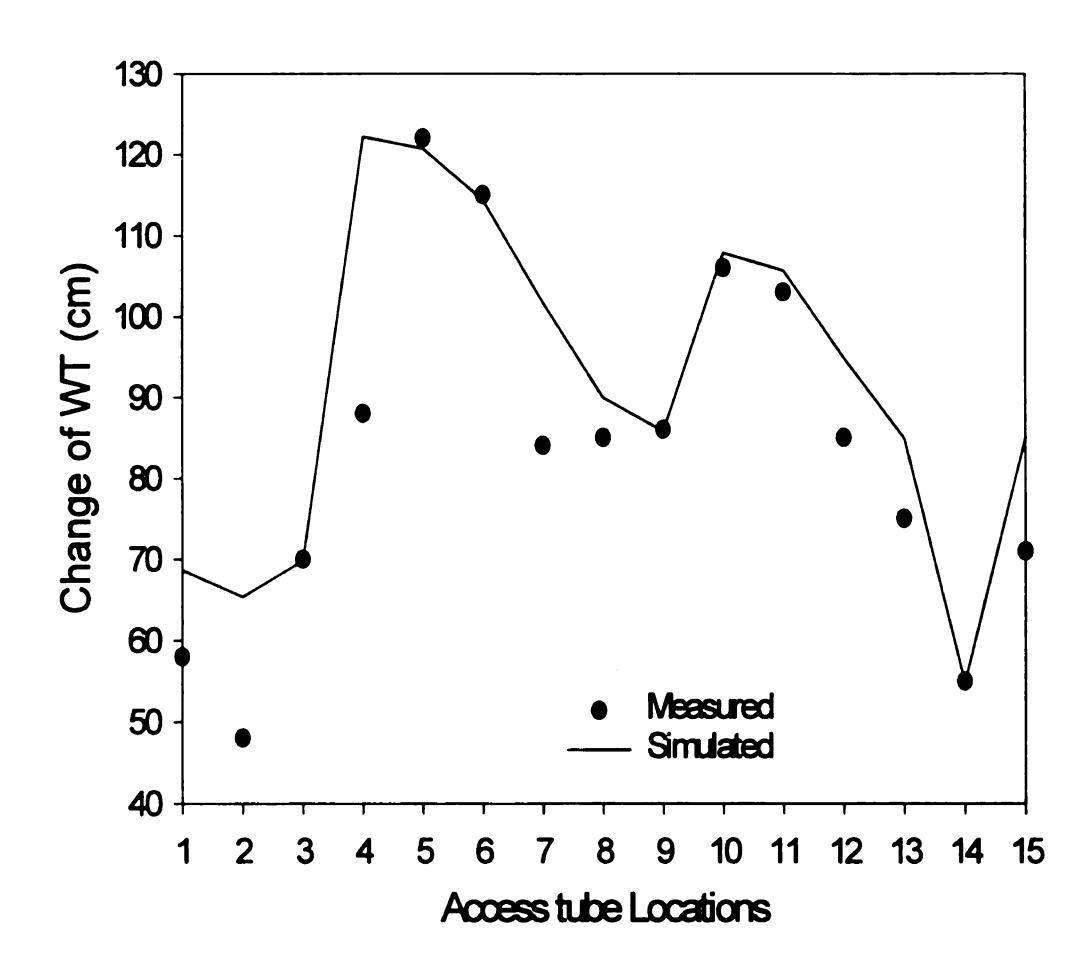


Figure 3.8. Measured and simulated change of soil water table depth (cm) from DOY 124 to 146.

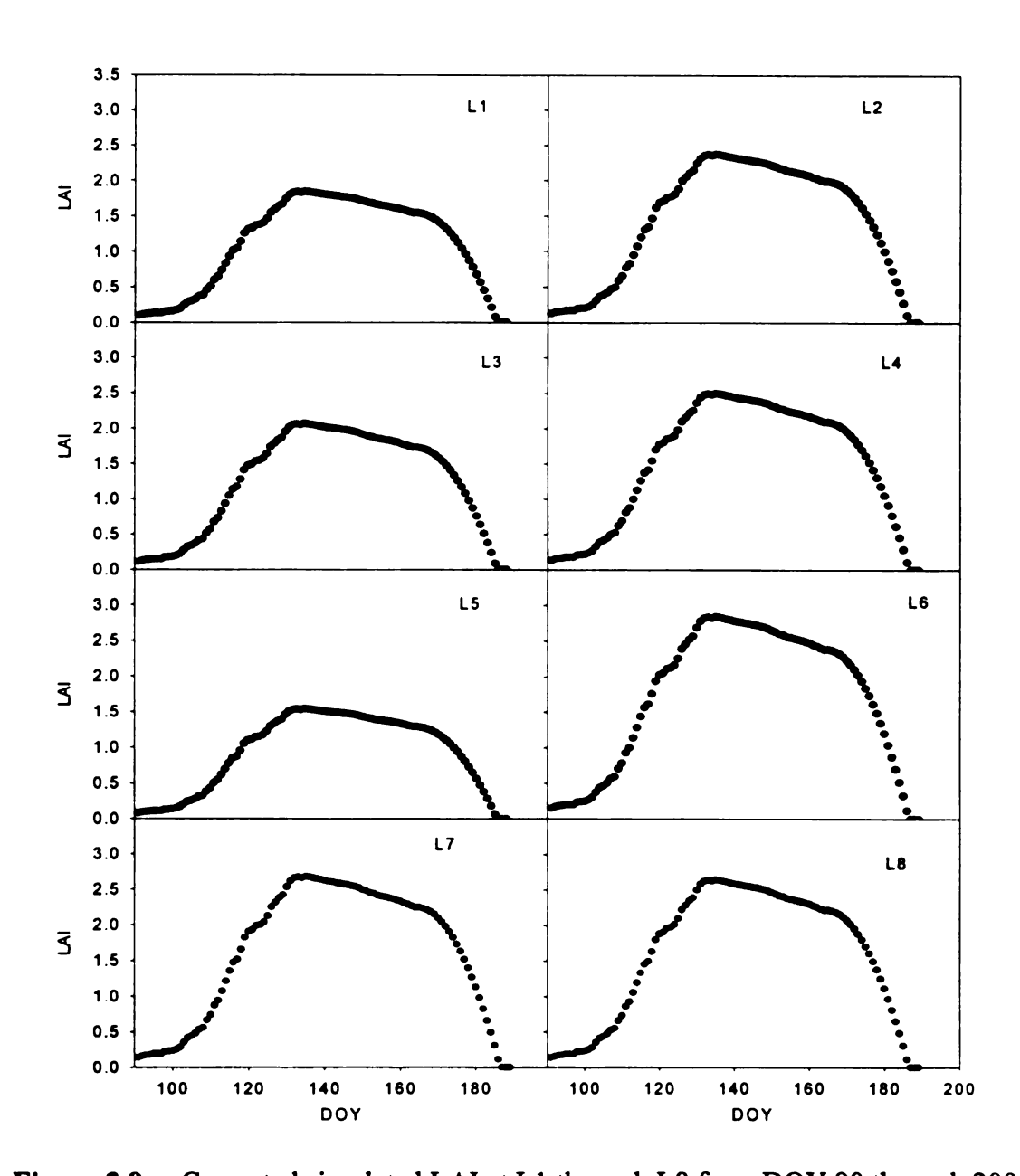


Figure 3.9.a. Corrected simulated LAI at L1 through L8 from DOY 90 through 200.

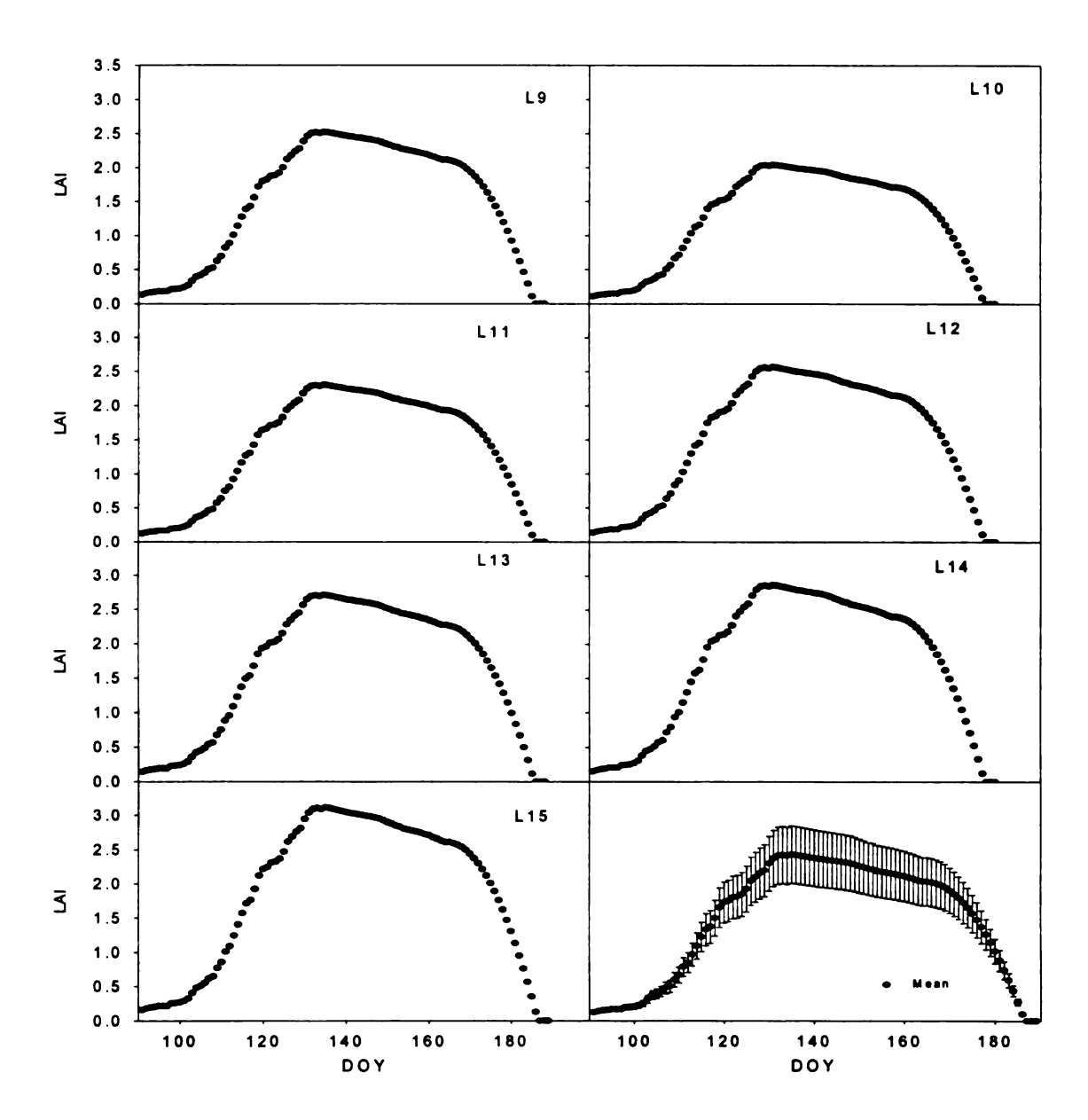


Figure 3.9.b. Corrected simulated LAI at L9 through L15 from DOY 90 through 200 and mean and standard deviation of LAI for the 15 locations.

Total Evaporation and Infiltration

Mean and standard deviation of simulated actual (E_{ta}) and potential (E_{tp}) daily evapotranspiration at all locations during the entire growing season are shown in Figure 3.10. There were no significant differences at different locations in respect to E_{ta} and E_{tp} . Daily E_{ta} ranged from 0.5 mm to 4.5 mm, whereas daily E_{tp} ranged from 1.5 mm to 7.5 mm. The highest E_{ta} occurred when soil surface was wet as on DOY 100 and 180. It was noticed that daily simulated E_{ta} decreased continuously from about 3.5 mm on DOY 125 to about 0.8 mm at DOY 151 because of dry conditions from DOY 125 through 151. The CERES-WHEAT underestimated E_{ta} because it is sensitivity to water stress. Because the water table could have supplied enough water to wheat root to prevent any water stress, it was assumed that E_{ta} was equal to E_{tp} during the period from DOY 124 to 146.

There was clear evident in the field that significant runoff took place between DOY 95 and DOY 124. The runoff mainly resulted because of the heavy rainfall events that occurred during that period (Figure 3.3) and because the soil was saturated. On the other hand, only six rainfall events occurred from DOY 125 through DOY 151 on DOY 125, 126, 129, 132, 134, and 145. The infiltration at all these dates was assumed to be equal to rainfall because each one of these rainfall events was less than 3.1 mm (Figure 3.3).

Lateral downslope soil water flow

The duration from DOY 124 through 146 was selected in order to study the lateral downslope soil water flow during it because during this period infiltration could be estimated accurately and a shallow water table was present at all locations. Estimated C ranged from about 5 to about 35, whereas estimated C sin γ ranged from about 0.12 to

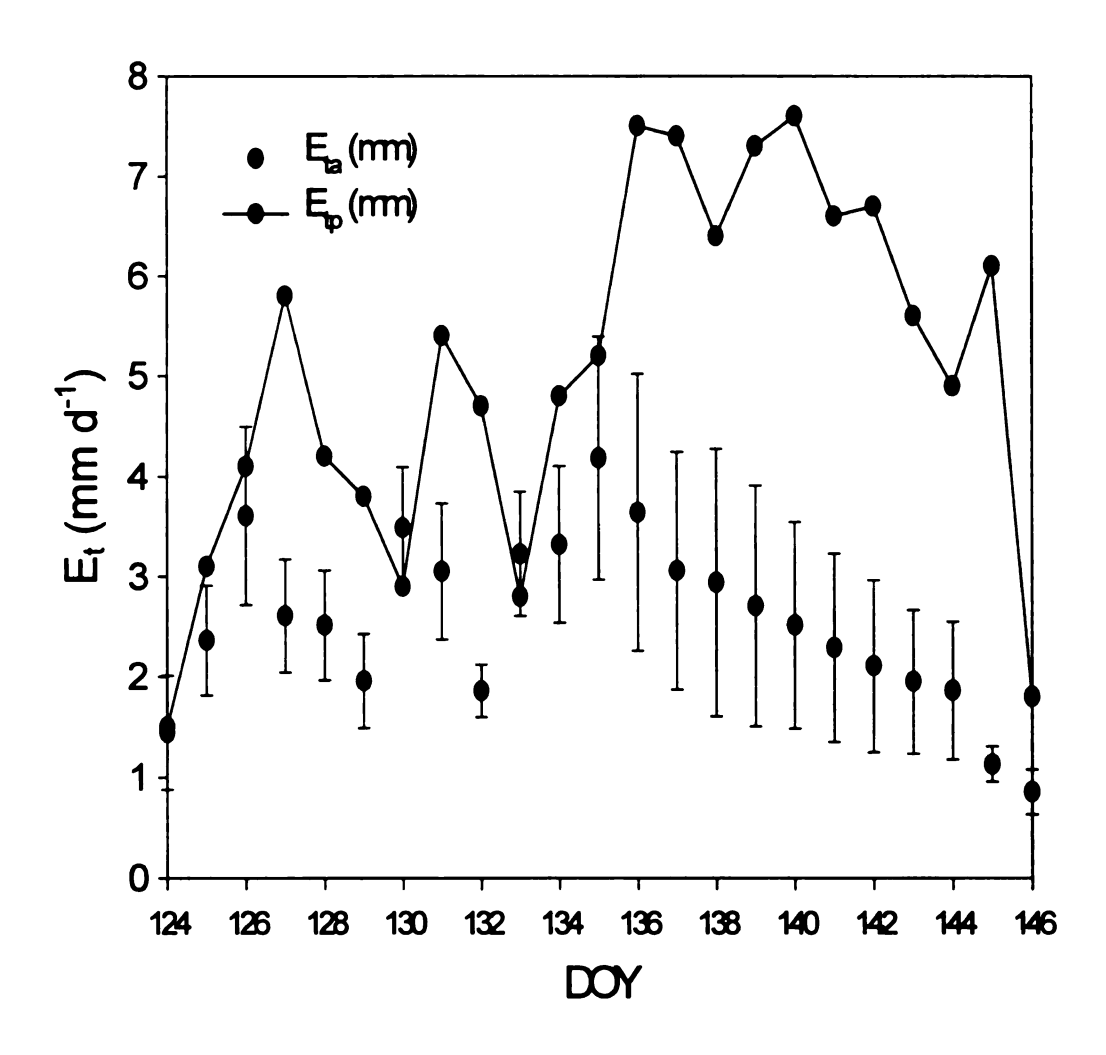


Figure 3.10. Mean and standard deviation of simulated daily actual (E_{ta}) and potential (E_{tp}) evapotranspiration from DOY 124 to 146.

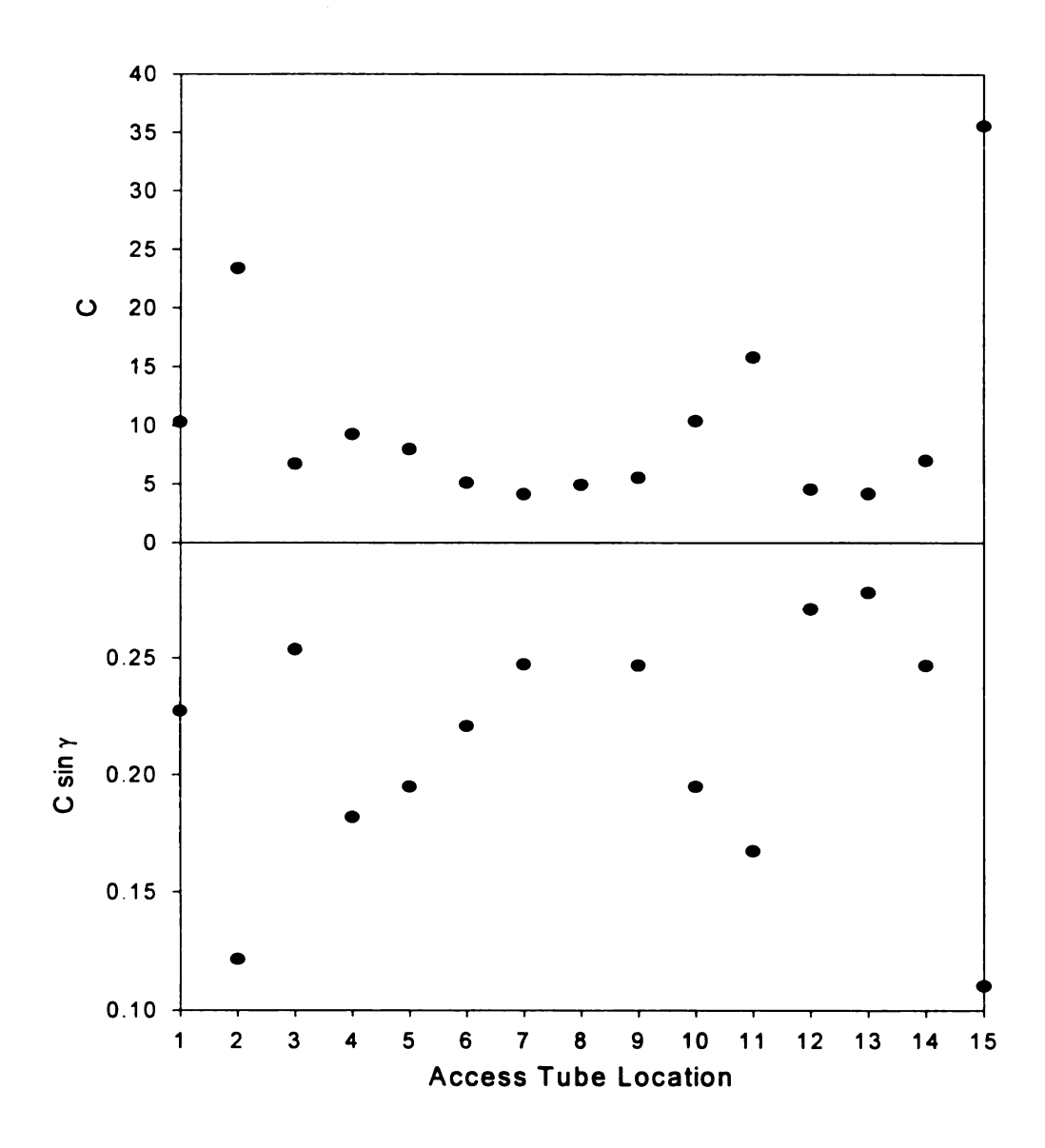


Figure 3.11. Estimated C and C $\sin \gamma$ at all access tube locations.

28 through May 22. On May 26, the water table level was below 150-cm for most of the meanwhile $C \sin \gamma$ was highest at these locations. On the contrast, C was greatest at L2, and L15 and $C \sin \gamma$ was minimum at these locations. The driving force for lateral downslope soil water flow is $\sin \gamma$ (slope), yet $C \sin \gamma$ determines the amount of lateral downslope drainage.

Estimated and measured cumulative lateral downslope drainage (L, mm) during that duration (22 days) for 3 different periods (124-132, 132-140, 140-146) at different access tubes locations are shown in Figure 3.12. During 124-132, estimated and measured cumulative L was in good agreement with RMSE of 4.41 mm. The L ranged from about 30 mm to 55 mm during DOY 124-132. During 132-140 and 140-146, estimated and measured cumulative L was relatively in good agreement with RMSE of 16.3 mm and 8.7 mm, respectively. The higher RMSE in these two periods, 132-140 and 140-146, could have resulted from uncertainties of estimating E₁₆. However, in general the new lateral downslope soil water flow model performed good in estimating the downslope lateral soil water flow at most access tube locations during the 3 periods.

Time domain reflectometry (TDR) measurements at the middle between L12 and L13 showed more details about lateral downslope results than was obtained from neutron probe measurements (Figure 3.13). The estimated daily L was in good agreement with the measured ones with RMSE of 1.81 mm d⁻¹. The simulated L was close to measured L on DOY 125, 126, 127, and 128 and 136 through 146. From DOY 129 though 135, deviation between measured and simulated daily L was evident. This deviation can be contributed to uncertainties of estimating E_{ta}. The maximum absolute difference between daily measured and simulated L was about 4 mm on DOY 131. From DOY 137 through 146,

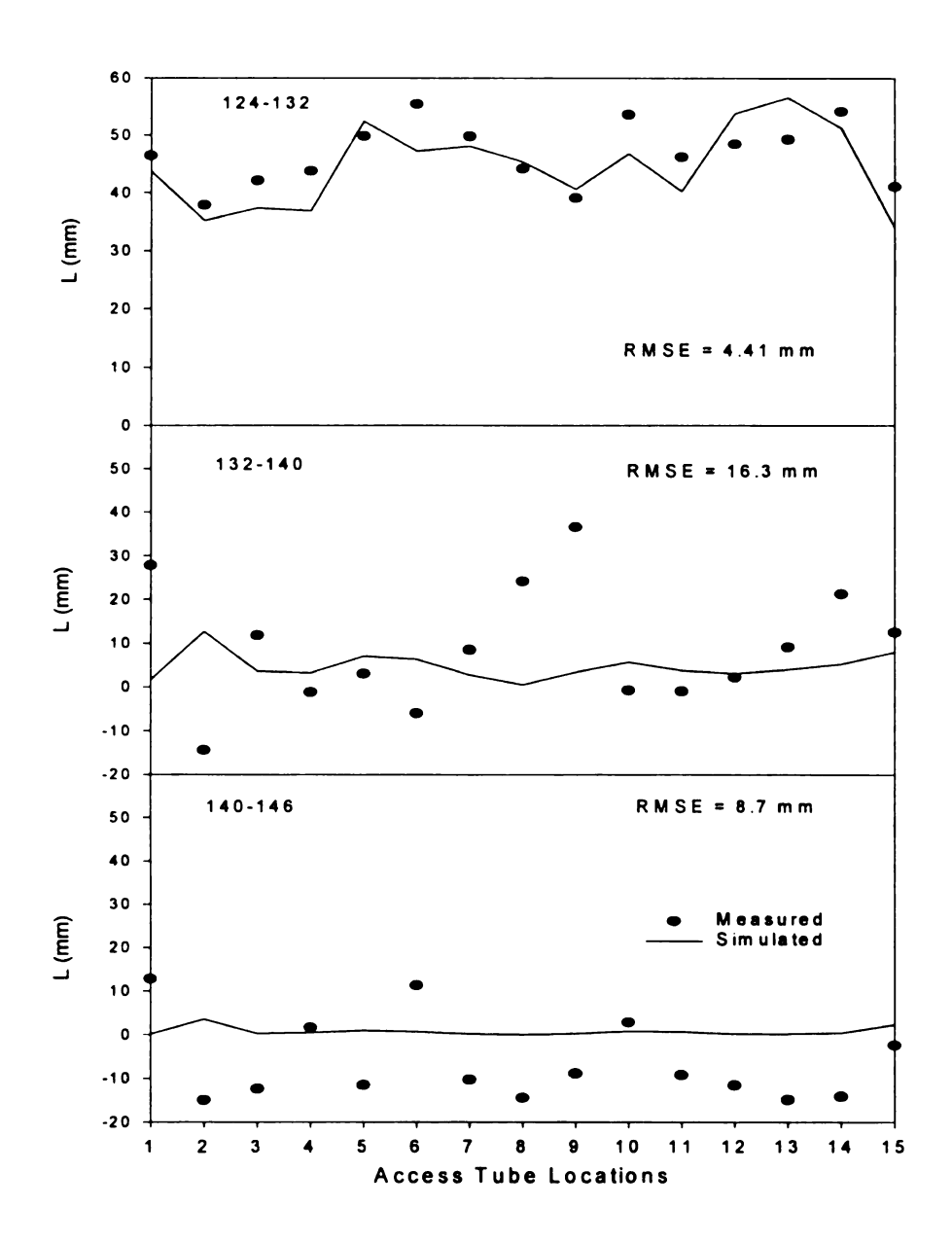


Figure 3.12. Measured and simulated cumulative lateral down slope (L) flow at all access tube locations from DOY 124-132, 132-140, and 140-146.

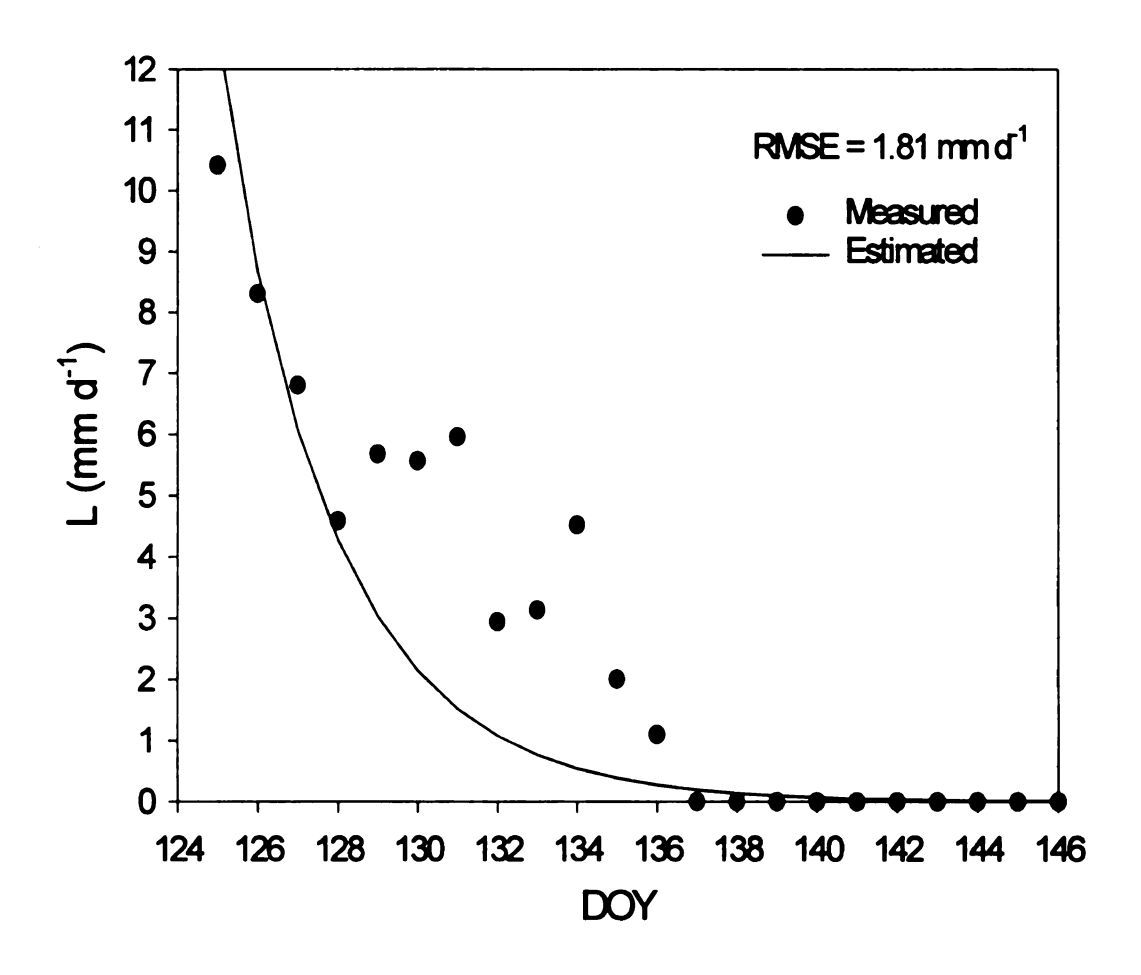


Figure 3.13. Measured and simulated daily lateral downslope soil water flow (L) at the middle of L12 and L13.

measured daily L was assumed 0 whenever negative values was calculated.

Conclusions

A generic simple functional model was developed to simulate daily lateral downslope drainage along a hillside. Saturated and drained upper limit soil water contents and slope angle (or the hydraulic gradient) are needed to run the new lateral downslope soil water flow model. The developed model was built based on physical basis and tested with real field data. Although the new model is simple, it performed well under field conditions.

The developed lateral downslope soil water flow model was built in a way that makes it possible to link it to a GIS package. A GIS can determine the directions of stream flow lines, while the lateral downslope model can account for the amount of soil water that may drain in a day at any position of a landscape. Such combination will produce a two-dimensional lateral downslope soil water flow.

Future studies are necessary to evaluate the developed lateral downslope model under different environmental conditions and for diverse soils within different landscapes. Minimizing the soil water balance variables (as studying lateral downslope soil water flow from a saturated soil with its surface covered) will help verify the model more accurately. Other useful studies will be that link the new lateral downslope model to a GIS framework because that will produce simple yet powerful functional two dimensional lateral downslope soil water flow models.

References

- Baker, J.M, and R.R. Allmaras. 1990. System for automating and multiplexing soil moisture measurements by time-domain reflectometry. Soil. Sci. Soc. Am. J. 54:1-6.
- Beven, K. 1982. On subsurface stormflow: predictions wish simple kinematic theory for saturated and unsaturated flows. Water Resour. Res. 18(6):1627-1633.
- Bouraoui, F., G. Vachaud, R. Haverkamp, and B. Normand. 1997. A distributed physical approach for surface-subsurface water transport modeling in agricultural watersheds. J. Hydrol. 203:79-82.
- Gerakis, A., and J.T. Ritchie. 1998. Simulation of atrazine leaching in relation to water table management using CERES model.
- Hillel, D. 1977. Computer simulation of soil-water dynamics: a compendium of recent work. Ottawa, IDRC.
- Jackson, C.R. 1992. Hillslope infiltration and lateral downslope unsaturated flow. Water Resour. Res. 28 (9):2533-2539.
- Jackson, C.R. 1993. Reply. Water Resour. Res. 29 (12):4169.
- McCord, J.T., D.B. Stephen, and J.L. Wilson.1991. Hysteresis and state-dependent anisotropy in modeling unsaturated hillslope hydrologic processes. Water Resour Res. 27 (7):1501-1518.
- Nieber, J.L., and M.F. Walter. 1981. Two-dimensional soil moisture flow in a sloping rectangular region: experimental and numerical studies. Water Resour Res. 17(6):1722-1730.
- Nielsen, D.R., J.W. Biggar, and K.T. Erh. 1973. Spatial variability of field-measured soilwater properties. Hilgardia 42:215-259.
- Philip, J.R. 1991. Hillslope infiltration and lateral downslope unsaturated flow. Water Resour Res. 27(1):109-117.
- Ritchie, J.T. 1972. Model for predicting evaporation from a row crop with incomplete cover. Water Resour. Res. 8:1204-1213.
- Ritchie, J.T., A. Gerakis, and A.A. Suleiman. 1999. Simple Model to Estimate Field-Measured Soil Water Limits. Trans. ASAE. (In review).

- Rosek, M.J. 1995. Spatial and temporal soil water content changes within a sloping landscape. Doctoral Dissertation. Crop and Soil Department. Michigan State University. Michigan. USA.
- Smith, R.E., and R.H.B. Hebbert. 1983. Mathematical simulation of interdependent surface and subsurface hydrologic processes. J.Y. Parlange. Water Resour Res. 19 (4):987-1001.
- Stagnitti, F., M.B. Parlange, T.S. Steenhuis, and J.Y. Parlange. 1986. Drainage from a uniform soil layer on a hillslope. Water Resour Res. 22 (5):631-634.
- Stagnitti, F., J.Y. Parlange, T.S. Steenhuis, M.B. Parlange, and C.W. Rose. 1992. A mathematical model of hillslope and watershed discharge. Stagnitti, F., M.B. Parlange, T.S. Steenhuis, and J.Y. Parlange. 1986.
- Suleiman, A.A., and J.T. Ritchie. 1999. Estimating saturated hydraulic conductivity from drained upper limit water content and bulk density. Trans. ASAE. (In review).
- Teich, A.H., J. Fregeau-Reid, and L. Seaman. 1992. AC Ron winter wheat. Can. J. Plant Sci. 72:1235-1238.
- Topp, G.C., J.L. Davis. 1985. Measurement of soil water content using time-domain reflectometry (TDR): A field evaluation. Soil Sci. Soc. Am. J. 49:19-24.
- Tsuboyama, Y., R.C. Sidle, S. Noguchi, and I. Hosoda. 1994. Flow and solute transport through the soil matrix and macropores of a hillslope segment. Water Resour. Res. 30 (4):879-890.
- Wallach, R., and D. Zaslavsky. 1991. Lateral flow in a layered profile of an infinite uniform slope. Water Resour. Res. 27 (8):1809-1818.
- Warrick, A.W., P.J. Wierenga, and L. Pan. 1997. Downward water flow through sloping layers in the vadose zone: analytical solutions for diversions. J. Hydrol. 192:321-337.

CHAPTER FOUR

ASSESSING AND MODELING THE SPATIAL VARIABILITY OF WHEAT YIELD WITHIN A SLOPING LANDSCAPE

Introduction

Differences in crop production within agricultural fields vary by a factor of two to four (Bouma et al., 1995). Field variability of crop yield is a consequence of variations in the genetic properties of plants and in the microenvironment (Bresler et al., 1981). Within a field, variability of crop yield is a primarily consequence of environmental factors since the genetic properties of the plants are similar. Among environmental factors, soil variability is the major cause of variation of crop yield in a given field. Although, climatic variables (solar radiation, air temperature, and precipitation) do vary within a field, they can be assumed to be constant. Soil variability can be attributed to variations in soil properties, such as hydraulic conductivity, drained upper limit soil water content, and cation exchange capacity, and variations in other soil variables, such as soil water, soil nutrients, and organic matter. (Berndtsson and Bahri, 1995).

Among the various environmental stress factors that limit global crop productivity, water deficit is probably the most limiting factor (Boyer, 1982). The nature and extent of damage, the ability of a plant to recover, and the degree to which the economic yield of a crop is affected depend on the developmental stage at which a plant encounters water deficit (Saini and Lalonde, 1998). Movement of water from one soil profile to another may be enough to prevent such water deficit or reduce its impact in some areas within a field.

Sloping landscapes enhance the spatial variability of crop yield within a field

because they heighten the variability of soil properties as well as soil variables. The soil water downslope flow, surface and subsurface, causes differences in amount of soil water available to plants (Verity and Anderson, 1990; Halvorson and Doll, 1991), depth of topsoil (Pennock and de Jong, 1990), and nutrient availability. A significant relationship between crop yield and landscape position has been demonstrated by several researchers (Fiez and Miller, 1995; Halvorson and Doll, 1991; and Moulin et al., 1994). Measurements and analysis of the spatial variability of fields are two important aspects of site-specific crop management (Yang et al., 1998). However, assessing the spatial variability of soil properties and crop yield by classical techniques is time consuming and expensive. Remote sensing, on the other hand, could provide inexpensive large-area estimates of crop variability within a field. In a study on a wheat field, Mass (1993) demonstrated that the use of remotely sensed infrared images enabled a crop simulation model to predict the crop yield quite accurately. The CERES-Wheat model, as described by Ritchie and Otter (1985), has been used to simulate crop yield accurately when all the input data are available. Integrating CERES-WHEAT model with remote sensing is a good approach to simulate crop yield variability within a field because in most cases data that characterize soil variability within a field are not available.

The objectives of this research were to (1) assess the spatial variability of soil properties and variables, leaf area index (LAI), and wheat yield within a sloping landscape, (2) evaluate the performance of CERES-WHEAT model within a sloping landscape, and (3) integrate remote sensing and CERES-WHEAT to simulate the spatial variability of wheat yield within a sloping landscape.

Materials and Methods

A field experiment was conducted to (1) assess the spatial variability of soil properties and variables, leaf area index (LAI), and wheat yield within a sloping landscape, (2) evaluate the performance of the CERES-WHEAT model within a sloping landscape, and (3) integrate remote sensing and CERES-WHEAT to simulate the spatial variability of wheat yield within a sloping landscape. A 100 m x 600 m field was planted to AC Ron (described by Teich et al., 1992) winter wheat variety on October 19, 1997 and harvested on July 15, 1998 in East Lansing, MI. In order to monitor the soil water content at different landscape positions along the slope, fifteen 150-cm access tubes were installed 20-m apart after planting along a transect perpendicular to the contour lines (Figure 4.1). To label the locations in which access tubes installed, the further north location was labeled as L1, the second further north was labeled as L2, and so on until L15. A neutron probe reading was taken on November 15, 1997, right after the installation of the access tubes. Other neutron probe readings were taken from April 15, until harvest in 1998 at one week intervals and after rain events. Measurements were made at depths of 15, 30, 45, 60, 90, 120, and 150 cm. Another access tube (L16) was installed in an area that showed less plant growth within the southern part of the field in mid May 1998. This area was selected based on a remotely sensed image that was captured on April 28. The location access tubes is shown in Figure 4.1. Daily maximum and minimum temperatures, solar radiation, and rainfall were recorded and shown in Figure 4.2 and Appendix B. Three other rain gauges were installed 150-m apart parallel to the access tubes transect to assess the spatial variability of rainfall. Manual measurements of these rain gauges were done after rain events. Along the transect of

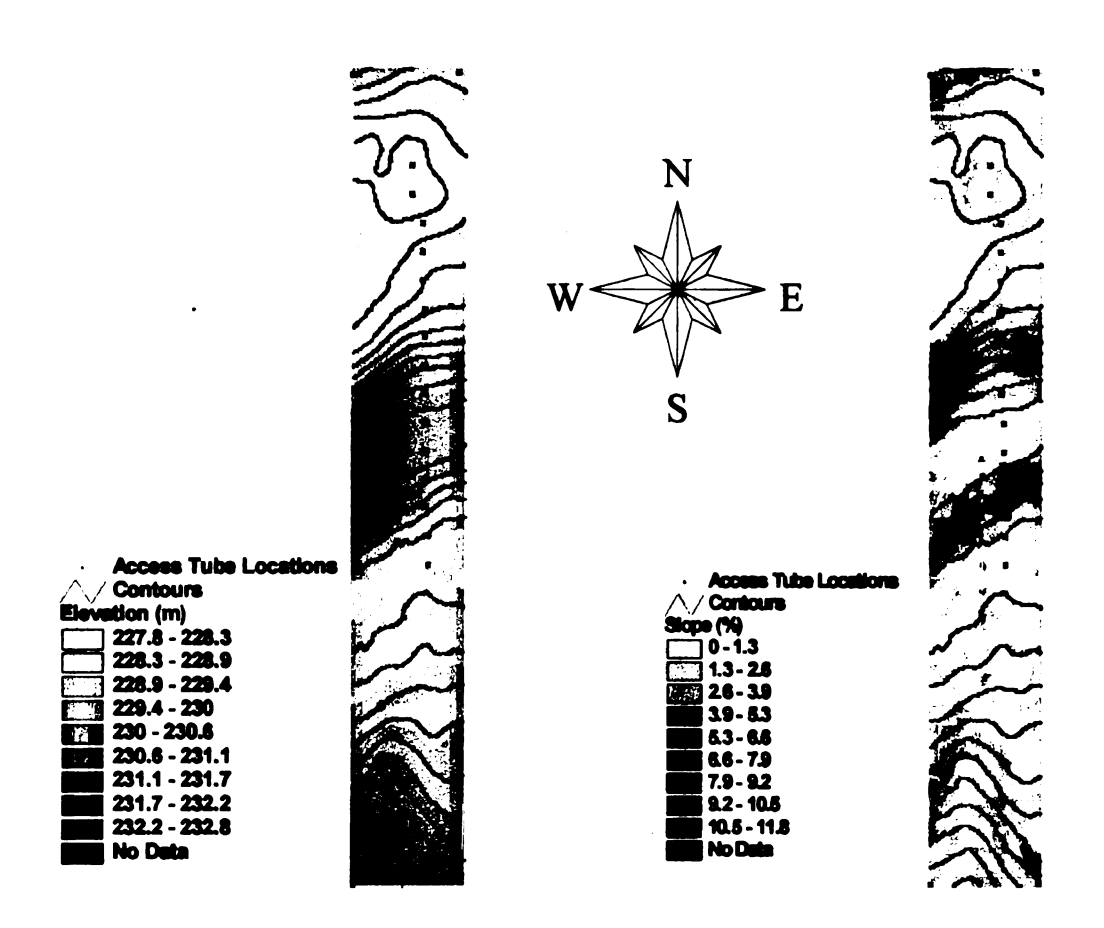


Figure 4.1. Elevation, contours, slope, and access tube locations within the experimental field.

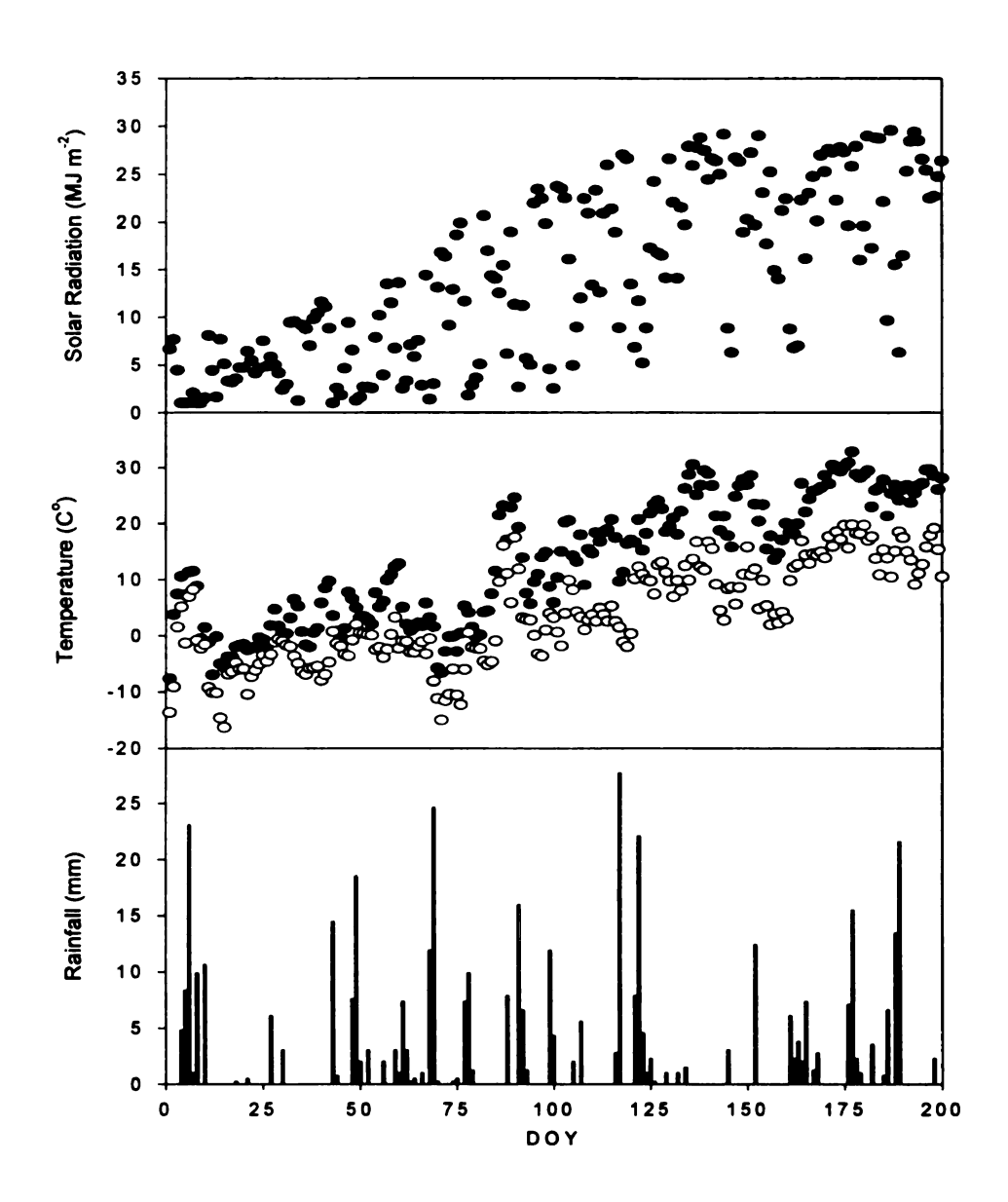


Figure 4.2. Daily solar radiation, maximum (Tmax) and minimum (Tmin) temperature, and rainfall from DOY 1 through 200 in 1998.

access tubes, leaf area index (LAI) was measured near each of the access tubes weekly from April 15 until anthesis date (June 4) using LAI-2000 (LI-COR, model LAI-2000) (Welles and Norman, 1991). Four infrared images were captured by an airplane on April 4, April 28, June 4, and July 10, 1998 to assess the spatial variability of wheat growth within the field (Figure 4.3).

Using a square of 1 m², plant density was counted near each access tube location on April 15, 1998. Two 1 m² wheat samples were harvested manually near each of the access tube locations to measure heads number, grain per head, head weight, unit grain weight, grain number, and grain yield on July 10, 1998. The field was harvested on July 15, 1998 using a combine equipped with Global Positioning System (GPS) and yield monitor.

Site Description

The soil of the 6 ha field is classified as Capac series. According to soil survey, a Capac series consists of somewhat poorly drained, moderately and moderately slowly permeable soils on till plains and moraines. These soils formed in medium- and moderately fine-textured deposits. While installing the access tubes, disturbed soil samples were taken at depths of 0-15, 15-30, 30-60, 60-90, 90-120 and 120-150 cm at each access tube location. Clay and sand, total nitrogen, and organic matter content were determined for each soil sample and are shown in appendix A. The soil water limits were estimated using the procedure described by Ritchie et al. (1999). Three trenches were opened at L10, L15, and L16 to study the soil profile at these locations. The elevation was measured at about 300 representative locations in the field using a theodolite. The range of elevation was approximately 227 to 231 m, and the slope ranged from

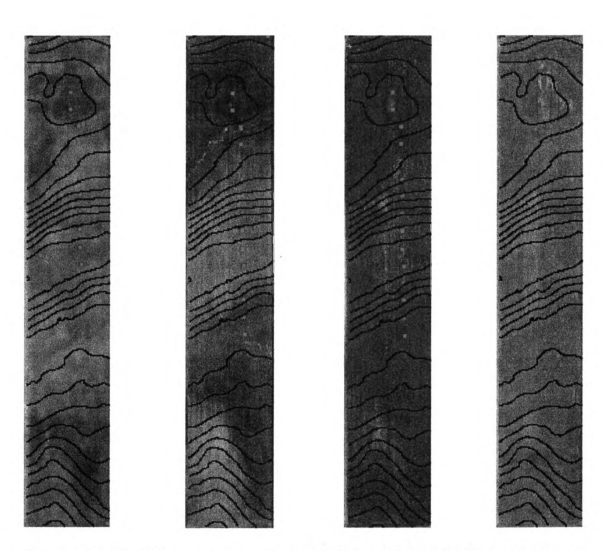


Figure 4.3. Infrared images were captured (from left to right) on April 4, April 28, June 4, and July 14, 1998.

approximately 0 to 12 % (Figure 4.1).

Field Management

The eastern part of the field was planted to corn in 1995, 1996 and 1997, while the western part of the field was planted to corn in 1995, 1996, and to wheat in 1996-1997.

Manure was spread on September 4, 1997 and then the field was plowed then disced on October 14. AC Ron winter wheat (325 seeds m⁻²) was sown on October 19, 1998.

Harmong Extra (0.3 oz/ac) was spread in the field on April 22, 1998 for weed control.

Urea (150lbs/ac) was spread on April 23, 1998. Drainage pipes were installed in the northen part of the field.

Normalized Difference Vegetation Index and LAI

The Normalized Difference Vegetation Index (NDVI), also referred to as vegetation index, was developed by Kriegler et al. (1969). This index can vary between -1 and 1 and is calculated as follows:

$$NDVI = \frac{NIR - R}{NIR + R} \tag{1}$$

where NIR and R are near infrared and red bands, respectively.

A linear relationship was assumed between LAI and NDVI as follows:

$$LAI = a + bNDVI (2)$$

where a and b are constants. Both a and b can vary significantly from one infrared image to another. On April 28 and June 4, measured LAIs near the access tube locations were

used as reference points to estimate a and b for the corresponding images. On the other dates, LAI was not estimated from infrared images since April 4 and July 14 images showed no spatial variability within the field.

Integrating CERES-WHEAT Model and Remote Sensing

The CERES-WHEAT model estimates the grain number per square meter based on stem weight per square meter at anthesis, adjusted using a genetic coefficient (G1). Because LAI can be obtained from infrared images, a relationship between stem weight and LAI is needed to allow the use of the CERES-WHEAT model for estimating yield by using infrared imagery. A linear relationship between LAI and stem weight (S, kg ha⁻¹) at anthesis was proposed as follows:

$$S = c + dLAI \tag{3}$$

where c and d are constants. To find c and d, CERES-WHEAT was run for different environmental conditions. A relationship between simulated S and LAI was built.

To simulate grain yield for each pixel (1 m²) within the field, the following steps were followed:

- (1) Estimating LAI from NDVI using Eq. [2] for each pixel of June 4th image. In our experiment the anthesis was on June 4th.
- (2) Eq. [3] was then used to estimate S at each pixel of June 4th image. Then, CERES-WHEAT was run to simulate grain number at each pixel. Assuming no nitrogen and water stress, a unit weight of a grain was simulated and assumed to be constant within the field. By definition grain yield can be calculated by multiplying grain number by unit grain weight.

Results and Discussion

Spatial Variability Along Access Tube Transect

Total nitrogen content of the soil surface layer varied spatially and ranged from about 0.1 % at L11 to 0.7 % at L2 (Figure 4.4). The organic matter content of the soil surface layer also varied spatially and ranged from about 1.9 % at L15 to 12 % at L2. The clay and sand contents of the soil surface layer were correlated with elevation and landscape position. The sand content of the soil surface layer increased with increasing elevation, whereas the clay content of this layer tended to decrease with increasing elevation. The clay content of the soil surface layer ranged from about 10 % at L16 to 34% at L2, while the sand content of this layer ranged from about 20 % at L2 to about 55 % at L16. The bulk density of the soil surface layer varied from 1.31 g cm⁻³ to 1.47 g cm⁻³ at L14.

There was significant variability of plant density (PD) within the field (Figure 4.5). It varied from about 190 plants m⁻² at L6 to about 325 m⁻² at L1. A continuous significant decrease of PD occurred from L1 though L6. Maximum PD was found at the bottom of the hill, intermediate at top of the hill, and minimum at hillside. Heads number (HN) ranged from 270 heads m⁻² at L4 to about 445 heads m⁻² at L16. Highest HN was found at L16 and then at southern bottom of the hill, intermediate at top of the hill and northern bottom of the hill, and lowest at hillside. Number of grains per head (GNPH) varied from about 20 grain per head at L2 to 16 grain per head at L6. Greatest GNPH was found at the northern bottom of the hill, intermediate at top of the hill and southern bottom of the hill, and lowest at hillside. Head weight (HW) ranged from 1.4 g at L15 to 0.85 g at L5. Maximum HW was found at the bottom of the hill, intermediate at top

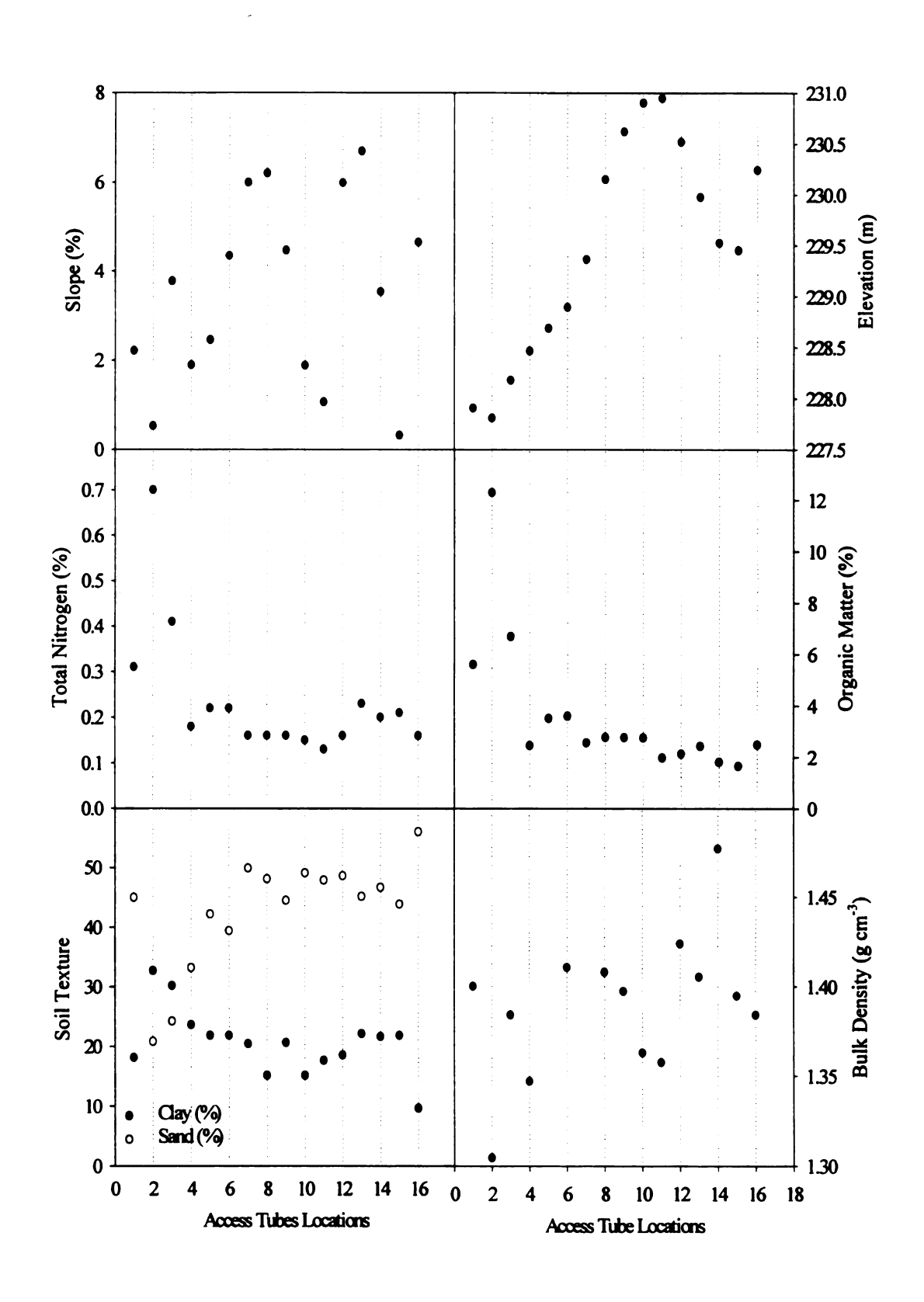


Figure 4.4. Elevation, slope, and some soil properties (total nitrogen, organic matter, soil texture, and bulk density) of the surface layer.

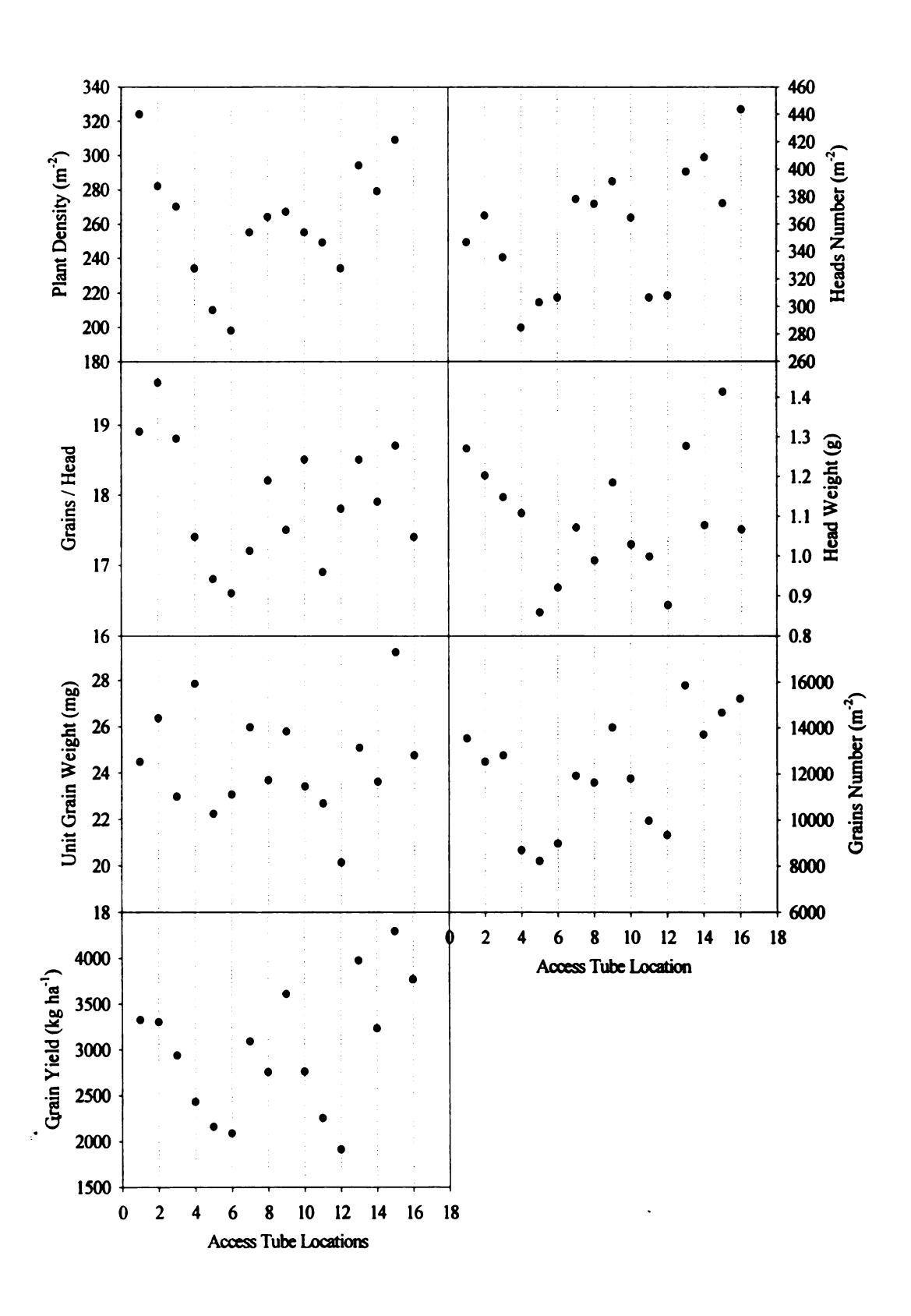


Figure 4.5. Crop characteristics at harvest time (plant density, heads number, number of grains per head, head weight, unit grain weight, grain number, and grain yield.

of the hill, and minimum at hillside. No significant variation was found among access tube locations in respect to unit grain weight. An average unit grain weight was 24.5 mg. Grain number (GN) varied significantly and ranged from about 8000 grains m⁻² to 16000 grains m⁻² at L13. Highest GN was found at L16 and southern bottom of the hill, intermediate at top of the hill and northern bottom of the hill, and lowest at hillside. Grain Yield (GY) varied significantly and ranged from 4400 kg ha⁻¹ at L15 to 1900 kg ha⁻¹ at L12. Greatest GY was found at southern bottom of the hill and L16, intermediate at top of the hill and northern bottom of the hill, and lowest at hillside.

Model Performance Along Access Tube Transect

Measured PD near each access tube location was used to run CERES-WHEAT in order to simulate GY accurately. Measured wheat grain yield ranged from 1827 kg ha⁻¹ at L5 to 4268 kg ha⁻¹ at L15 with an average of 2943 kg ha⁻¹ (Table 4.1). Simulated grain yield ranged from 1814 kg ha⁻¹ at L4 to 3791 kg ha⁻¹ at L15 with an average of 3251 kg ha⁻¹ (Table 4.1). It was clear that CERES-WHEAT gave good estimate of mean, minimum, and maximum GY. The difference between simulated and measured grain yield ranged from -615 kg ha⁻¹ at L4 to 1454 kg ha⁻¹ at L5 with an average of 308 kg ha⁻¹. However, the ratio of absolute error to measured grain yield ranged from 3% at L2 to 79% at L5. Simulated GY was within 15% error margin at 10 access tube locations; L1, L2, L6, L7,L9, L10, L13, L14, L15, and L16. The ratio of error to measured grain yield was 21, -25, 79, 19, 43, and 71 % at L3, L4, L5, L8, L11, and L12, respectively. The CERES-WHEAT performed best at bottom of the hill and least at hillside landscape position.

Table 4.1. Measured and simulated grain yield near all access tube locations.

Access tube	Measured Grain	Simulated Grain	Error
location	Yield	Yield	
		kg ha ⁻¹	
L1	3325	3574	204(7%)*
L2	3301	3408	107(3%)*
L3	2936	3549	613(21%)
L4	2429	1814	-615(-25%)
L5	1827	3281	1454(79%)
L6	2087	2411	324(15%)*
L7	3089	3287	198(6%)*
L8	2753	3290	537(19%)
L9	3608	3255	-353(-10%)*
L10	2759	3194	435(15%)*
L11	2252	3224	972(43%)
L12	1910	3274	1364(71%)
L13	3974	3395	-579(-14%)*
L14	3231	3572	341(10%)*
L15	4268	3791	-477(-11%)*
L16	3333	3693	360(10%)*
Mean	2942	3251	308
Standard deviation	714	490	620
Minimum	1827	1814	-615
Maximum	4268	3791	1454

^{*} Absolute error is less than 15%.

Infrared Images Interpretation

The infrared image of April 4 did not show any clear variability within the field (Figure 4.3). That could be because (1) there was no significant variability of wheat growth and/or crop stands, or (2) there was significant variability of wheat density and/or wheat growth and infrared images did not show it. The second possibility was considered to be right because counting plant stands near the access tube locations on April 15, 1998 showed significant variability of plant density along access tube transect. The inability of early-season infrared images to identify and show crop growth is due to the fact that soil reflectance mask plant reflectance when plant cover is too small.

Spatial variability of wheat growth was evident in April 28, 1998 infrared image (Figure 4.3). Four distinguishable wheat growth zones were observed within the field from April 28 infrared image: (1) best wheat growth at the northern bottom of the hill, (2) less wheat growth at hillside and top of the hill, (3) good wheat growth at the southern bottom of the hill and the south-eastern corner of the field, and (4) less growth at the corner of the south-western part of the field. As shown in Figure 4.5, PD was greater in zone (1) and zone (3) than zone (2). In zone 4, wheat plants had less PD and were behind about 8 days in respect to their development stage. Variability of PD may have happened as a result of interaction between soil surface conditions, management, and weather conditions at the time of planting through emergence. For instance, at L16 (in zone 4), the sand content of soil surface layer was the highest within the field. That could have resulted of deep planting depth if the soil surface was too wet. A deeper planting depth could have resulted in less plant stands directly by preventing some seeds from emerging or indirectly by delaying plant emergence. A sensitivity analysis of CERES-WHEAT on

planting depth showed that seeds which were planted at 6 cm depth or below, could have their emerged wheat plants killed on January 15, 1998 as a result of cold damage.

Another reason of wheat variability could have been the presence of an E horizon within the root zone. An E Horizon (white, infertile, and high bulk density) was found in the field at a depth of 90 cm in zone 4, at depth of 90-120 cm in zone 2, and at depth of 150 cm in zone 1 and zone 3. Before April 28, 1998, wheat could not have had any water deficit stress because soil water was available. However, wheat plants could have had excess water stress (oxygen shortage) because of long term saturation conditions. A shallow E horizon could have forced such saturation conditions for longer period resulting in a severe water stress. Such severe water stress could have resulted in delaying the wheat development in zone 4.

Accumulation of crop residue was captured by infrared image of April 28 (Figure 4.3) as curved light color lines. Two of them were seen; one near location L3 and the other one near L15. Such residue accumulation resulted from significant runoff and erosion occurred in the period between April 4 and April 28. Two heavy rain storms occurred within that period; one on April 9 (12 mm d⁻¹) and the other one on April 27 (28 mm d⁻¹) (Figure 4.2). Both of them could have resulted in significant runoff and/or erosion or most probably only the later generated that significant runoff and erosion. If another infrared image was taken between these two rainfall storms more certain interpretation could have been made.

Although some of zone 4 can be noticed, not much variability of wheat growth was evident in June 4 (anthesis date) 1998 infrared image (Figure 3.4). That is mainly because wheat growth masked the variability of wheat within the field and partially

because the relative difference between wheat growth within the field became less. The residue lines were not seen either because the accumulated crop residue was covered by wheat.

The infrared image of July 14 did not show any variability of wheat growth within the field (Figure 4.3) because it was captured one day before wheat harvesting. That indicated that it was impossible to assess grain yield using remotely sensed infrared images at time of maturity. Some weed populations were evident within the field such as near L1 and L2.

Similar spatial variability of wheat growth within the field from each image was obtained by transforming raw reflectance data into NDVI maps (Figure 4.6). Although, features like crop residue accumulation lines or soil color cannot be seen on NDVI maps, they can give a more quantitative way of studying the spatial variability of wheat growth within the field. The NDVI ranged from -0.3 to 0.6. It ranged from -0.3 to 0 on April 4, from -0.2 to 0.2 on April 28, 0 to 0.6 on June 4, and from -0.3 to 0.1 on July 14.

Leaf area index maps did not show any improvement in identifying wheat growth spatial variability over NDVI (Figures 4.6 and 4.7) because LAI was a linear transform from NDVI. However, LAI can be linked with a crop simulation model in order to better estimate the spatial variability of wheat growth, grain yield, and evapotranspiration.

Modeling Spatial Variability of Grain Yield

Testing the relationship between stem weight and LAI at anthesis in different environmental conditions showed that simulated stem weight was highly correlated to simulated LAI at anthesis with r^2 =0.99 (Figure 4.8). Such a relationship demonstrated

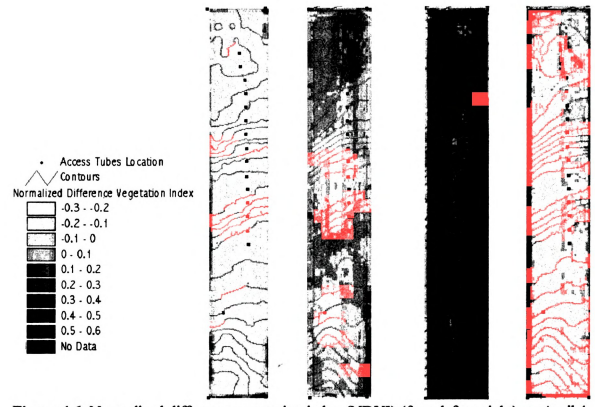


Figure 4.6. Normalized difference vegetation index (NDVI) (from left to right) on April 4, April 28, June 4, and July 14, 1998.

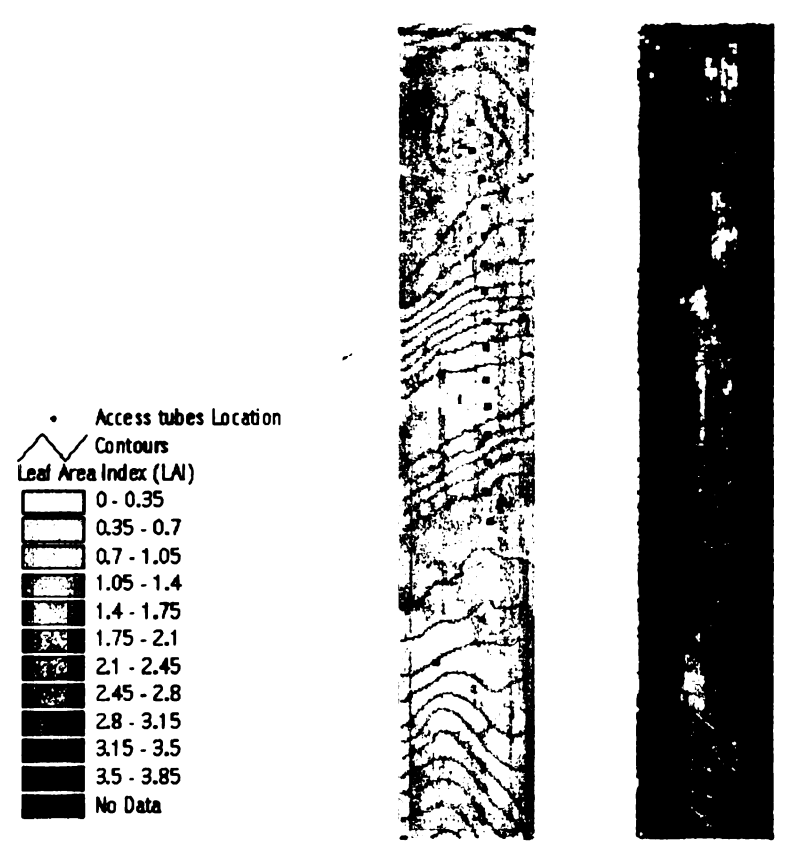


Figure 4.7. Leaf area index (LAI) (from left to right) on April 4, April 28, June 4, and July 14, 1998.

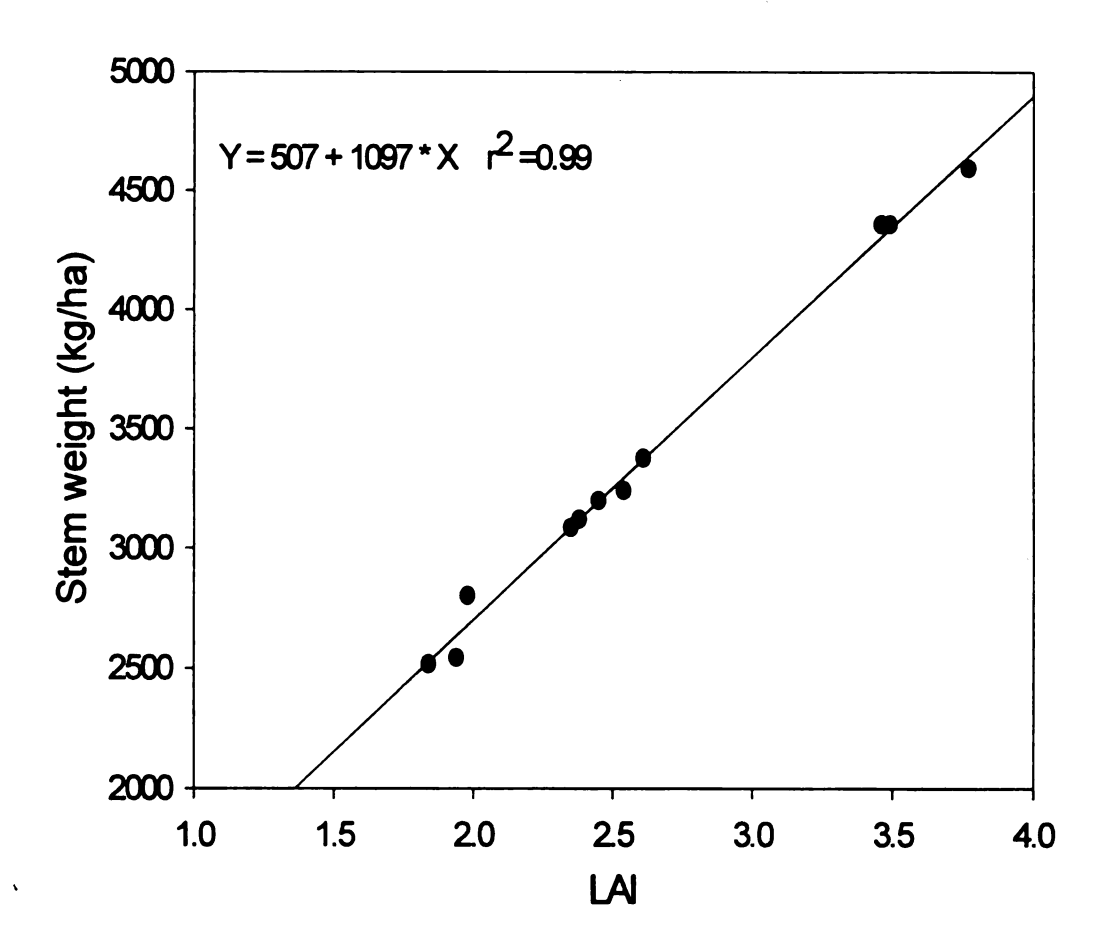


Figure 4.8. Relationship between simulated stem weight and simulated leaf area index at anthesis.

that LAI map at anthesis can be converted accurately into stem weight map at anthesis which was needed to use June 4 infrared image in estimating wheat grain yield. This relationship was used to convert LAI on June 4 into stem weight as first step of integrating CERES-WHEAT and remotely sensed infrared image to simulate spatial variability of grain yield. Then, the calculated stem weight was used to estimate seed number at each pixel using the CERES-WHEAT procedure. In future, CERES-WHEAT can be modified to estimate grain number directly from LAI.

Assuming a constant unit grain weight was valid within the field (Figure 4.5 and 4.9), using an average value of 0.245 mg of a unit grain weight estimated measured grain yield at 33 locations accurately with $r^2 = 0.92$. That allowed us to estimate a unit grain weight by running CERES-WHEAT just once using a representative soil profile data. The estimated (0.25 mg) and measured unit grain weight were in good agreement.

The simulated spatial variability of grain yield was in good agreement with the measured one (Figure 4.10). Most of the high yield, intermediate yield and low yield areas within the field were simulated quite accurately. At the southern-east bottom of the hill, an overestimation of grain yield was evident. Error of simulating total grain yield (16500 kg) was about 7 % of measured total grain yield (15655 kg).

Conclusions

Significant spatial variability of soil properties and wheat growth and yield was evident within the field. Total nitrogen, organic matter, and texture of soil surface layer were correlated with landscape position. Plant density, heads number, grain number, and grain yield were correlated with both soil and landscape position. Unit grain weight was

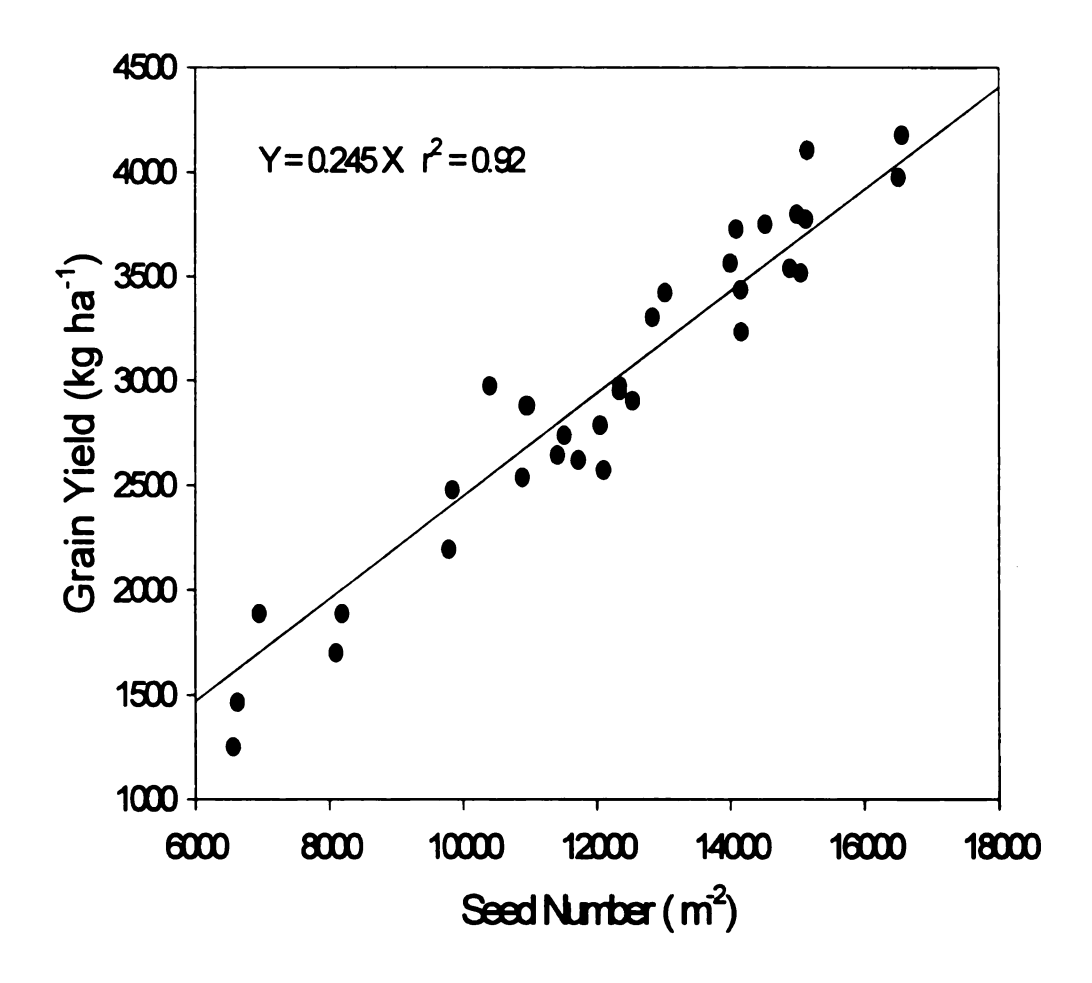


Figure 4.9. Relationship between measured grain yield and measured seed number near access tube locations.

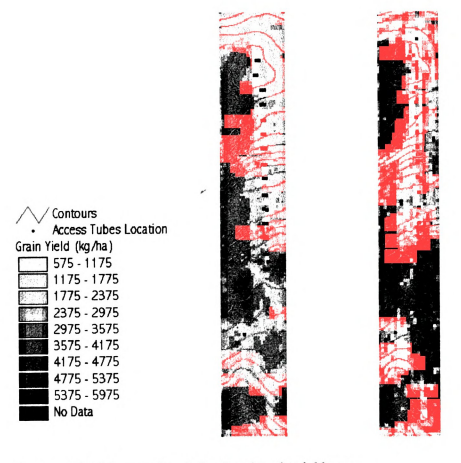


Figure 4.10. Measured and simulated grain yield maps.

not correlated to either soil nor landscape position.

The CERES-WHEAT model estimated grain yield within error margin of 15 % at 10 locations out of 16. Minimum, mean, and maximum grain yield along access tube transect were estimated reasonably well by CERES-WHEAT. Measured plant density at each access tube location was needed to simulate grain yield reasonably near most of access tubes locations.

Spatial variability of grain yield within the field could be estimated reasonably well by integrating CERES-WHEAT and remote sensing. The new developed procedure did not require intensive spatial sampling of soil properties nor many infrared images. An infrared image near anthesis date is needed for best outcomes of the CERES-WHEAT and remote sensing integration.

Although the integration procedure has answered a question, many other questions are yet to be answered such as (1) can such an approach be used for other crops like maize?, (2) can infrared images of one year be linked with a crop model in order to estimate another year grain yield variability, (3) can infrared images be used to estimate spatial variability of plant density, and (4) can infrared images help in building minimum sampling set? Future studies are needed to address these questions.

References

- Berndtsson, R., and A. Bahri. 1995. Field variability of element concentrations in wheat and soil. Soil Sci. 159(5):311-320.
- Bouma, J., J. Brouwer, A. Verhagen, and H.W.G. Booltink. 1995. Site specific management on field level: high and low tech approaches. Kluwer Academic Publishers in cooperation with International Potato Center. Netherlands. Boyer, J.S. 1982. Plant productivity and environment. Science 218:443-448.
- Boyer, J.S.1982. Plant productivity and environment Potential for increasing crop plant productivity, genotypic selection. Science. 218 (4571):443-448.
- Bresler, E, S. Dasbreg, D. Russo, and G. Dagan. 1981. Spatial variability of crop yield as stochastic soil process. Soil. Sci. Soc. Am. J. 45:600-605.
- Fiez, T.E., and B.C. Miller. 1995. Varying winter wheat seeding rates among landscape positions. J Prod. Agric. 8(3):346-350.
- Halvorson, G.A., and E.C. Doll. 1991. Topographic effects on spring wheat yields and water use. Soil Sci. Am. J. 55:1680-1685.
- Kriegler, F. J., Malila, W. A., Nalepka, R. F., and Richardson, W. 1969. Preprocessing transformations and their effects on multispectral recognition, in _Proceedings of the Sixth International Symposium on Remote Sensing of Environment_, University of Michigan, Ann Arbor, MI, pp.97-131.
- Maas, S. 1993. Within-season calibration of modeled wheat growth using remote sensing and field sampling. Agron. J. 85:669-672.
- Moulin, A.P., D.W. Anderson, and M. Mellinger. 1994. Spatial variability of wheat yield, soil properties and erosion in hummocky terrain. Can J. Soil Sci. 74 (2):219-228.
- Pennock, D.J., and E. de Jong. 1990. Spatial pattern of soil redistribution in boroll landscapes, southern Saskatchewan, Canada. Soil Sci. 150:867-873.
- Ritchie, J.T. and S. Otter. 1985. Description and performance of CERES-Wheat: A user-oriented wheat yield model. USDA-ARS. ARS-38. p. 159-175.
- Ritchie, T.J., A. Gerakis, and A.A Suleiman. 1999. Simple Model to Estimate Field-Measured Soil Water Limits. Trans. ASAE (In review)
- Saini, H.S., and S. Lalonde. 1998. Injuries to reproductive development under water stress, and their consequences for crop productivity. J. Crop Prod. 1(1):223-248.

- Teich, A.H., J. Fregeau-Reid, and L. Seaman. 1992. AC Ron winter wheat. Can. J. Plant Sci. 72:1235-1238.
- Verity, G.E., and D.W. Anderson. 1990. Soil erosion effects on soil quality and yield. Can-J-Soil-Sci. 70(3):471-484.
- Welles, J.M., and J.M. Norman. 1991. Instrument for indirect measurements of canopy architecture. Agron. J. 83:818-825.
- Yang, C., C.L. Peterson, G.J. Shorpshire, and T. Otawa. 1998. Spatial variability of field topography and wheat yield in the Palouse region of the pacific northwest. Trans. ASAE 41(1):17-27.

SUMMARY AND CONCLUSIONS

ASSESSING AND MODELING THE SPATIAL VARIABILITY OF SOIL WATER
REDISTRIBUTION AND WHEAT YIELD ALONG A SLOPING LANDSCAPE

By

AYMAN ABDALLAH AHMED SULEIMAN

Assessing and modeling the spatial variability of soil water redistribution and wheat yield along a sloping landscape is a prerequisite for best site-specific-management within sloping landscapes. The objective of this research was to (1) test upward soil water flow during second stage evaporation and downward soil water flow during vertical drainage in the water balance of CERES, (2) develop a simple functional model to simulate lateral downslope soil water flow, and (3) integrate remote sensing and CERES-WHEAT to simulate the spatial variability of wheat yield within a sloping landscape.

Upward soil water flow dynamics during second stage soil water evaporation model in the water balance of CERES was evaluated in laboratory and field conditions. In laboratory, columns were filled with soils of contrasting texture. The soils were saturated and then allowed to drain for 14 days while their surfaces were covered. After the drainage cycle their surfaces were uncovered for 60 days under high potential evaporative losses. Soil water content was monitored at 11 different depths using TDRs during the evaporation cycle. In the field, soil water content was monitored at 11 different depths of

a bare soil using TDRs for about 60 days.

Results showed that, the two constants (n and a) that used in the model were soil specific since α was soil specific. However, they did not vary much and were highly correlated to θ_{dul} . New linear relationships between α , n, and a with θ_{dul} were developed. These relationships enabled the second stage evaporation model in the water balance of CERES to simulate better soil water distribution and soil water evaporation for diverse soils. It was found that the impact of water table on second stage evaporation could not be captured by second stage evaporation theory because soil water contents at different depths had different relationships with Boltzmann transform.

Downward soil water flow dynamics during vertical drainage in the water balance of the CERES model was evaluated theoretically and in laboratory and field conditions. A theory was introduced on the basis of Darcy's Law, using the assumption of a unit gradient for a vertical drainage cycle, and the validity of Brooks and Corey (1964) equation for unsaturated hydraulic conductivity estimation. In laboratory, columns were filled with soils of contrasting texture, then soils were saturated and allowed to drain for 14 days while their surfaces were covered. Soil water content was monitored at 11 different depths using TDRs during the drainage cycle. In the field, soil water content was monitored at 11 different depths of a bare soil using TDRs for about 14 days during a drainage cycle.

It was found that the drainage coefficient is soil dependent. It was clear also that the drainage coefficient depends on the initial soil water content. However, using a sole value of the drainage coefficient for each soil is reasonable and simplifies soil water drainage modeling. Two methods were introduced to estimate the drainage coefficient

from drained upper limit water content and saturated water content. The new models gave good estimate of the drainage coefficient. Therefore, these new models are recommend to be used in the water balance of CERES instead of a constant value of 0.55. Also Eq. [21], which calculates the drainage coefficient, could be incorporated in the drainage model in the water balance of CERES because it is easier and gave as good results as Eq. [20]. A new definition of the drainable soil water was introduced. The new definition made the drainage model in the water balance of CERES applicable under shallow soil water table conditions.

A generic simple functional model to simulate daily lateral downslope soil water flow was developed based on Darcy's Law and the Brooks and Corey (1964) equation for the estimation of unsaturated hydraulic conductivity. Saturated and drained upper limit soil water contents and slope angle (or the hydraulic gradient) were needed to run the new lateral downslope soil water flow model. In order to evaluate the model, a field study was conducted along a sloping landscape in Lansing, Michigan in 1997-1998. Although the new model is simple, it performed well under field conditions. The developed lateral downslope soil water flow model was built in a way that makes possible to link it to a GIS package. A GIS can determine the directions of stream flow lines, while the lateral downslope model can account for the amount of soil water that may drain in a day at any position of a landscape. Such combination will produce a two-dimensional lateral downslope flow.

To integrate CERES-WHEAT with remote sensing, a 6 ha field was planted to wheat on October 19, 1997 and harvested using a combine equipped with GPS and yield monitor on July 15, 1998. Four infrared images were captured during the growing season

in order to estimate the wheat growth spatial variability. Soil and plant samples were taken along a transect.

Significant spatial variability of soil properties and wheat growth and yield was evident within the field. Total nitrogen, organic matter, and texture of soil surface layer were correlated with landscape position. Plant density, heads number, grain number, and grain yield were correlated with both soil and landscape position. Unit grain weight was not correlated to either soil properties nor landscape position. The CERES-WHEAT model estimated grain yield within error margin of 15 % at 10 locations out of 16.

Minimum, mean, and maximum grain yield along access tube transect were estimated reasonably well by CERES-WHEAT. Measured plant density at each access tube location was needed to simulate grain yield reasonably near most of access tubes locations. Spatial variability of grain yield within the field could be estimated reasonably well by integrating CERES-WHEAT and remote sensing. The new developed procedure did not require intensive spatial sampling of soil properties nor many infrared images. An infrared image near anthesis date is needed for best outcomes of the CERES-WHEAT and remote sensing integration.

APPENDICES

Appendix A

Soil properties at access tube locations.

Access Tube Location	Depth	Clay	Sand	Carbon	Total Nitrogen	EC	pН
	cm	-		%		dS m ⁻¹	
L1	0-15	18.1	45.0	3.68	0.31	0.85	7.27
L1	15-30	19.5	47.5	3.53	0.31		
L1	30-60	20.3	56.0	2.66	0.23	0.49	7.58
L1	60-90	21.3	54.8	2.20	0.19		
L2	0-15	32.7	20.8	8.09	0.70	0.42	6.81
L2	15-30	32.7	24.1	7.58	0.65		
L2	30-60	29.1	23.9	12.37	1.02		
L2	60-90	31.0	9.6	4.96	0.36	0.47	7.10
L2	90-120	29.5	15.5	6.84	0.49	2.82	7.13
L2	120-150	23.6	14.5	3.08	0.08	2.91	7.20
L3	0-15	30.2	24.2	4.39	0.41	0.66	7.69
L3	15-30	32.8	16.0	2.15	0.17	0.46	7.88
L3	30-60	12.6	63.8	0.74	0.03	0.52	7.58
L3	60-90	10.5	76.2	0.86	0.04	0.52	8.03
L3	90-120	8.5	66.3	1.36	0.23	0.62	7.97
L4	0-15	23.6	33.2	1.61	0.18	0.78	7.84
L4	15-30	23.6	32.6	0.37	0.03	0.30	7.77
L4	30-60	21.9	34.9	0.92	0.04	0.36	7.69
L4	60-90	23.6	33.2	0.63	0.01	0.63	7.73
L5	0-15	21.8	42.2	2.31	0.22	0.53	7.78
L5	15-30	21.8	42.7	1.27	0.11		
L5	30-60	19.6	44.2	0.48	0.05	0.28	7.67
L5	60-90	23.6	35.0	1.44	0.05	0.33	8.03
L5	90-120	22.4	43.0	2.70	0.01	0.33	7.94
L6	0-15	21.8	39.4	2.36	0.22	0.39	7.60
L6	15-30	21.8	36.1	1.12	0.11		
L6	30-60	27.2	36.5	0.39	0.04	0.28	7.86
L6	60-90	23.7	25.3	2.20	0.03	0.34	7.98
L6	90-120	25.0	30.7	2.42	0.04	0.42	8.04
L6	120-150	25.6	24.2	3.06	0.02	0.32	7.73

Access Tube	Depth	Clay	Sand	Carbon	Total Nitrogen	EC	»U
Location Location	cm			%		dS m ⁻¹	pН
L7	30-60	21.2	48.0	0.62	0.06	0.32	7.62
L7	60-90	16.3	12.0	2.29	0.02	0.38	7.57
L7	90-120	14.6	10.9	2.43	0.01	0.34	7.61
L7	120-150	19.6	1.8	1.61	0.00	0.34	7.54
L8	0-15	15.1	48.1	1.82	0.16	0.60	7.15
L8	15-30	21.8	46.3	1.43	0.14		
L8	30-60	21.8	49.3	0.52	0.05	0.27	7.48
L8	60-90	13.9	83.6	0.48	0.02	0.38	7.52
L8	90-120	8.5	62.3	0.52	0.01	0.47	7.42
L8	120-150	18.9	44.1	1.71	0.00	0.42	7.89
L9	0-15	20.6	44.5	1.82	0.16	0.60	7.68
L9	15-30	20.6	44.0	1.44	0.13		
L9	30-60	28.5	45.9	0.48	0.05	0.34	7.71
L9	60-90	13.9	48.1	0.96	0.04	0.43	7.74
L10	0-15	15.1	49.1	1.81	0.15	0.56	8.02
L10	15-30	15.1	48.2	1.37	0.13		
L10	30-60	21.8	52.4	0.34	0.03	0.31	7.01
L10	60-90	19.2	54.7	0.34	0.04	0.33	7.62
L10	90-120	16.3	49.5	0.39	0.02	0.38	7.84
L11	0-15	17.6	47.9	1.30	0.13	0.49	7.68
L11	15-30	18.5	47.7	1.54	0.14		
L11	30-60	16.3	49.3	0.62	0.05	0.34	7.56
L11	60-90	31.8	36.3	0.47	0.04	0.51	7.95
L11	90-120	10.5	46.7	0.28	0.01	0.40	7.64
L11	120-150	18.3	43.1	0.44	0.01	0.36	7.88
L12	0-15	18.5	48.6	1.40	0.16	0.77	7.62
L12	15-30	15.1	42.8	0.72	0.13		
L12	30-60	24.4	43.5	0.48	0.06	0.32	7.64
L12	60-90	17.0	64.2	0.26	0.02	0.32	7.62
L12	90-120	19.3	56.7	0.25	0.02	0.46	7.74
L12	120-150	10.6	49.6	0.18	0.00	0.35	7.70
L12	150-180	20.4	42.4	0.30	0.01	0.38	7.60
L12	180-210	19.1	43.0	0.26	0.00	0.34	7.62
L12	210-240	20.2	42.0	0.29	0.01	0.35	7.63
L13	0-15	22.1	45.2	1.60	0.23		
L13	15-30	19.7	43.6	1.26	0.17		
L13	30-60	20.5	40.3	0.58	0.07	0.38	7.60

4 70 1	Depth	Clay	Sand	Carbon	Total Nitrogen	EC	**
Access Tube Location	cm			%			pН
L14	15-30	18.0	48.6	0.64	0.10		-
L14	30-60	18.0	51.2	0.35	0.04	0.24	7.55
L14	60-90	14.7	55.5	0.20	0.01	0.32	7.87
L14	90-120	13.8	58.5	0.19	0.01	0.32	7.80
L14	120-150	12.3	60.3	0.17	0.01	0.35	7.70
L15	0-15	21.8	43.9	1.09	0.21	0.39	7.08
L15	15-30	23.5	43.0	0.79	0.15		
L15	30-60	20.9	43.4	0.61	0.08	0.30	7.43
L15	60-90	22.7	39.5	0.39	0.05	0.28	7.40
L15	90-120	20.8	44.0	0.22	0.02	0.26	7.38
L15	120-150	15.5	52.2	0.21	0.01	0.41	7.49
L16	0-15	9.6	56.0	1.63	0.16		
L16	15-30	10.5	54.7	1.72	0.16		
L16	30-60	9.4	48.8	1.33	0.12		
L16	60-90	12.1	49.7	1.48	0.15		
L16	90-120	16.0	44.8	0.33	0.02		
L16 .	120-150	14.0	47.9	0.29	0.01		

Appendix B

Daily solar radiation (SR), maximum (T_{max}) and minimum temperature (T_{min}) , and Rainfall (R) for the sloping landscape.

Year	DOY	SR	Tmax	T _{min}	R
		MJ m ⁻²		C °	mm
97	152	8.7	16.9	9.1	0.0
97	153	7.5	15.9	9.9	1.8
97	154	4.6	15.8	12.4	2.3
97	155	17.5	21.5	9.6	0.3
97	156	27.9	23.3	4.9	0.0
97	157	25.9	24.3	6.5	0.0
97	158	26.3	23.7	11.1	0.0
97	159	29.6	21.4	12.9	0.0
97	160	28.6	23.0	10.0	0.0
97	161	28.8	26.2	8.3	0.0
97	162	29.0	28.2	9.6	0.0
97	163	21.1	27.5	11.8	0.0
97	164	15.1	23.4	15.1	5.1
97	165	21.6	26 .0	13.5	4.3
97	166	29.9	21.8	9.7	0.0
97	167	29.3	25.3	8.4	0.0
97	168	10.7	22.3	15.6	7.4
97	169	23.6	21.8	9.8	0.0
97	170	25.9	25.3	12.7	0.0
97	171	21.1	26.8	13.2	0.0
97	172	8.1	26.0	17.8	8.1
97	173	13.6	28.4	17.3	10.9
97	174	28.8	27.7	16.0	0.0
97	175	18.9	29.4	14.2	4.3
97	176	25.8	30.8	21.6	0.0
97	177	23.8	27.2	21.3	0.0
97	178	29.1	26.1	15.6	0.0
97	179	30.0	28.4	11.0	0.0
97	180	27.6	29.6	13.4	0.0
97	181	27.2	30.4	15.6	0.0
97	182	17.6	27.3	18.2	2.0
97	183	16.0	26.4	19.0	1.3
97	184	22.0	29.7	16.8	0.3
97	185	6.1	20.4	16.2	0.0
97	186	14.4	19.4	12.1	0.0
97	187	25.8	23.9	7.3	0.0
97	188	23.0	24.5	10.6	1.3
97	189	28.1	22.6	12.5	0.0
97	190	10.6	24.1	14.6	4.8
97	191	26.5	21.6	11.3	0.0

Year	DOY	SR	T _{mex}	T _{min}	R
, , ,		MJ m ⁻²	- max (3°	mm
97	192	29.7	24.4	8.7	0.0
97	193	29.3	26.3	9.0	0.0
97	194	29.2	27.9	11.2	0.0
97	195	25.0	30.2	13.3	0.0
97	196	24.4	33.0	20.0	5.1
97	197	27.7	27.1	17.3	0.0
97	198	26.5	30.8	17.4	0.0
97	199	13.2	27.4	17.8	20.3
97	200	27.3	29.5	16.7	0.3
97	201	29.2	24.1	14.5	0.0
97	202	25.1	27.3	9.4	0.0
97	203	6.6	22.2	16.2	14.4
97	204	16.4	25.0	13.1	0.0
97	205	13.9	23.8	14.4	0.0
97	206	16.0	26.4	17.2	0.0
97	207	21.2	27.7	14.6	0.0
97	208	20.3	30.5	20.2	4.3
97	209	21.3	29.0	17.7	0.0
97	210	23.9	27.2	14.9	0.0
97	211	27.7	23.6	11.6	0.0
97	212	26.5	25.5	9.1	0.0
97	213	28.1	27.7	10.1	0.0
97	214	11.3	24.9	12.2	0.0
97	215	23.5	28.7	17.8	0.0
97	216	6.6	23.0	15.7	19.0
97	217	18.1	23.5	14.7	0.3
97	218	24.9	20.7	10.5	0.0
97	219	22.1	24.0	7.8	4.3
97	220	24.7	25.1	9.6	0.3
97	221	21.5	26.9	10.4	0.0
97	222	21.5	28.1	13.1	0.0
97	223	12.4	24.1	17.2	0.8
97	224	3.8	17.6	13.0	7.6
97	225	4.7	19.7	13.1	9.1
97	226	17.9	22.6	14.0	0.3
97	227	21.3	22.7	6.7	0.0
97	228	13.0	27.1	15.4	8.9
97	229	10.4	27.6	18.1	3.0
97	230	3.4	18.7	12.2	7.1
97	231	17.8	21.5	11.0	0.0
97	232	22.1	22.7	10.5	0.0
97	233	3.5	15.6	13.8	2.5
97	234	10.1	18.3	12.4	4.6
97	235	9.5	19.6	11.6	0.0
97	236	23.6	21.7	7.4	0.0
97	237	4.7	17.6	13.5	0.0
97	238	8.8	20.6	12.6	0.0
97	239	13.8	23.6	10.8	0.0
٠.			_0.0		5.5

Year	DOY	SR	T _{mex}	T _{min}	R
		MJ m ⁻²		3°	mm
97	240	21.4	27.7	14.4	0.0
97	241	12.7	19.6	12.7	0.0
97	242	11.0	20.7	11.2	0.0
97	243	17.8	23.6	10.0	0.0
97	244	8.7	21.2	15.7	1.0
97	245	13.7	24.8	14.7	0.0
97	246	8.4	22.8	13.0	0.0
97	247	23.0	17.9	7.5	0.0
97	248	22.9	20.6	2.7	0.0
97	249	16.0	21.4	2.2	0.8
97	250	19.8	26.8	14.3	0.0
97	251	14.5	21.5	11.3	0.0
97	252	10.6	23.0	13.6	0.0
97	253	1.9	16.2	13.6	46.2
97	254	4.2	17.1	14.3	22.6
97	255	5.1	16.6	12.8	0.0
97	256	5.2	17.4	12.7	0.5
97	257	14.4	22.4	12.9	0.0
97	258	8.9	21.5	12.1	0.8
97	259	17.9	26.5	10.9	0.0
97	260	13.0	26.0	13.8	0.0
97	261	15.7	23.3	12.4	30.4
97	262	19.6	25.7	8.9	0.0
97	263	10.5	26.2	17.4	2.0
97	264	8.6	19.3	7.4	1.0
97	265	19.8	15.4	2.6	0.0
97	266	10.7	16.5	4.1	0.0
97	267	13.0	17.6	6.7	1.0
97	268	19.3	17.9	0.8	0.0
97	269	17.4	22.6	8.9	0.0
97	270	18.1	17.4	6.0	0.0
97	271	17.6	20.3	3.9	0.0
97	272	12.7	23.7	9.7	4.1
97	273	13.7	20.9	10.2	0.3
97	274	4.8	14.5	8.9	0.3
97	275	17.8	12.7	1.9	0.0
97	276	16.3	19.6	0.6	0.0
97	277	15.8	25.6	11.2	0.0
97	278	5.5	22.9	12.0	1.8
97	279	15.6	26.6	7.1	0.3
97	280	14.6	27.2	12.3	0.0
97	281	14.0	27.3	11.8	0.0
97	282	13.1	26.7	12.2	0.0
97	283	3.4	20.4	11.2	4.3
97	284	15.9	16.5	5.3	0.0
97	285	15.1	19.1	3.3	0.0
97	286	13.4	24.6	6.0	0.0
97	287	2.6	21.2	7.9	7.9

Year	DOY	SR	T _{mex}	T _{min}	R
		MJ m ⁻²		2 °	mm
97	288	10.4	9.6	1.0	0.0
97	289	11.6	10.4	0.6	0.0
97	290	6.3	9.7	-1.5	0.0
97	291	8.7	9.6	-0.6	0.0
97	292	14.2	13.5	-3.3	0.0
97	293	12.9	14.5	-1.4	0.0
97	294	10.5	11.5	-1.6	0.0
97	295	10.3	7.8	-2.4	0.0
97	296	5.4	3.2	-3.5	0.0
97	297	6.1	5.5	-4.8	0.0
97	298	2.0	6.3	2.6	1.3
97	299	5.1	7.1	-0.1	0.0
97	300	1.2	3.8	-0.5	7.6
97	301	3.4	-0.2	-3.2	0.0
97	302	11.8	7.6	-4 .8	11.9
97	303	10.6	12.7	0.9	0.0
97	304	9.2	15.2	-2.4	0.0
97	305	4.5	14.4	8.9	0.3
97	306	1.8	12.1	8.3	12.9
97	307	1.6	8.7	0.9	1.3
97	308	6.0	4.0	-1.2	0.0
97	309	2.1	5.4	-0.5	1.8
97	310	4.3	5.6	1.4	0.0
97	311	6.6	16.5	2.5	11.1
97	312	3.6	7.2	1.3	0.0
97	313	9.5	9.9	-0.4	0.0
97	314	3.4	5.4	-0.2	0.0
97	315	7.9	6.1	-2.5	0.8
97	316	5.3	2.7	<i>-</i> 5.5	0.0
97	317	5.8	-1.3	-8.9	0.0
97	318	5.1	0.0	-8.9	8.0
97	319	3.6	-0.2	-2.0	2.5
97	320	3.4	-0.9	-5 .1	2.3
97	321	6.8	-1.9	-10.6	0.0
97	322	9.7	0.5	-6.1	0.8
97	323	7.7	3.4	-8.1	0.0
97	324	3.9	0.8	-1.6	0.0
97	325	4.2	5.5	-3.6	0.5
97	326	2.4	3.8	-1.5	1.0
97	327	6.9	6.1	-3.1	0.0
97	328	2.6	1.6	-6.4	0.0
97	329	5.6	-1.0	-8.7	0.0
97	330	7.4	10.9	-4.2	0.5
97	331	1.8	8.6	1.1	0.5
97	332	5.1	7.6	-3.3	1.8
97	333	1.8	10.4	3.9	0.0
97	334	1.0	6.8	4.4	3.8
97	335	1.0	4.8	1.9	0.5
					-

Year	DOY	SR	T _{mex}	T _{min}	R
ı vai	50.	MJ m ⁻²	' mex	<u>'min</u>	mm
97	335	1.0	4.8	1.9	0.5
97	336	4.2	2.3	-0.8	0.0
97	337	4.5	2.7	-3.2	0.0
97	338	1.2	2.3	-2.3	0.3
97	339	2.3	2.1	-2.1	1.8
97	340	4.5	-0.8	-3.6	0.0
97	341	3.2	1.2	-3.2	0.5
97	342	2.9	2.2	-0.5	0.0
97	343	2.4	0.5	-2.0	0.0
97	344	1.6	0.3	-2.1	0.0
97	345	1.5	-0.7	-2.4	0.3
97	346	4.6	-1.5	-5.7	0.0
97	347	2.5	-1.4	-6.0	0.0
97	348	2.2	-0.2	-4 .5	0.0
97	349	7.1	4.7	-8.2	2.8
97	350	7.9	6.5	-4 .9	0.0
97	351	7.4	5.8	-0.7	0.0
97	352	7.9	6.3	-7.0	0.0
97	353	5.8	5.4	-4.4	0.0
97	354	5.1	7.2	0.3	0.0
97	355	1.8	1.1	-2.6	0.3
97	356	2.8	-1.8	-4 .1	0.0
97	357	1.0	-0.5	-3.4	2.0
97	358	2.3	0.0	-2 .0	2.8
97	359	2.1	0.2	-2.8	0.5
97	360	1.3	0.2	-0.9	7.4
97	361	1.5	-0.2	-2.9	0.0
97	362	4.6	-1.5	- 9.7	0.5
97	363	6.2	0.0	-10.6	0.0
97	364	5.1	2.1	-2.8	0.0
97	365	5.5	-1.9	-10.6	0.3
98	1	6.7	-7.7	-13.6	0.0
98	2	7.7	3.7	-9.1	0.0
98	3	4.4	7.4	1.5	0.0
98	4	0.9	10.5	5.1	4.8
98	5	0.8	7.2	-1.4	8.4
98	6	0.9	11.3	6.9	23.1
98	7	2.0	11.4	8.2	1.0
98	8	0.7	8.8	-0.9	9.9
98	9	1.0	-0.6	-2.3	0.0
98	10	1.6	1.4	-1.6	10.6
98	11	8.1	-1.2	-9.3	0.0
98	12	4.4	-7.0	-10.1	0.0
98	13	1.6	-0.2	-10.2	0.0
98	14	7.7	-5.0	-14.6	0.0
98	15	5.1	-5.7	-16.3	0.0
98	16	3.3	-3.8	-6.9	0.0
98	17	3.2	-3.9	-6.5	0.0
	• •			3.0	

Year	DOY	SR	T _{mex}	T _{min}	R
		MJ m ⁻²		<u>;° </u>	<u>mm</u>
98	18	3.5	-2.1	-4 .9	0.3
98	19	4.7	-1.8	-6.0	0.0
98	20	4.7	-1.6	-5.9	0.0
98	21	6.4	-2.6	-10.4	0.5
98	22	5.4	-2.3	-7.4	0.0
98	23	4.1	-2.1	-6.2	0.0
98	24	4.6	-0.5	-5.1	0.0
98	25	7.5	-0.8	-3.6	0.0
98	26	4.8	-1.8	-4 .6	0.0
98	27	5.8	1.7	-3.4	6.1
98	28	5.0	4.6	-1.2	0.0
98	29	4.1	1.6	-0.7	0.0
98	30	2.4	0.3	-1.1	3.0
98	31	3.0	0.3	-1.8	0.0
98	32	9.4	3.1	-2.0	0.0
98	33	9.5	6.4	-3.7	0.0
98	34	1.2	5.2	-5.0	0.0
98	35	9.1	0.6	-6 .5	0.0
98	36	8.8	-1.7	-7.0	0.0
98	37	7.0	-2.1	-5.9	0.0
98	38	9.8	0.5	-5.8	0.0
98	39	10.4	1.2	-5.5	0.0
98	40	11.6	5.8	-8.0	0.0
98	41	11.1	8.4	-7.0	0.0
98	42	8.8	9.7	-4.8	0.0
98	43	0.9	3.5	0.7	14.4
98	44	2.6	0.7	-1.4	0.8
98	45	1.8	-0.3	-2.0	0.0
98	46	4.6	1.2	-3.4	0.0
98	47	9.4	7.7	-3.7	0.0
98	48	6.5	6.5	-0.8	7.6
98	49	1.3	4.9	2.0	18.5
98	50	1.6	3.2	0.5	2.0
98	51	2.7	3.3	0.4	0.0
98	52	2.7	2.9	0.1	3.0
98	53	2.6	2.0	0.0	0.0
98	54	7.9	7.6	-2.5	0.0
98	55	10.2	5.0	-2.2	0.0
98	56	3.9	6.1	-3.9	2.0
98	57	13.5	9.9	-2.5	0.0
98	58	11.5	10.8	0.2	0.0
98	59	6.7	12.2	3.2	3.0
98	60	13.6	12.2	-2.3	3.0 1.0
98	61	2.5	5.0	-2.3 -1.0	7.4
98	62	2.5 3.3	2.0	-1.0 -1.1	7. 4 3.0
98	63				
		7.1 5.0	0.9 1.5	-3.0	0.3
98 08	64 65	5.9 7.5	1.5	-3.0 1.0	0.5
98	65	7.5	2.2	-1.9	0.0

Year	DOY	SR	T _{mex}	T _{min}	R
		MJ m ⁻²		<u>, </u>	mm
98	66	2.8	1.7	-1.1	1.0
98	67	14.4	5.8	-3.3	0.0
98	68	1.4	3.1	-0.6	11.9
98	69	3.0	1.6	-8.1	24.6
98	70	13.1	-5.8	-11.2	0.3
98	71	16.8	-6.6	-15.0	0.0
98	72	16.4	-2 .8	-11.5	0.0
98	73	9.1	-0.2	-10.4	0.0
98	74	12.9	-0.2	-6.0	0.3
98	75	18.6	-2 .9	-10.6	0.5
98	76	19.9	0.4	-12.3	0.0
98	77	11.7	5.2	-6.0	7.4
98	78	1.8	4.1	0.5	9.9
98	79	2.9	1.4	-2.1	1.3
98	80	3.6	-0.3	-2.3	0.0
98	81	5.1	0.1	-2.3 -2.3	0.0
98	82	20.7	4.1	-2.5 -4.6	0.0
98	83	20.7 16.9	4.3	-5.2	0.0
98	84	14.3	4.3 7.4	-5.2 -4.7	0.0
98	85				
		14.0 42.5	11.4	-1.0	0.0
98	86	12.5	21.5	9.6	0.0
98	87	15.4	23.2	16.0	0.0
98	88	6.2	17.0	11.0	7.9
98	89	18.9	22.9	5.8	0.0
98	90	11.3	24.6	17.5	0.0
98	91	2.7	19.2	11.8	16.0
98	92	11.2	13.8	3.1	6.6
98	93	5.7	7.5	2.9	1.3
98	94	5.0	5.6	2.7	0.0
98	95	22.0	9.5	0.0	0.0
98	96	23.4	10.9	-3.3	0.0
98	97	22.5	14.0	-3.7	0.0
98	98	19.8	14.8	0.9	0.0
98	99	4.5	8.7	3.9	11.9
98	100	2.5	5.8	3.2	4.3
98	101	23.7	10.3	0.6	0.0
98	102	23.5	14.9	-1.9	0.0
98	103	22.5	20.2	3.9	0.0
98	104	16.1	20.5	9.8	0.0
98	105	4.9	14.2	8.1	2.0
98	106	8.9	13.2	4.2	0.0
98	107	12.0	18.0	3.2	5.6
98	108	22.4	9.0	1.0	0.0
98	109	20.9	15.3	2.8	0.0
98	110	13.3	14.7	3.6	0.0
98	111	23.3	18.4	2.5	0.0
98	112	12.6	16.7	4.8	0.0
-		12.0	10.7	٦.٠	J.U

Year	DOY	SR	T _{mex}	Tmin	R
		MJ m ⁻²		C°	mm
98	114	25.9	18.9	2.5	0.0
98	115	21.4	20.7	5.2	0.0
98	116	18.9	17.5	2.4	2.8
98	117	8.9	9.6	1.4	27.6
98	118	27.0	11.2	-1.2	0.0
98	119	26.6	16.3	-2.0	0.0
98	120	13.4	17.0	0.3	0.0
98	121	6.8	16.6	10.1	7.9
98	122	11.7	20.7	12.2	22.1
98	123	5.2	15.2	10.9	4.6
98	124	8.9	18.2	9.9	1.0
98	125	17.3	21.8	9.7	2.3
98	126	24.2	23.4	7.3	0.3
98	127	16.7	24.0	12.6	0.0
98	128	16.4	22.6	13.0	0.0
98	129	14.1	18.5	11.2	1.0
98	130	26.6	19.5	9.7	0.0
98	131	22.1	20.9	6.9	0.0
98	132	14.1	18.0	9.7	1.0
98	133	21.5	22.1	8.0	0.0
98	134	19.7	26.3	12.4	1.5
98	135	27.9	28.8	9.8	0.0
98	136	25.9	30.6	13.6	0.0
98	137	27.8	25.1	16.7	0.0
98	138	28.8	26.9	12.2	0.0
98	139	27.5	29.4	11.6	0.0
98	140	24.4	28.9	16.6	0.0
98	141	26.6	26.8	15.5	0.0
98	142	26.4	21.3	9.1	0.0
98	143	25.0	18.8	4.4	0.0
98	144	29.1	21.3	2.7	0.0
98	145	8.8	17.8	8.3	3.0
98	146	6.3	15.8	8.6	0.0
98	147	26.7	24.8	5.6	0.0
98	148	26.3	26.8	8.6	0.0
98	149	18.9	27.9	10.9	0.0
98	150	20.3	27.0	15.8	0.0
98	151	27.2	28.6	10.8	0.0
98	152	19.7	23.4	11.8	12.4
98	153	29.0	20.4	4.7	0.0
98	154	23.1	23.3	9.8	0.0
98	155	17.7	15.4	5.3	0.0
98	156	25.2	17.7	1.9	0.0
98	157	14.9	13.5	3.8	0.0
98	158	14.0	14.6	2.2	0.0
98	159	21.2	17.0	4.1	0.0
98	160	22.4	20.0	2.9	0.0
98	161	8.7	18.3	9.8	6.1
	. • .			J. -	

Year	DOY	SR		T .	R
i vai	DO 1	MJ m ⁻²	T _{max}	T _{min} C°	mm
98	162	6.8	18.1	12.1	2.3
98	163	7.0	19.9	12.6	3.8
98	164	22.3	27.2	16.8	2.0
98	165	16.1	22.0	14.3	7.4
98	166	23.0	24.4	12.8	0.0
98	167	24.7	25.8	14.5	1.3
98	168	20.1	26.0	14.3	2.8
98	169	27.0	26.4	14.9	0.0
98	170	25.3	28.6	13.8	0.0
98	171	27.6	27.1	17.6	0.0
98	172	27.3	30.5	15.9	0.0
98	173	22.3	29.7	18.5	0.0
98	174	27.7	29.4	17.1	0.0
98	175	27.3	30.2	19.6	0.0
98	176	19.6	30.9	15.6	7.1
98	177	25.8	32.9	19.7	15.4
98	178	27.9	28.8	18.3	2.3
98	179	16.0	28.2	18.1	1.0
98	180	19.6	28.8	19.6	0.0
98	181	28.9	29.5	16.9	0.0
98	182	17.2	22.9	17.6	3.6
98	183	28.8	25.9	13.7	0.0
98	184	28.7	26.4	10.8	0.0
98	185	22.1	27.8	15.2	0.8
98	186	9.6	21.3	13.8	6.6
98	187	29.5	25.3	10.4	0.0
98	188	15.5	26.9	15.0	13.4
98	189	6.3	24.1	18.4	21.5
98	190	16.4	26.1	17.4	0.0
98	191	25.3	26.8	14.9	0.0
98	192	28.4	23.7	13.4	0.0
98	193	29.4	25.4	9.1	0.0
98	194	28.5	26.8	11.0	0.0
98	195	26.6	27.2	12.6	0.0
98	196	25.4	29.6	15.7	0.0
98	197	22.5	29.6	17.8	0.0
98	198	22.7	28.6	19.1	2.3
98	199	24.7	26.1	15.3	0.0
98	200	26.4	28.1	10.4	0.0
98	201	16.2	29.1	17.4	1.8
98	202	26.8	30.5	18.4	0.0
98	203	16.0	31.7	18.0	10.4
98	204	16.4	26.8	19.1	0.0
98	205	25.7	24.6	14.1	0.0
98	206	20.5	23.0	10.7	0.0
98	207	17.0	23.8	11.1	0.0
98	208	26.7	26.3	9.5	0.0
98	209	19.0	25.6	13.9	0.0

Year	DOY	SR	T _{mex}	T _{min}	R
		MJ m ⁻²	C°		mm
98	210	26.5	28.2	16.3	0.0
98	211	25.3	26.5	14.9	0.0
98	212	14.2	25.5	16.1	0.0
98	213	22.2	25.9	11.9	0.0
98	214	27.4	26.7	9.9	0.0
98	215	26.0	27.9	9.6	0.0
98	216	14.9	26.8	12.0	0.0

Appendix C

LIST OF ABBREVIATIONS

Chapter 1

a	Constant
В	Bulk density
α	The slope of the relationship between cumulative soil evaporation and the square
	root of time during second stage evaporation
θ	Volumetric soil water content
θ_{i}	Initial soil water content
θ_{s}	Saturated soil water content
θ_{ss}	Soil water content at the soil surface
$\theta_{ ext{dul}}$	Drained upper limit soil water content
$\theta_{\sf ad}$	Air dry soil water content
Δθ	The daily change of soil water content
C	The percent of evaporable soil water that can be evaporated in a day at a certain
	depth
d	Soil depth
E	Evaporation rate
\mathbf{E}_{p}	Potential evaporation
E_s	Soil water evaporation
E_{sa}	Actual soil water evaporation
E_c	Cumulative soil evaporation
$D(\theta)$	Soil water diffusivity
$K(\theta)$	Soil water hydraulic conductivity
K _s	Saturated soil water hydraulic conductivity
n	Constant
t	Time
Z	Distance
λ	Boltzmann transform

Chapter 2

Distance

Z

Constant a b Constant α Function of both saturated and drained upper limit soil water contents θ Volumetric soil water content θ_1 Soil water content at the end of first day during a drainage cycle Soil water content at the end of second day during a drainage cycle θ_2 Initial soil water content θ_{i} Residual soil water content θ, Saturated soil water content θ, Drained upper limit soil water content θ_{dul} Δθ The daily change of soil water content ∂h/∂z Hydraulic gradient The percent of drainable soil water that can be drained in a day at a certain depth C C_1 The fraction of drainable soil water that can be drained from a soil layer in the first day during a drainage cycle. The fraction of drainable soil water that can be drained from a soil layer in the C_2 second day during a drainage cycle. Soil water evaporation E, Soil water hydraulic conductivity $K(\theta)$ $K_1(\theta)$ The first day hydraulic conductivity $K(\theta_1)$ Hydraulic conductivity at θ_1 $K_2(\theta)$ The second day hydraulic conductivity $K(\theta_2)$ Hydraulic conductivity at θ_2 Saturated soil water hydraulic conductivity K, n Function of drained upper limit soil water content Soil water flux q t Time

Chapter 3

a	Constant
$\mathbf{a_1}$	Constant
b	Constant
b_1	Constant
α	Function of both saturated and drained upper limit soil water contents
θ	Volumetric soil water content
θ_1	Soil water content at the end of first day during a drainage cycle
θ_2	Soil water content at the end of second day during a drainage cycle
$\boldsymbol{\theta}_{i}$	Initial soil water content
θ_{s}	Saturated soil water content
$\theta_{ ext{dul}}$	Drained upper limit soil water content
Δθ	The daily change of soil water content
∂h/∂z	Hydraulic gradient
γ	The slope angle
C siny	The percent of drainable soil water that can be drained laterally in a day at a
	certain depth
E_s	Soil water evaporation
$K(\theta)$	Soil water hydraulic conductivity
$K_1(\theta)$	First day hydraulic conductivity
$K(\theta_1)$	Hydraulic conductivity at θ_1
K _s	Saturated soil water hydraulic conductivity
L	Integer
n	Function of drained upper limit soil water content
q	Soil water flux
q_s	Saturated soil water flux

t Time

WT Water table depth

x,z Cartesian rectangular space coordinates

x., z. Rotated Cartesian rectangular space coordinates

z Distance

MICHIGAN STATE UNIV. LIBRARIES
31293020611806